AWARD NUMBER: W81XWH-17-1-0147
PR161377

TITLE: Establishing Sts-1 as a Novel Target to Treat Deadly Pathogen Infections

PRINCIPAL INVESTIGATOR: Nicholas Carpino

CONTRACTING ORGANIZATION: Stony Brook University
Department of Molecular Genetics and Microbiology
Stony Brook, NY 11794

REPORT DATE: JUNE 2018

TYPE OF REPORT: Annual Report

PREPARED FOR: U.S. Army Medical Research and Materiel Command
Fort Detrick, Maryland 21702-5012

REPORT DOCUMENTATION PAGE

Form Approved
OMB No. 0704-0188

1. REPORT DATE	2. REPORT TYPE	3. DATES COVERED
JUNE 2018	Annual	15 May 2017– 14 May 2018

4. TITLE AND SUBTITLE

Establishing Sts-1 as a Novel Target to Treat Deadly Pathogen Infections

5a. CONTRACT NUMBER
W81XWH-17-1-0147

5b. GRANT NUMBER
PR161377

5c. PROGRAM ELEMENT NUMBER

6. AUTHOR(S)

Nick Carpino
Jarrod French

E-Mail: nicholas.carpino@stonybrook.edu; jarrod.french@stonybrook.edu

5d. PROJECT NUMBER

5e. TASK NUMBER

5f. WORK UNIT NUMBER

7. PERFORMING ORGANIZATION NAME(S) AND ADDRESS(ES)

Stony Brook University
Stony Brook, NY 11794

8. PERFORMING ORGANIZATION REPORT NUMBER

9. SPONSORING / MONITORING AGENCY NAME(S) AND ADDRESS(ES)

U.S. Army Medical Research and Materiel Command
Fort Detrick, Maryland 21702-5012

10. SPONSOR/MONITOR'S ACRONYM(S)

11. SPONSOR/MONITOR'S REPORT NUMBER(S)

12. DISTRIBUTION / AVAILABILITY STATEMENT

Approved for Public Release; Distribution Unlimited

13. SUPPLEMENTARY NOTES

14. ABSTRACT

This proposal addresses a unique approach to improving clinical outcomes for individuals who have contracted life-threatening bacterial and fungal infections. Two homologous phosphatases, Sts-1 and Sts-2, have been established as negative regulators of signaling pathways within mammalian immune cells. Experimental mice in which the Sts proteins are functionally inactivated have been shown to be profoundly resistant to infection with high doses of different microbial pathogens, including *Candida albicans*, *Francisella tularensis LVS*, and *Staphylococcus aureus*. Resistance was characterized by an altered immune response and enhanced pathogen clearance. We propose to develop pharmacological inhibitors of Sts-1, in order to enhance anti-microbial immune responses. Proposed aims are to **1)** determine how leukocyte anti-microbial effector functions are regulated by Sts-1 activity; **2)** conduct a 20,000 compound pilot screen for Sts-1 inhibitors; **3)** solve X-ray crystal structures of Sts-1-drug complexes to characterize the active site architecture; and **4)** assess how HTS lead compounds alter leukocyte microbicidal responses and survival curves following infection.

15. SUBJECT TERMS
Immune regulation; signal transduction; inflammation; microbial infections; high-throughput screening.

16. SECURITY CLASSIFICATION OF:			17. LIMITATION OF ABSTRACT	18. NUMBER OF PAGES	19a. NAME OF RESPONSIBLE PERSON
a. REPORT	b. ABSTRACT	c. THIS PAGE			19b. TELEPHONE NUMBER *(include area code)*
Unclassified	Unclassified	Unclassified	Unclassified	84	USAMRMC

Table of Contents

Page

1. Introduction

Subject: This proposal, in the FY16 PRMRP Topic Area of **Anti-Microbial Resistance**, addresses a unique approach to improving clinical outcomes for individuals who have contracted life-threatening bacterial and fungal infections. **Purpose:** Overall, we propose to develop an improved clinical strategy to fight deadly human pathogens. Our approach relies on pharmacological inhibition of an important immune regulator (Sts-1), in order to enhance anti-microbial immune responses. **Scope:** Two homologous phosphatases, Sts-1 and Sts-2, have been established as negative regulators of signaling pathways within mammalian immune cells. Experimental mice in which the Sts proteins are functionally inactivated have been shown to be profoundly resistant to infection with high doses of different microbial pathogens, including *Candida albicans*, *Francisella tularensis LVS*, and *Staphylococcus aureus*. Of the two, Sts-1 displays the more predominant role. The resistance of *Sts*-/- animals was characterized by an altered immune response and enhanced pathogen clearance. We propose to **1)** determine how leukocyte anti-microbial effector functions are regulated by Sts activity; **2)** conduct a 20,000 compound pilot screen for Sts-1 inhibitors; **3)** solve X-ray crystal structures of Sts-1- drug complexes to characterize the active site architecture; and **4)** assess how HTS lead compounds alter leukocyte microbicidal responses and survival curves following infection.

2. Keywords:

Sts-1&2 (Suppressor of TCR Signaling-1 & -2); immune regulation; signal transduction; phosphatase activity; phagocyte; inflammation; microbial infection; inhibitory molecules; high-throughput screening; combination therapy.

3. Accomplishments

a. What were the major goals of the project?

1) Determine leukocyte effector responses regulated by Sts activity (1-12 months); establish role of Sts-1 in human cells (1-12 months).
2) Establish the feasibility of inhibiting Sts-1 phosphatase activity with small molecules;
3) Determine effects of small molecule-mediated inhibition of Sts-1 phosphatase activity on leukocyte anti-microbial responses (6-18 months).

b. What was accomplished under these goals?

1) To identify phagocyte effector functions regulated by Sts, we compared wild type and Sts-/- bone marrow derived phagocytic populations for responses to *ex vivo C. albicans* stimulation (see *Figures 3-6 in Frank et al, Appendix 2*). We also evaluated *Sts*-/- bone marrow-derived monocytic cells for response to *F. tularensis* infection (*Appendix 3*). We identified Dectin-1 – dependent ROS production downstream of fungal ligand stimulation as a target of Sts inhibitory activity within BMDCs (*Figures 4&5, Frank et al, Appendix 2*). The ROS response was evaluated using a luminol-based chemiluminescence assay. Other effector responses, such as inflammasome activation, cytokine production, or induction of the NO response do not appear to be regulated by Sts activity, as they were unaffected by the absence of Sts expression (*Figure 4, Frank et al, Appendix 2*). We also identified the IFNγ signaling pathway as a target of Sts regulatory activity in bacterially infected monocytes (*Appendix 3*). Achieving these results delayed the initiation of the HL-60 mutagenesis project.

2) To establish the feasibility of selectively inhibiting Sts-1 phosphatase activity we first miniaturized a phosphatase assay for transfer to 1,536-well plates, and then conducted a 20,000 compound pilot screen in collaboration with the Molecular Screening Center at the

Scripps Research Institute (*Appendix 4, Figures 1 and 2*). The assay behaved well (good signal to noise and Z' scores) and we identified 51 active compounds (from 115 initial hits; 0.56% hit rate) after counter-screening and titration assays (*Appendix 4, Figure 2*). Several clear classes of inhibitors were identified. We chose two of the classes of compounds identified in the screen, the tetracyclines (10 variants identified as hits) and the azo dyes (6 variants identified), for further investigation (*Appendix 4, Figures 3 and 4*, respectively). Both classes of compounds were determined to be competitive inhibitors and were selective for Sts-1 over other canonical PTPs (*Appendix 4, Figure 5*). The azo dyes had selectivity indices of at least 20 and 50 for PTP1B and SHP1, respectively; the tetracyclines showed no inhibition for either PTP1B or SHP1 (*Appendix 4, Table 4*). We also conducted site-directed mutagenesis of the phosphatase domain of Sts-1 and determined that an active site tyrosine residue and an active site tryptophan residue contribute to inhibitor binding (*Appendix 4, Figure 6 and Table 5*). In parallel with these studies, we have been actively pursuing crystal structures of Sts-1 phosphatase in complex with inhibitors. We have solved a high-resolution structure of human Sts-1 phosphatase domain with sulfate bound in the active site, as well as unliganded structures of Sts-1 and Sts-2 phosphatase domains (*Appendix 1*). In addition, we have recently identified conditions for co-crystallization of an inhibitor fragment in the active site. Our current data shows clear electron density for a portion of the inhibitor in the active site – we attribute the incomplete density to partial occupancy of the compound and are currently optimizing conditions to obtain the fully occupied structure (*Appendix 5, Figures 1 – 3*). Taken together, these feasibility studies demonstrate that Sts-1 has a 'druggable' binding pocket that can be selectively inhibited by small molecules, and that we can effectively identify inhibitors using our high-throughput screening approach.

3) We have developed an *in cellulo*-based assay to look at the inhibition of Sts activity via small molecule competitive inhibition (see *Figure 5, Zhou et al, Appendix 1*). Briefly, Sts-1 is co-expressed in 293T cells with a putative substrate (phosphorylated Zap-70). In the absence of Sts-1 inhibition, Zap-70 is dephosphorylated. Following Sts-1 inhibition, Zap-70 remains phosphorylated. We will utilize this assay as an initial *in cellulo* assay to evaluate leads obtained in our screening program. Derivation of additional *in cellulo* and *in vivo* assays to evaluate small compound inhibitors is also in progress.

c. What opportunities for training and professional development has the project provided?

This work has provided the opportunity to train graduate students David Frank and Kaustubh Parashar in basic research involving the mammalian immune response and host-pathogen reactions. In addition, this work has provided the opportunity to train two additional graduate students (Weijie Zhou and Yue Yin) in various aspects of drug discovery, enzyme kinetics, cell biology and structural biology. These students have reported their findings at regional and national conferences. The training and the networking opportunities/exposure at meetings, in part, have contributed to the students' thesis projects and ultimate transition into the job market. Finally, Ms. Zhou was awarded the department of Chemistry Award for Outstanding Doctoral Student and has accepted a position at Genentech as of the summer of 2018.

d. How were the results disseminated to communities of interest?

Publications:

1. *in print*: 1 manuscript (Zhou et al, 2017; PMID 28759203; see *Appendix 1*);

2. *under review*: 1 manuscript (Frank et al, 2018, see Appendix 2);
3. *in preparation:* 2 manuscripts: **i)** Parashar et al, "Negative regulation of the monocyte IFNγ response by the Sts proteins"; (*Appendix 3*) and **ii)** Zhou et al, "Discovery and characterization of two classes of selective inhibitors of the Suppressor of TCR Signaling proteins" (to be submitted to *Antimicrobial Agents and Chemotherapy* summer of 2018) (*Appendix 4*).

Poster Presentations:
1. CSHL Meeting (2018): *Negative regulation of Gene expression and signaling in the immune system, 2018.* "Phagocytes from mice lacking the Sts phosphatases have an enhanced anti-fungal response to *C. albicans,*" Frank et. al.
2. SBU Biochemistry and Cell Biology Department annual retreat (2017) "Phosphatase Suppressor of T cell Receptor Signaling Pathway As a Novel Drug Target for Pathogenic Infections" Zhou *et al.*
3. American Crystallographic Association Annual Meeting (2016) "Structural and Functional Characterization of Human Sts-1HP targeting the T cell signaling pathway" Zhou *et al.*

e. What do you plan to do during the next reporting period to accomplish the goals?

1) **a.** Evaluate role of Sts-1 in regulating fungal-dependent transcriptional activation.
b. Determine elements of Dectin-Syk-ROS pathway targeted by Sts-1
2) **a.** Ongoing structural studies will continue, aimed at solving an X-ray crystal structure of protein-drug complexes
b. Further characterization of hits and initial SAR studies will be carried out
3) Lead compounds from pilot screen will be evaluated for biological efficacy in selected *in cellulo* and *in vivo* assays.

4. Impact

a. What was the impact on the development of the principal disciplines of the project?

1) Feasibility of a large-scale high-throughput screen for Sts-1 inhibitors established.
2) Identification of individual phagocyte anti-fungal effector functions regulated by Sts.

b. What was the impact on other disciplines?

Nothing to report.

c. What was impact on technology transfer?

Nothing to report.

d. What was the impact on society beyond science and technology?

Nothing to report.

5. Changes/problems

a. Changes in approach and reasons for change.

Nothing to report.

b. Actual or anticipated problems or delays and actions or plans to resolve them.

1) Specific Aim 1.2: Delays in generating *Sts-1*$^{-/-}$ HL60 cells. Resolution: utilize new guide RNAs.
2) Initial attempts to co-crystallize inhibitors (identified in the screen) with Sts-1 for co-crystal structures were unsuccessful. Resolution: using smaller inhibitor fragments, we have identified a condition to obtain co-crystal structures. This condition will be used as a starting point for further protein-inhibitor structure studies

c. Changes that had a significant impact on expenditures

Nothing to report.

d. Significant changes in use or care of human subjects, vertebrate animals, biohazards, and/or select agents.

Nothing to report.

6. Products

a. Publications, conference papers, and presentations. See 3d.

b. Websites/Internet sites.

Nothing to report.

c. Technologies or techniques.

Strategy to develop specific Sts-1 inhibitors for future therapeutic use has been successfully validated.

d. Inventions, patent applications, and/or licenses.

Nothing to report.

e. Other products.

Nothing to report.

7. Participants and other collaborating organizations

a. What individuals have worked on the project?

Name: Nick Carpino
Project Role: PI
Research Identifier: ORCID ID 0000-0002-9231-9160
Nearest person-month worked: 1

Contribution to Project: Supervisory role

Name: Jarrod French
Project Role: PI
Research Identifier: ORCID ID 0000-0002-6762-1309
Nearest person-month worked: 1
Contribution to Project: Supervisory role

Name: David Frank
Project Role: Graduate student
Research Identifier:
Nearest person-month worked: 12
Contribution to Project: experimentalist

Name: Weijie Zhou
Project Role: Graduate student
Research Identifier:
Nearest person-month worked: 12
Contribution to Project: experimentalist

Name: Yue Yin
Project Role: Graduate student
Research Identifier:
Nearest person-month worked: 6
Contribution to Project: experimentalist

Name: Kaustubh Parashar
Project Role: Graduate student
Research Identifier:
Nearest person-month worked: 12
Contribution to Project: experimentalist

b. Has there been a change in the active other support of the PD/PI(s) or senior/key personnel since the last reporting period?

<u>Carpino, Completed Research Support</u>

Dean's Office Bridge Funding 1/1/16-6/30/17 0.6 calendar months
SBU School of Medicine
"Role of the Sts proteins in regulating the immune response to *C. albicans* infection."
The goal of this project is to determine role of the Sts proteins in regulating the host immune response to systemic infection by wild type C. albicans species.

RCH23267 (U01HL127522) 5/15/16-5/14/17 1.2 calendar months
Stony Brook University (NIH/NHBLI)
"Developing a small molecule drug to treat systemic C. albicans infections."

The major goal of this work is to evaluate Sts-1 as a drug target for the treatment of systemic candidiasis and to lay the foundation for an HTS inhibitor campaign.

Dean's Office Targeted Research Award 7/1/16-6/30/17 0.6 calendar months
SBU School of Medicine
"Developing a small molecule inhibitor to treat C. albicans infections."
The goal of this project is to develop a small molecule Sts inhibitor to prevent life - threatening C. albicans infections.

Carpino, New Research Support

R21 AI130859 (Carpino) 12/15/17 – 11/30/19 1.2 calendar
NIH/NIAID
Establishing Sts-1 as a novel target for treatment of systemic candidiasis.
The major goal of this project is to establish the feasibility of treating systemic C. albicans infection by targeting Sts-1 via small molecule inhibition.

R21 AI133381 (Carpino) 01/01/18 – 12/31/20 1.2 calendar
NIH/NIAID
Role of Sts-1 and -2 in the host response to bacterial pathogens
The major goals of this project are to define the mechanistic role of the Sts proteins in regulating leukocyte responses to bacterial infections.

French, Completed Research Support

RCH23267 (U01HL127522) 5/15/16-5/14/17 1.2 calendar months
Stony Brook University (NIH/NHBLI)
"Developing a small molecule drug to treat systemic C. albicans infections."
The major goal of this work is to evaluate Sts-1 as a drug target for the treatment of systemic candidiasis and to lay the foundation for an HTS inhibitor campaign.

Dean's Office Targeted Research Award 7/1/16-6/30/17 0.6 calendar months
SBU School of Medicine
"Developing a small molecule inhibitor to treat C. albicans infections."
The goal of this project is to develop a small molecule Sts inhibitor to prevent life - threatening C. albicans infections.

French, New Research Support

Cottrell Scholar Award (French) 07/01/19 – 06/30/22 0.1 calendar
Research Corporation for Science Advancement
Structural dynamics of photoactive proteins and crowdsourcing structural biology
This is a 'young investigator' career development award that will support the research, professional development and educational pursuits of the PI

R21 AI130859 (Carpino) 12/15/17 – 11/30/19 1.2 calendar
NIH/NIAID

Establishing Sts-1 as a novel target for treatment of systemic candidiasis.
The major goal of this project is to establish the feasibility of treating systemic C. albicans infection by targeting Sts-1 via small molecule inhibition.

NSF MCB 1750637 (French) 05/01/18 – 04/30/23 0.9 calendar
National Science Foundation
CAREER: Structural dynamics of photoactive proteins
The goal of this work is to determine the mechanisms of signal transduction in flavoprotein photoreceptors.

R35GM124898 (French) 09/15/17 – 08/30/22 3.8 calendar NIH/ NIGMS
Mechanisms that govern assembly and function of higher order protein structures of purine metabolic enzymes
This is a program grant to support the PI's investigations into the trafficking, functions and assembly mechanisms of higher order protein structures involved in nucleotide metabolism

c. What other organizations were involved as partners?

Name: Scripps High-Throughput Screening Facility
Scripps Research Institute
Location: Jupiter, FL
Contribution: Pilot high-throughput screen of 20,000 compounds

8. Special reporting requirements

N/A

9. Appendices 1-5:

APPENDIX 1

Published manuscript, Zhou et al, 2017

Biochemistry

Article

pubs.acs.org/biochemistry

Structural and Functional Characterization of the Histidine Phosphatase Domains of Human Sts-1 and Sts-2

Weijie Zhou,[†] Yue Yin,[†] Alexandra S. Weinheimer,[‡] Neena Kaur,[§] Nick Carpino,*[,§] and Jarrod B. French*[,†,‡]

[†]Department of Chemistry, Stony Brook University, Stony Brook, New York 11794, United States

[‡]Department of Biochemistry and Cell Biology, Stony Brook University, Stony Brook, New York 11794, United States

[§]Department of Molecular Genetics and Microbiology, Stony Brook University, Stony Brook, New York 11794, United States

ABSTRACT: The suppressor of T cell signaling (Sts) proteins, Sts-1 and Sts-2, are homologous phosphatases that negatively regulate signaling pathways downstream of the T cell receptor. Functional inactivation of Sts-1 and Sts-2 in a murine model leads to resistance to systemic infection by the opportunistic pathogen, *Candida albicans*. This suggests that modulation of the host immune response by inhibiting Sts function may be a viable strategy for treating these deadly fungal pathogen infections. To better understand the molecular determinants of function and structure, we characterized the structure and steady-state kinetics of the histidine phosphatase domains of human Sts-1 (Sts-1_{HP}) and Sts-2 (Sts-2_{HP}). We determined the X-ray crystal structures of unliganded Sts-1_{HP} and Sts-1_{HP} in complex with sulfate to 2.5 and 1.9 Å, respectively, and the structure of Sts-2_{HP} with sulfate to 2.4 Å. The steady-state kinetic analysis shows, as expected, that Sts-1_{HP} has a phosphatase activity significantly higher than that of Sts-2_{HP} and that the human and mouse proteins behave similarly. In addition, comparison of the phosphatase activity of full-length Sts-1 protein to Sts-1_{HP} reveals similar kinetics, indicating that Sts-1_{HP} is a functional surrogate for the native protein. We also tested known phosphatase inhibitors and determined that the SHP-1 inhibitor, PHPS1, is a potent inhibitor of Sts-1 (K_i = 1.05 ± 0.15 μM). Finally, we demonstrated that human Sts-1 has robust phosphatase activity against the substrate, Zap-70, in a cell-based assay. Collectively, these data suggest that the human Sts proteins are druggable targets and provide a structural basis for future drug development efforts.

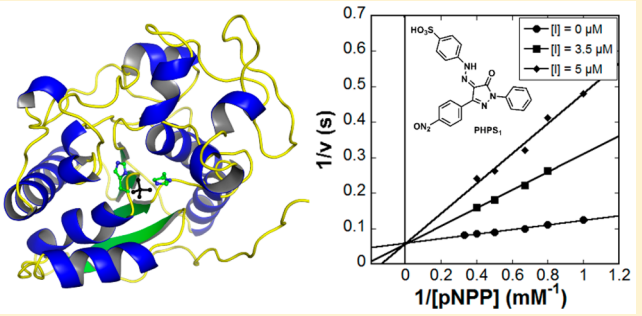

T cells play critical roles in the recognition and elimination of foreign pathogens in the host immune system. The T cell receptor (TCR) is responsible for activating T cells as well as recognizing and responding to foreign antigens or inappropriately expressed endogenous proteins.[1] Control of T cell signaling occurs through both positive and negative regulation. Two members of the suppressor of TCR signaling (Sts) family of proteins, Sts-1 and Sts-2, have been shown to be functionally redundant negative regulators of signaling pathways downstream of the TCR.[2] Sts-1 and -2 share 40% sequence identity and have a multidomain structure containing an N-terminal ubiquitin-association (UBA) domain and a Src-homology 3 (SH3) domain. Both of these domains are believed to be involved in protein−protein interactions.[3,4] Current models of Sts function suggest that these two domains play critical roles in localizing Sts enzymatic functions to specific intracellular regions.[5] In addition, both Sts-1 and Sts-2 contain a C-terminal histidine phosphatase (HP) catalytic domain that is homologous to phosphoglycerate mutase (PGM), part of the histidine phosphatase superfamily.[6−8] The C-terminal HP domain of mouse Sts-1 has been shown to have an intrinsic phosphatase activity that contributes to the ability of Sts proteins to negatively regulate signaling pathways downstream of the TCR.[6]

The roles of Sts-1 and -2 were discovered from analysis of T cells isolated from mice lacking Sts-1 and -2.[2] In particular, naive Sts-1/2$^{-/-}$ T cells exhibit a pronounced increase in their level of TCR-induced proliferation compared with that of wild-type cells. The HP domain of Sts-1 (Sts-1_{HP}) was shown to have robust tyrosine phosphatase activity that could dephosphorylate numerous proteins, including Zap-70.[2,6] Zap-70 is a tyrosine kinase that plays a critical role in propagating signals initiated by TCR engagement.[6,9] Hyperphosphorylated and ubiquitinated Zap-70 was identified and characterized in Sts-1/2$^{-/-}$ stimulated T cells.[10] Moreover, Sts-knockout mice displayed significantly enhanced survival after infection with the fungal pathogen *Candida albicans*. In a mouse model that mimics disseminated candidiasis in humans, mice were found to be profoundly resistant to infection without a hyperinflammatory response that would cause tissue damage.[11] In addition, the mice lacking the Sts proteins were associated with a significant

Received: July 6, 2017
Revised: July 27, 2017
Published: July 31, 2017

DOI: 10.1021/acs.biochem.7b00638
Biochemistry XXXX, XXX, XXX−XXX

reduction in fungal burden.[11] This result underscores the role of the Sts proteins in regulating host responses to fungal pathogens and their potential as host-modulatory drug targets for antifungal therapies.

Previous structural studies of Sts-1_{HP} and Sts-2_{HP} have been conducted for the murine proteins.[6,12−16] These structures (97 and 81% sequence identity with human Sts-1_{HP} and Sts-2_{HP}, respectively) revealed that these proteins have a conserved phosphoglycerate mutase fold. A comparison of MmSts-1_{HP} to MmSts-2_{HP} showed a high degree of structural similarity, yet some notable structural differences in the active site.[6,12,14] Functional studies, both *in vitro* and *in vivo*, showed that Sts-1 has a phosphatase activity much higher than that of Sts-2, both on non-native substrates and on the putative protein substrate, Zap-70.[6,11,14,17] The mechanism of catalysis is believed to resemble that of other histidine phosphatases, proceeding through a covalent phosphor−histidine intermediate.[8,18−20]

To improve our understanding of how the human Sts proteins function and as a basis for structure-guided drug discovery, we determined the X-ray crystal structures of human Sts-1_{HP}, both unliganded and with a sulfate occupying the active site, and of human Sts-2_{HP} with sulfate bound. Analogous to those of the murine Sts proteins, the structures of the human homologues have a high degree of similarity with some subtle yet distinct structural differences. Comparison of the steady-state kinetics shows that, as with the mouse proteins, Sts-1 is a much more efficient phosphatase. In addition, we demonstrate that the intact Sts-1 protein displays phosphatase kinetics similar to that of the isolated Sts-1_{HP} domain. This indicates that Sts-1_{HP} is an effective surrogate for the full-length protein upon measurement of phosphatase activity. We also report several potent Sts inhibitors, including the phenylhydrazono-pyrazolone sulfonate PHPS1, which is known to be a cell-permeable inhibitor of the phosphatase Shp2.[21] Finally, we demonstrate that human Sts-1 dephosphorylates the protein substrate Zap-70 in a cell-based assay. Taken together, these results confirm the druggability of Sts-1 and provide a framework for structure-based drug development. In addition, these findings confirm the structural and functional similarity of the mouse and human Sts proteins, suggesting that findings in the murine model should translate well to humans.

MATERIALS AND METHODS

Cloning, Expression, and Purification of Human Sts-1_{HP} and Sts-2_{HP}. A cDNA fragment encoding Sts-1_{HP} (residues 369−636) was amplified by polymerase chain reaction, cloned as a His-tagged protein in the pTHT vector (a modified form of pET-28 with a tobacco etch virus protease site in place of the thrombin site), and expressed in *Escherichia coli* strain BL21 (DE3). Bacterial cultures were grown in terrific broth supplemented with 50 mg/L kanamycin for 6 h at 310 K and induced with 0.3 mM isopropyl thiogalactopyranoside (IPTG) at 291 K overnight. The cells were harvested by centrifugation and lysed using sonication in lysis buffer [500 mM NaCl, 5 mM imidazole, and 20 mM Tris-HCl (pH 8.0)]. The protein was then purified on a Ni-NTA column (Qiagen) equilibrated with lysis buffer. Nonspecifically bound proteins were washed away with lysis buffer supplemented with 20 mM imidazole. The protein was eluted with elution buffer (lysis buffer with 300 mM imidazole). The six-His tag was removed with tobacco etch virus (TEV) protease in TEV protease buffer [20 mM Tris-HCl (pH 8.0), 150 mM NaCl, and 1 mM EDTA]. The N-terminal sequence remaining after cleavage, and preceding residue 369 of Sts-1_{HP} of the crystallized protein, was QGHMASMTGGQQMGRGS. The untagged protein was concentrated to 20−24 mg/mL, buffer exchanged into storage buffer [10 mM HEPES (pH 7.5), 150 mM NaCl, and 5 mM BME] and stored at −80 °C. The Sts-2_{HP} protein domain (residues 393−657) was expressed and purified in the same way as Sts-1_{HP}. The N-terminal sequence remaining after cleavage, and preceding residue 393 of Sts-2_{HP}, was QGHM-ASMTGGQQMGRGS. The untagged protein was concentrated to 16−18 mg/mL and stored in buffer containing 20 mM Tris (pH 8.0), 50 mM NaCl, 10% glycerol, and 5 mM DTT. For full-length human Sts-1, we cloned the gene from cDNA into the pDB-NusA vector. The protein was expressed as a fusion with the NusA protein linked by a TEV cleavage site. The cells were lysed, and the protein was initially purified as detailed above for the HP domains. After the initial purification step, the NusA solubility tag was removed by treatment with TEV protease and the liberated tag was separated from the untagged protein with a second round of immobilized-metal affinity chromatography using Ni-NTA. The protein was further purified by size exclusion chromatography using a HiLoad 26/600 Superdex 200 (GE Life Sciences) column in 50 mM MES buffer (pH 7.5) and 150 mM NaCl.

Crystallization and Data Collection. *Unliganded Human Sts-1_{HP}.* Initial crystallization screening of human Sts-1_{HP} was conducted at 18 °C, using the hanging-drop vapor diffusion method, based on the conditions under which the mouse Sts-1_{HP} is known to crystallize.[16] Rod-shaped crystals were obtained overnight when 1 μL of Sts-1_{HP} was mixed with 1 μL of the reservoir solution containing 0.1 M HEPES (pH 7.0), 5% ethylene glycol, 0.3 M magnesium chloride, and 13% PEG 8000. The crystal size and quality were improved by seeding. Prior to be being flash-frozen in liquid nitrogen, the crystals were soaked in a solution containing the crystallization buffer with a final PEG 8000 concentration of 30%.

Human Sts-1_{HP} with Sulfate. Initial crystallization screening of human Sts-1_{HP} was conducted at 18 °C, using the hanging-drop vapor diffusion method, based on the conditions under which mouse Sts-1_{HP} is known to crystallize.[15] Lozenge-shaped crystals were obtained overnight when Sts-1_{HP} was mixed with the reservoir solution in a ratio of 1:1.5. The reservoir solution consisted of 0.1 M sodium acetate (pH 5.5), 0.2 M ammonium sulfate, 23% PEG 2000 MME, and 2 mM DTT. These crystals were cryoprotected by being soaked in the crystallization solution with PEG 2000 MME added to a final concentration of 30%, before being flash-frozen in liquid nitrogen.

Human Sts-2_{HP}. Sparse matrix screening was conducted for Sts-2_{HP} using the hanging-drop vapor diffusion method at 291 K. Cubic-shaped crystals were obtained after 2 days under a condition that included equal volumes of Sts-2_{HP} and a solution consisting of 0.1 M HEPES (pH 7.0), 22% PEG 4000, 0.2 M potassium acetate, and 0.2 M lithium sulfate. Crystals of a similar morphology were also obtained using a reservoir solution consisting of 0.1 M Tris (pH 8.0), 30% PEG 4000, 0.2 M lithium sulfate, and 15 mM strontium chloride. Crystals were first soaked in a solution containing the crystallization solution with a PEG 4000 final concentration of 30% before being flash-frozen in liquid nitrogen. In all three cases, data were collected at 100 K at the Advanced Photon Source on beamlines 24 ID-C and 24 ID-E. Data collection statistics are listed in Table 2.

DOI: 10.1021/acs.biochem.7b00638
Biochemistry XXXX, XXX, XXX−XXX

Structure Determination and Refinement. In all cases, diffraction data were indexed, integrated, and scaled using HKL-2000.[22] Structures were determined by molecular replacement using MolRep[23] with the equivalent mouse protein structures (coordinate files 2H0Q and 3D4I) as search models.[12,15,16] The models were refined using iterative rounds of manual model building with Coot[24] and restrained refinement with Refmac5.[25] Water molecules were added using Coot only after the refinement had converged. Sulfates in and around the active site were directly inserted into the corresponding difference electron density, and the model was then subjected to an additional round of refinement. The refinement statistics for the models are listed in Table 2. Note that the unstructured N-termini of the proteins (upstream of R373 in Sts-1_{HP} and upstream of R395 in Sts-2_{HP}) were not ordered in the crystal structures.

Phosphatase Assays. Three commonly used spectrophotometric or fluorescent phosphatase assays were used to quantify the phosphatase activities of human Sts-1_{HP} and Sts-2_{HP}.[26−28] These assays make use of three different substrates: *p*-nitrophenyl phosphate (pNPP), 3-*O*-methylfluorescein phosphate (OMFP), or 6,8-difluoro-4-methylumbelliferyl phosphate (DifMUP). For the pNPP substrate, the reaction buffer contained 20 mM Tris (pH 7.5), 150 mM sodium chloride, 5 mM magnesium chloride, and 1 mM BME. The reaction was initiated by adding the protein to the pNPP in the reaction buffer. The rate of reaction was measured continuously at 298 K by quantifying the appearance of the nitrophenol product at 405 nm on a SpectraMax Plus instrument (Molecular Devices). For the OMFP substrate, a 10× assay buffer, consisting of 300 mM Tris (pH 7.4), 750 mM NaCl, and 10 mM EDTA, was diluted 10-fold and DTT added to a final concentration of 1 mM. OMFP was added to the assay buffer from a freshly made 10 mM stock in DMSO. The production of OMF was measured continuously at 298 K by fluorescence (excitation at 485 nm and emission at 525 nm) on a SpectraMax Gemini instrument (Molecular Devices). For the DifMUP substrate, a 10× assay buffer, consisting of 500 mM Bis-Tris (pH 7.5), 750 mM NaCl, and 20 mM EDTA, was diluted 10-fold and fresh DTT added to a final concentration of 1 mM. DifMUP was added from a freshly made 10 mM stock in DMSO. The rate of reaction was measured continuously at 298 K by quantifying the production of DifMU by fluorescence (excitation at 360 nm and emission at 450 nm) on a SpectraMax Gemini instrument (Molecular Devices).

Steady-State Kinetics. Initial velocities (v_0) were determined from slopes of linear segments of progress curves using time points well before the reaction had reached 10% completion. Initial velocities were determined at varying substrate concentrations and plotted against substrate concentration. The data were fit with a rectangular hyperbola using the Michaelis−Menten equation, and values for K_m and k_{cat} were determined (Kaleidagraph, Synergy Software).

Analysis of Inhibition of Sts-1_{HP} and Sts-2_{HP}. The phosphatase assays were used to analyze the inhibition of the two enzymes. To determine the mode of inhibition, double-reciprocal plots of $1/v_0$ versus 1/[substrate] were constructed using measurements of rate as described above. As the mode of inhibition was determined to be competitive, the data were fit using the following equation:

$$v = \frac{v_{max}[\text{substrate}]}{K_m\left(1 + \frac{[\text{inhibitor}]}{K_i}\right) + [\text{substrate}]} \quad (1)$$

The value of the inhibition constant, K_i, was determined either from the fit of the data to eq 1 or by analyzing the steady-state kinetics (as detailed above) in the presence of the inhibitor and using the following equation:

$$K_m^{app} = K_m\left(1 + \frac{[\text{inhibitor}]}{K_i}\right) \quad (2)$$

In all cases, the determination of inhibition constants was performed in triplicate experiments at multiple inhibitor concentrations, and the final amount of DMSO added during the assay was <2% of the total volume. The error values provided are standard errors from triplicate measurements.

Zap-70 Dephosphorylation Assay. Human embryonic kidney 293 (HEK-293) cells were cultured in DMEM (Dulbecco's modified Eagle's medium, Gibco/Life Technologies) supplemented with 10% FBS (Fisher Hyclone) and 100 units/mL penicillin and 100 units/mL streptomycin. Zap-70 dephosphorylation was assessed as described previously.[6] Briefly, either human or murine Sts-1 expression constructs (Flag-tagged) were co-transfected into cells using Lipofectamine 2000 transfection reagent, along with plasmids encoding Lck (lymphocyte-specific protein tyrosine kinase), Zap-70 (T7-tagged), and a CD8-ζ chain chimera. Twenty-four hours after being transfected, cells were lysed in buffer containing 50 mM Tris-HCl (pH 7.6), 150 mM NaCl, 5 mM EDTA, and 1% NP-50 and clarified by centrifugation for 15 min at 16000*g*. Lysates were suspended in Laemmli sample buffer, and proteins were resolved by sodium dodecyl sulfate−polyacrylamide gel electrophoresis and transferred to nitrocellulose. Levels of phosphorylated Zap-70 were determined by immunoblotting with an antibody directed at Zap-70 pTyr-493 (Cell Signaling Technologies). Levels of Zap-70 and Sts-1 were determined by immunoblotting with antibodies to T7 (Novagen) and Flag (Sigma), respectively. The experiment was performed in triplicate, and the blot shown is a representative example of typical data collected.

RESULTS AND DISCUSSION

Activity of Human Sts-1_{HP} and Sts-2_{HP}. Knockout of the Sts proteins in mice confers a profound resistance to fungal infection without deleterious immunopathology.[11] This highlights the clinical relevance of the Sts proteins as potential immunomodulatory targets for the treatment of deadly pathogen infections. The enzymatic activity of the Sts proteins is performed by a C-terminal histidine phosphatase domain that is structurally homologous to the phosphoglycerate mutase family.[6] This phosphatase domain is believed to have tyrosine phosphatase activity and can act on protein substrates such as Zap-70.[2,6] To better understand the molecular details of the human proteins and to provide a basis for future drug discovery efforts, we set out to characterize the activity and structure of human Sts-1_{HP} and Sts-2_{HP}. The histidine phosphatase domains of the human Sts proteins (Sts-1_{HP} and Sts-2_{HP}) expressed and purified well using conventional methods. To determine the activity of these proteins, we used three established phosphatase assays that employed the substrates *p*-nitrophenyl phosphate (pNPP), 3-*O*-methylfluorescein phosphate (OMFP), and 6,8-difluoro-4-methylumbelliferyl phosphate

DOI: 10.1021/acs.biochem.7b00638
Biochemistry XXXX, XXX, XXX−XXX

(DifMUP).[26,28] The steady-state kinetic parameters of Sts-1_{HP} and Sts-2_{HP} for the three phosphatase substrates are listed in Table 1. As expected, the phosphatase activity of Sts-2_{HP} is considerably slower than that of Sts-1_{HP}. In addition to the characterization of the phosphatase domain, we determined the kinetics of the full-length Sts-1 protein (Table 1). These data illustrate two key points about the human Sts proteins. The kinetics of the human Sts proteins follow the same trends and are quite similar to what has been observed for the mouse proteins,[6,12] and the kinetics of the isolated Sts-1 HP domain are reasonably similar to those of the native, full-length protein. These findings are important for long-term drug discovery efforts aimed at targeting Sts-1. They highlight the utility of the mouse model to make physiologically relevant observations that are consistent with the activity of the human protein. Furthermore, the data illustrate that the isolated HP domain, which is considerably easier to produce and work with, is a viable surrogate for measuring the phosphatase activity of the full-length protein.

Table 1. Kinetic Constants of Human Sts Proteins

substrate/enzyme	K_m (mM)	k_{cat} (s^{-1})	k_{cat}/K_m (M^{-1} s^{-1})
pNPP			
human Sts-1_{HP}	2.64 ± 0.48	13.62 ± 0.63	5.16×10^3
human Sts-2_{HP}	5.61 ± 1.69	1.23 ± 0.15	2.19×10^2
full-length Sts-1	3.31 ± 0.27	158.6 ± 6.48	4.77×10^4
OMFP			
human Sts-1_{HP}	0.19 ± 0.03	786.1 ± 52.4	4.14×10^6
human Sts-2_{HP}	1.07 ± 0.24	5.86 ± 0.78	5.48×10^3
full-length Sts-1	ND	ND	ND
DifMUP			
human Sts-1_{HP}	0.002	100.68	5.03×10^7
human Sts-2_{HP}	0.85 ± 0.23	4.92 ± 0.76	5.79×10^3
full-length Sts-1	ND	ND	ND

Structures of Human Sts-1_{HP}. To characterize the phosphatase active site of Sts-1 for future structure-guided drug discovery efforts, we determined the X-ray crystal structure of human Sts-1_{HP}, both unliganded (to 2.5 Å resolution) and with the phosphate mimic, sulfate (to 1.9 Å resolution), bound in the active site. Data collection and refinement statistics are listed in Table 2. The overall structure of the human Sts-1_{HP} protomer is shown in Figure 1A. The protein has the conserved phosphoglycerate mutase (PGM) fold and is a dimer in solution (Figure 1B). Dimerization is mediated by multiple interactions between the intertwined C-terminal dimerization domains of the protomers. This observation is consistent with reports that the physiologically relevant state of Sts-1 is a dimer and the dimerization occurs through the HP domain of the protein.[29]

Table 2. Data Collection and Refinement Statistics[a]

	Sts-1_{HP} unliganded	Sts-1_{HP} sulfate	Sts-2_{HP} sulfate
	Data Collection		
Protein Data Bank entry	5W5G	5VR6	5WDI
resolution range (Å)	50.0−2.48 (2.53−2.48)	50.0−1.87 (1.90−1.87)	50.0−2.43 (2.47−2.43)
wavelength (Å)	0.97910	0.97910	0.97910
space group	*C*2	$P2_12_12_1$	$P2_12_12$
unit cell dimensions			
a, *b*, *c* (Å)	116.6, 74.5, 101.7	62.6, 79.2, 105.1	77.5, 113.1, 61.0
α, *β*, *γ* (deg)	90, 100.9, 90	90.0, 90.0, 90.0	90.0, 90.0, 90.0
no. of measured reflections	64585	211226	73594
no. of unique reflections	28546 (1401)	41518 (1693)	20513 (958)
mean I/σ	11.5 (1.7)	14.9 (4.4)	14.1 (1.8)
completeness	93.8 (93.9)	94.4 (77.7)	98.3 (94.2)
redundancy	2.3 (2.1)	5.1 (4.1)	3.6 (3.4)
R_{merge}	0.12 (0.49)	0.08 (0.20)	0.06 (0.47)
	Refinement		
resolution range (Å)	50.0−2.48	50.0−1.87	50.0−2.43
total no. of reflections	27105	39428	19484
test set	5% (1441)	5% (2033)	5% (996)
R_{work}	19.4	19.4	20.6
R_{free}	24.9	24.1	25.0
no. of protein atoms	5816	4163	4040
no. of ligand atoms	0	80	25
no. of water atoms	98	336	122
root-mean-square deviation from ideal			
bonds (Å)	0.005	0.006	0.005
angles (deg)	0.966	1.1	1.006
mean *B* factor (Å^2)	61.8	20.6	38.3
Ramachandran (%)			
favored	95.82	97.7	97.3
outliers	0.26	0.19	0
Clashscore[b]	1.5 (100%)	3.2 (98%)	1.0 (100%)

[a]Numbers in parentheses correspond to values for the highest-resolution shell. [b]Value calculated by MolProbity. The value in parentheses corresponds to the percentile (100% is best) when compared to a representative set of structures of comparable resolution.[39]

DOI: 10.1021/acs.biochem.7b00638
Biochemistry XXXX, XXX, XXX−XXX

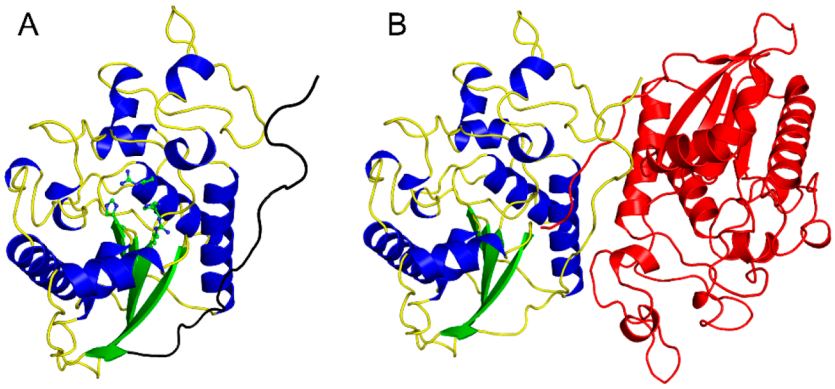

Figure 1. Overall structure of human Sts-1_{HP}. The overall fold of the Sts-1_{HP} protomer is shown in panel A with the conserved active site histidine residues (H380 and H565) and arginine residues (R379 and R462) shown in ball-and-stick representation (carbon atoms colored green and nitrogen atoms colored blue). The dimerization domain is at the C-terminus of the protein and is colored black. The physiologically relevant dimeric form of Sts-1_{HP} is given in panel B with one chain colored by secondary structure as in panel A and the other colored red.

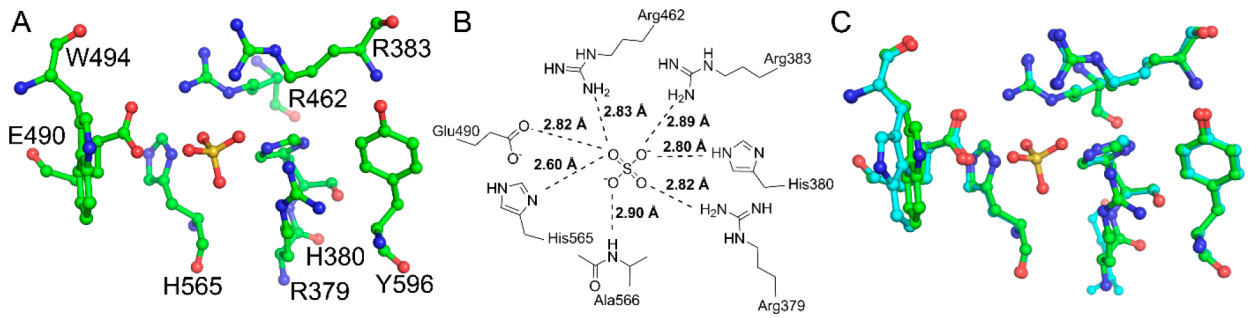

Figure 2. Active site of human Sts-1_{HP}. A ball-and-stick diagram (A, carbon atoms colored green, nitrogen atoms colored blue, oxygen atoms colored red, and the sulfur atom colored yellow) shows the active site residues of Sts-1_{HP} around the phosphate binding pocket (marked by the sulfate in this structure). In addition to the conserved histidine residues and arginine residues, additional hydrogen bonding contacts are made to the sulfate by an additional arginine residue and a glutamate residue (B). The superposition of the human and murine Sts-1_{HP} (C, overall root-mean-square deviation of 0.35 Å) illustrates that the architecture of the active site is highly structurally conserved. The only observed difference is a slight change in the orientation of the tryptophan (W494 in the human protein) at the edge of the active site.

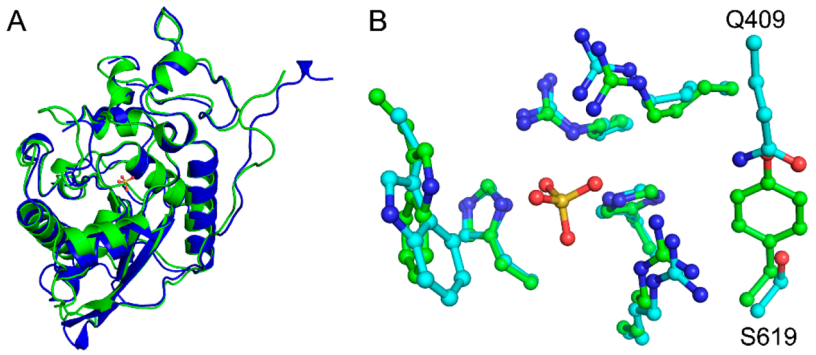

Figure 3. Structure of human Sts-2_{HP}. The overall fold of human Sts-2_{HP} is nearly identical to that of Sts-1_{HP}. A superposition of the Sts-2_{HP} protomer with the equivalent Sts-1_{HP} protomer (A, Sts-1 colored green and Sts-2 colored blue, RMSD of 1.02 Å) shows only subtle differences in peripheral loop regions. Similarly, the active sites of the two proteins align well (in panel B, Sts-1 has green carbon atoms and Sts-2 has cyan carbon atoms; in both structures, the nitrogen atoms are colored blue, oxygen atoms are colored red, and the sulfur atom is colored yellow) but do show some subtle yet distinct differences. Whereas the conserved histidine and arginine residues line up well, a tyrosine and a valine in Sts-1 (Y596 and V386, respectively) are replaced with a glutamine and a serine, respectively, in Sts-2 (Q409 and S619, respectively). It is these differences that likely account for the substrate selectivity of the Sts proteins.

The active site of Sts-1_{HP} (Figure 2A,B) is distinguished by the two catalytic histidine residues (H380 and H565) and two highly conserved arginine residues (R379 and R462). These residues, as well as a glutamate (Q490) and an additional arginine (R383), act to optimally position the phosphate group of the ligand for efficient catalysis (Figure 2B). The phosphatase activity of Sts-1, like that of other PGM family histidine phosphatases, is proposed to proceed through a two-step mechanism that involves nucleophilic attack by one of the conserved histidine residues.[6,8,18−20,30] The active site glutamate is the likely proton donor during this attack. The second step of the reaction is a hydrolysis of the phosphor−histidine intermediate. The incoming water molecule is believed to be activated for attack by the same glutamate residue. The

DOI: 10.1021/acs.biochem.7b00638
Biochemistry XXXX, XXX, XXX−XXX

orientation and bond distances of the residues in the active site of sulfate-bound Sts-1_{HP} are consistent with the proposed mechanism (Figure 2B).

As mentioned in the previous section, the degree of similarity of the mouse and human Sts-1 is an important consideration for future drug discovery efforts. In particular, a high degree of similarity suggests that results from mouse model studies are more likely to be directly translatable to humans. Comparison of the mouse and human Sts-1_{HP} structures (Figure 2C) shows a very high degree of structural conservation in the active site [overall root-mean-square deviation (RMSD) of 0.35 Å]. The only modest difference observed is in the orientation of a tryptophan residue (W494) near the entrance to the active site. In the human and mouse Sts-1_{HP} structures, however, this tryptophan has the highest *B* factor of any of the active site residues. This suggests that this residue has a degree of conformational flexibility higher than that the otherwise immobile active site residues, which may account for the subtle differences observed between the two structures.

Structure of Human Sts-2_{HP}. The two Sts proteins from human, Sts-1 and Sts-2, share approximately 45% overall sequence identity and 50% sequence identity in the HP domain. Despite the high degree of sequence identity, the catalytic efficiency of Sts-2_{HP} is much lower than that of Sts-1_{HP} for all substrates tested (Table 1). To better understand the basis for these kinetic differences, we determined the X-ray crystal structure of human Sts-2_{HP} in the presence of sulfate (data collection and refinement statistics are listed in Table 2). As expected, the overall fold of Sts-2_{HP} is very similar to that of Sts-1_{HP} (RMSD of 1.02 Å) with only slight differences in flexible loops and the dimerization domain observed (Figure 3A). The active site is also highly structurally conserved but has some subtle yet distinct differences (Figure 3B). While the positions of the conserved histidine and arginine residues are nearly identical in the two structures, a valine−tyrosine pair (V386 and Y596) is replaced with a glutamine−serine pair (Q409 and S619) in the Sts-2_{HP} structure. This difference likely accounts for the lower rate of phosphatase activity of Sts-2. Mutation of these residues in mouse Sts-2_{HP} (Q372V and S582Y) increases the k_{cat}/K_m by a factor of 38 for the pNPP substrate.[12] The phosphatase substrates contain large aromatic groups, particularly the fluorescein and umbelliferone of the OMFP and DifMUP, respectively, that could make important π-stacking interactions with the tyrosine ring of Sts-1. This likely is indicative of the differences between the native Sts-1 and Sts-2 substrates. The Sts proteins have been implicated in negatively regulating TCR signaling via the dephosphorylation of key signaling proteins downstream of the TCR.[2,6] One of the putative substrates of Sts-1 is the tyrosine kinase, Zap-70, while much less is known about the possible substrates of Sts-2.[2,6,17,30] Sts-2 also shows activity against Zap-70, albeit at a level much lower than that of Sts-1.[17] This, and other data, suggests that Sts-1 and Sts-2 have distinct regulatory roles. This is supported by the observations that knockout of both Sts-1 and Sts-2 induces a degree of hyperactivation of signaling pathways greater than that seen for the loss of either protein alone.[2,6,11] The lower phosphatase activity of Sts-2 for Zap-70 and the substrates tested here does raise the possibility that the primary function of Sts-2 arises from one of the other domains of the protein and that the phosphatase activity is evolutionarily redundant. Alternative roles for Sts-2, driven by the UBA and SH3 domain interactions, have been proposed. These include the inhibition of tyrosine kinase receptor endocytosis and the promotion of caspase-independent apoptosis, proposed to be mediated by interactions of UBA or SH3 with the E3 ubiquitin ligase/adaptor protein, Cbl, and with apoptosis-inducing factor, respectively.[29,31] Further study is required to identify the physiologically relevant phosphatase substrates or binding partners of Sts-2.

Inhibitors of Sts-1_{HP}. Beyond the observation that phosphate and several phosphate mimics can inhibit the histidine phosphatase activity of Sts-1 and Sts-2,[12,13] there have been no reports of small molecule inhibitors of the Sts proteins. To test the feasibility of inhibiting Sts-1 with a drug-like compound and to compare the inhibition profile with those of other phosphatases, we tested a number of known phosphatase inhibitors (Table 3 and Figure 4A). Of those tested, the alkaline

Table 3. Inhibition Constants

inhibitor	Sts-1_{HP} K_i (μM)
orthovanadate	4.61 ± 0.62
β-glycerophosphate	NI[a]
(−)-tetramisole	NI[a]
methyl-dephostatin	NI[a]
1-naphthyl phosphate	NI[a]
2-bromo-4-hydroxyacetophenone	NI[a]
PHPS1[b]	1.05 ± 0.15
sulfanilic acid	480 ± 55
sulfanilamide	NI[a]
SMP[c]	48.3 ± 5.61

[a]No observable inhibition. [b]4-{2-[1,5-Dihydro-3-(4-nitrophenyl)-5-oxo-1-phenyl-4*H*-pyrazol-4-ylidene]hydrazinyl}benzenesulfonic acid. [c]1-(4-Sulfophenyl)-3-methyl-5-pyrazolone.

phosphatase inhibitor tetramisole,[32,33] the Ser/Thr phosphatase inhibitor glycerophosphate, and the PTP-1B/SHPTP-1 inhibitor 3,4-methyl-dephostatin[34−36] did not show any observable level of inhibition of Sts-1_{HP} phosphatase activity. The Src homology-2-containing phosphatase (SHP2) inhibitor, PHPS1 (4-{2-[1,5-dihydro-3-(4-nitrophenyl)-5-oxo-1-phenyl-4*H*-pyrazol-4-ylidene]hydrazinyl}benzenesulfonic acid),[21] however, is a potent competitive inhibitor of Sts-1_{HP} with a K_i of 1 μM (Figure 4B and Table 3). The compound 1-(4-sulfophenyl)-3-methyl-5-pyrazolone (SMP), which is a precursor of PHPS1, also inhibits Sts-1_{HP} (K_i = 48 μM). In addition, the phosphotyrosine analogue, sulfanilic acid, was found to be a modest inhibitor. From these data, we can draw several important conclusions. The phosphatase activity of Sts-1 can clearly be modulated by small molecule inhibitors, and as expected, the inhibition profile is distinct from that of canonical protein tyrosine phosphates (PTPs). For example, PTP-1B is more potently inhibited by methyl-3,4-dephostatin (IC_{50} of 3.5 μM) than by PHPS1 (IC_{50} of 19 μM), whereas Sts-1 activity is not affected by methyl-3,4-dephostatin.[21,36,37] These data, taken together with the structure that reveals a distinct binding pocket in the active site (Figure 4C), suggest that Sts-1 is likely a druggable target. Further *in vivo* studies will need to be conducted, however, to validate this conclusion.

Zap-70 Dephosphorylation by Human Sts-1. The Sts proteins have been implicated in the control of T cell activity as negative regulators of TCR signaling.[2,6] Previous work on the mouse proteins demonstrated that Zap-70 is one of the protein substrates of Sts-1 and Sts-2.[6,17] Our studies, detailed herein, have revealed a significant degree of structural and functional similarity between the mouse and human proteins. To confirm

DOI: 10.1021/acs.biochem.7b00638
Biochemistry XXXX, XXX, XXX−XXX

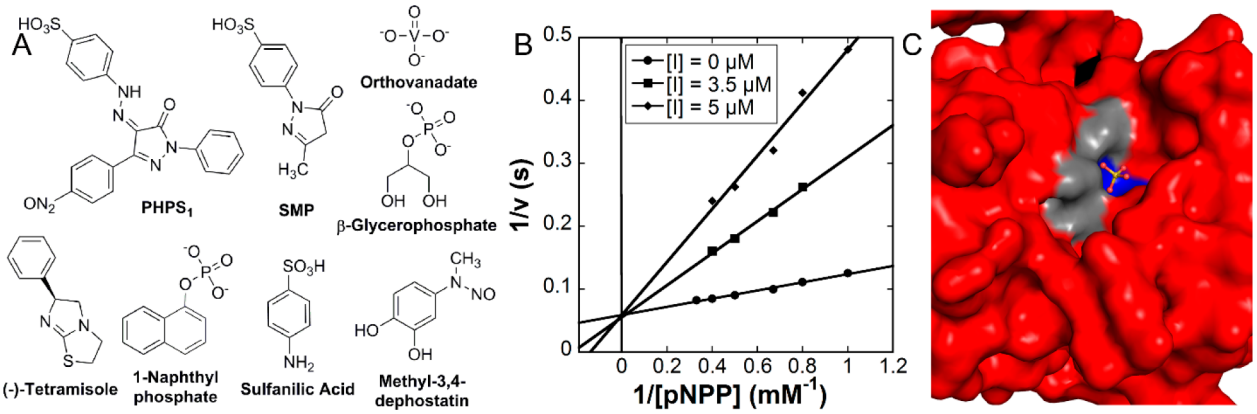

Figure 4. Inhibition of Sts-1_{HP}. A set of known phosphatase inhibitors (A) were screened for their capacity to inhibit the phosphatase activity of Sts-1_{HP}. The SHP-1 inhibitor, PHPS1, was shown to be a potent competitive inhibitor of Sts-1_{HP} (B, K_i of 1.05 ± 0.15 μM). Shown is a Lineweaver–Burk plot of the activity of Sts-1_{HP} (as measured by the pNPP assay) with three different concentrations of the inhibitor, PHPS1. Examination of the structure of Sts-1_{HP} shows that there is a clear binding cleft where the substrates and inhibitors bind (C, Sts-1_{HP} shown in surface representation colored red, conserved histidine residues colored blue, and conserved arginine residues colored gray).

that human Sts-1 also targets Zap-70 as a phosphatase substrate, we conducted an *in cellulo* assay measuring phosphorylation of Zap-70 in the presence and absence of Sts-1 (Figure 5). HEK-293 cells were cotransfected with T7-

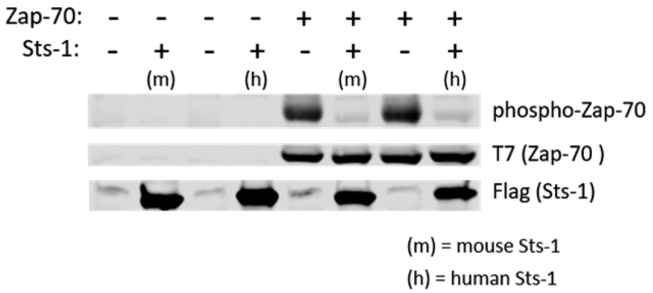

Figure 5. Human Sts-1_{HP} dephosphorylates Zap-70. Using a cell-based assay (see Materials and Methods), both mouse and human Sts-1_{HP} were tested for their ability to dephosphorylate the hyperphosphorylated substrate, Zap-70. In the absence of either Sts-1 protein, a dark band is seen for phosphorylated Zap-70 (phospho-Zap-70, top lane of the gel). When either mouse Sts-1 (m) or human Sts-1 (h) is also present in the cells, the amount of phosphorylated Zap-70 is significantly diminished without an effect on the overall expression level of the Zap-70 protein. This experiment was conducted in triplicate, and the blot shown is a representative example of these data.

tagged Zap-70, the cellular machinery to ensure Zap-70 phosphorylation [Lck and CD8-ζ chain chimera (see Materials and Methods)], and either murine or human Sts-1. In the absence of any Sts-1 protein, hyperphosphorylation of Zap-70 (Figure 5, phosphor-Zap-70) is observed as expected. When either the mouse or human Sts-1 protein is co-expressed, the amount of phosphorylated Zap-70 is reduced to nearly nil. These data verify not only that the purified proteins are structurally and functionally conserved but also that the human and mouse proteins behave similarly in cells. This further validates the mouse model as a viable surrogate for studies of human Sts-1.

In summary, this work details the first structural and functional characterization of the human Sts proteins. These proteins have recently been shown to have potential as targets for immune stimulation to treat deadly pathogen infections. The studies described illustrate that the phosphatase domain of human Sts-1 has a distinct active site pocket that can be potently inhibited by a competitive inhibitor with druglike properties.[21,38] This not only serves as a proof of principle that Sts-1 can be functionally inactivated by a small molecule drug but also may provide a scaffold from which to design more potent and selective Sts inhibitors. In addition, the structural and functional similarity of the mouse and human proteins underscores the utility of the mouse model for the discovery and characterization of inhibitors of the human protein. Comparison of the human Sts-1_{HP} and Sts-2_{HP} structures reveals a high degree of conservation but does show some subtle distinctions. These differences are likely the key determinants of substrate specificity and may be critical features for drug discovery if selective inhibition of one Sts protein is determined to be a requirement for biological efficacy. Overall, these data suggest that the Sts proteins are druggable, possess a well-defined binding pocket, and can bind to a known druglike molecule with high affinity. These distinct molecular features can be exploited for the development of specific and effective inhibitors of phosphatase activity. This work provides a foundation for drug discovery efforts and important tools for the structure-guided development of inhibitors of the Sts proteins.

■ ASSOCIATED CONTENT

Accession Codes

The coordinates of structures reported have been deposited in the Protein Data Bank as entries 5VR6, 5W5G, and 5WDI for structures of sulfate-bound Sts-1, unliganded Sts-1, and sulfate-bound Sts-2, respectively.

■ AUTHOR INFORMATION

Corresponding Authors

*Phone: 631-632-8015. E-mail: jarrod.french@stonybrook.edu.
*Phone: 631-632-4610. E-mail: nicholas.carpino@stonybrook.edu.

ORCID

Jarrod B. French: 0000-0002-6762-1309

Funding

This work was supported by Stony Brook University, the National Heart, Lung, and Blood Institute of the National Institutes of Health under Grant U01HL127522 (J.B.F. and

DOI: 10.1021/acs.biochem.7b00638
Biochemistry XXXX, XXX, XXX–XXX

N.C.), and the Office of the Assistant Secretary of Defense for Health Affairs through the Peer Reviewed Medical Research Program under Grant W81XWH17-1-0147 (J.B.F. and N.C.). Additional support was provided by the Center for Biotechnology, a New York State Center for Advanced Technology, Stony Brook University, Cold Spring Harbor Laboratory, Brookhaven National Laboratory, and the Feinstein Institute for Medical Research.

Notes

The authors declare no competing financial interest.

■ ACKNOWLEDGMENTS

This work is based upon research conducted at the Northeastern Collaborative Access Team beamlines, which are funded by the National Institute of General Medical Sciences from the National Institutes of Health (P41 GM103403). The Pilatus 6M detector on the 24-ID-C beamline is funded by a NIH-ORIP HEI grant (S10 RR029205). This research used resources of the Advanced Photon Source, a U.S. Department of Energy (DOE) Office of Science User Facility operated for the DOE Office of Science by Argonne National Laboratory under Contract DE-AC02-06CH11357.

■ REFERENCES

(1) Singer, A. L., and Koretzky, G. A. (2002) Control of T Cell Function by Positive and Negative Regulators. *Science 296*, 1639−1640.

(2) Carpino, N., Turner, S., Mekala, D., Takahashi, Y., Zang, H., Geiger, T. L., Doherty, P., and Ihle, J. N. (2004) Regulation of ZAP-70 Activation and TCR Signaling by Two Related Proteins, Sts-1 and Sts-2. *Immunity 20*, 37−46.

(3) Hicke, L., Schubert, H. L., and Hill, C. P. (2005) Ubiquitin-binding domains. *Nat. Rev. Mol. Cell Biol. 6*, 610−621.

(4) Musacchio, A. (2002) How SH3 domains recognize proline. *Adv. Protein Chem. 61*, 211−268.

(5) Tsygankov, A. Y. (2013) TULA-family proteins: a new class of cellular regulators. *J. Cell. Physiol. 228*, 43−49.

(6) Mikhailik, A., Ford, B., Keller, J., Chen, Y., Nassar, N., and Carpino, N. (2007) A phosphatase activity of Sts-1 contributes to the suppression of TCR signaling. *Mol. Cell 27*, 486−497.

(7) Carpino, N., Kobayashi, R., Zang, H., Takahashi, Y., Jou, S. T., Feng, J., Nakajima, H., and Ihle, J. N. (2002) Identification, cDNA cloning, and targeted deletion of p70, a novel, ubiquitously expressed SH3 domain-containing protein. *Molecular and cellular biology 22*, 7491−7500.

(8) Rigden, D. J. (2008) The histidine phosphatase superfamily: structure and function. *Biochem. J. 409*, 333−348.

(9) Chu, D. H., Morita, C. T., and Weiss, A. (1998) The Syk family of protein tyrosine kinases in T-cell activation and development. *Immunol. Rev. 165*, 167−180.

(10) Carpino, N., Chen, Y., Nassar, N., and Oh, H. W. (2009) The Sts proteins target tyrosine phosphorylated, ubiquitinated proteins within TCR signaling pathways. *Mol. Immunol. 46*, 3224−3231.

(11) Naseem, S., Frank, D., Konopka, J. B., and Carpino, N. (2015) Protection from systemic Candida albicans infection by inactivation of the Sts phosphatases. *Infect. Immun. 83*, 637−645.

(12) Chen, Y., Jakoncic, J., Carpino, N., and Nassar, N. (2009) Structural and functional characterization of the 2H-phosphatase domain of Sts-2 reveals an acid-dependent phosphatase activity. *Biochemistry 48*, 1681−1690.

(13) Chen, Y., Jakoncic, J., Parker, K. A., Carpino, N., and Nassar, N. (2009) Structures of the phosphorylated and VO(3)-bound 2H-phosphatase domain of Sts-2. *Biochemistry 48*, 8129−8135.

(14) Chen, Y., Jakoncic, J., Wang, J., Zheng, X., Carpino, N., and Nassar, N. (2008) Structural and functional characterization of the c-terminal domain of the ecdysteroid phosphate phosphatase from bombyx mori reveals a new enzymatic activity. *Biochemistry 47*, 12135−12145.

(15) Jakoncic, J., Sondgeroth, B., Carpino, N., and Nassar, N. (2010) The 1.35 A resolution structure of the phosphatase domain of the suppressor of T-cell receptor signaling protein in complex with sulfate. *Acta Crystallogr., Sect. F: Struct. Biol. Cryst. Commun. 66*, 643−647.

(16) Kleinman, H., Ford, B., Keller, J., Carpino, N., and Nassar, N. (2006) Crystallization and initial crystal characterization of the C-terminal phosphoglycerate mutase homology domain of Sts-1. *Acta Crystallogr., Sect. F: Struct. Biol. Cryst. Commun. 62*, 218−220.

(17) San Luis, B., Sondgeroth, B., Nassar, N., and Carpino, N. (2011) Sts-2 is a phosphatase that negatively regulates zeta-associated protein (ZAP)-70 and T cell receptor signaling pathways. *J. Biol. Chem. 286*, 15943−15954.

(18) Bond, C. S., White, M. F., and Hunter, W. N. (2001) High resolution structure of the phosphohistidine-activated form of Escherichia coli cofactor-dependent phosphoglycerate mutase. *J. Biol. Chem. 276*, 3247−3253.

(19) Bond, C. S., White, M. F., and Hunter, W. N. (2002) Mechanistic implications for Escherichia coli cofactor-dependent phosphoglycerate mutase based on the high-resolution crystal structure of a vanadate complex. *J. Mol. Biol. 316*, 1071−1081.

(20) Zheng, Q., Jiang, D., Zhang, W., Zhang, Q., Zhao, Q., Jin, J., Li, X., Yang, H., Bartlam, M., Shaw, N., Zhou, W., and Rao, Z. (2014) Mechanism of dephosphorylation of glucosyl-3-phosphoglycerate by a histidine phosphatase. *J. Biol. Chem. 289*, 21242−21251.

(21) Hellmuth, K., Grosskopf, S., Lum, C. T., Wurtele, M., Roder, N., von Kries, J. P., Rosario, M., Rademann, J., and Birchmeier, W. (2008) Specific inhibitors of the protein tyrosine phosphatase Shp2 identified by high-throughput docking. *Proc. Natl. Acad. Sci. U. S. A. 105*, 7275−7280.

(22) Otwinowski, Z., and Minor, W. (1997) Processing of X-ray diffraction data collected in oscillation mode. *Methods Enzymol. 276*, 307−326.

(23) Vagin, A., and Teplyakov, A. (2010) Molecular replacement with MOLREP. *Acta Crystallogr., Sect. D: Biol. Crystallogr. 66*, 22−25.

(24) Emsley, P., and Cowtan, K. (2004) Coot: model-building tools for molecular graphics. *Acta Crystallogr., Sect. D: Biol. Crystallogr. 60*, 2126−2132.

(25) Murshudov, G. N., Vagin, A. A., and Dodson, E. J. (1997) Refinement of macromolecular structures by the maximum-likelihood method. *Acta Crystallogr., Sect. D: Biol. Crystallogr. 53*, 240−255.

(26) Sergienko, E. A. (2013) Phosphatase high-throughput screening assay design and selection. *Methods Mol. Biol. 1053*, 7−25.

(27) Tautz, L., and Sergienko, E. A. (2013) High-throughput screening for protein tyrosine phosphatase activity modulators. *Methods Mol. Biol. 1053*, 223−240.

(28) Tierno, M. B., Johnston, P. A., Foster, C., Skoko, J. J., Shinde, S. N., Shun, T. Y., and Lazo, J. S. (2007) Development and optimization of high-throughput in vitro protein phosphatase screening assays. *Nat. Protoc. 2*, 1134−1144.

(29) Kowanetz, K., Crosetto, N., Haglund, K., Schmidt, M. H., Heldin, C. H., and Dikic, I. (2004) Suppressors of T-cell receptor signaling Sts-1 and Sts-2 bind to Cbl and inhibit endocytosis of receptor tyrosine kinases. *J. Biol. Chem. 279*, 32786−32795.

(30) San Luis, B., Nassar, N., and Carpino, N. (2013) New insights into the catalytic mechanism of histidine phosphatases revealed by a functionally essential arginine residue within the active site of the Sts phosphatases. *Biochem. J. 453*, 27−35.

(31) Collingwood, T. S., Smirnova, E. V., Bogush, M., Carpino, N., Annan, R. S., and Tsygankov, A. Y. (2007) T-cell ubiquitin ligand affects cell death through a functional interaction with apoptosis-inducing factor, a key factor of caspase-independent apoptosis. *J. Biol. Chem. 282*, 30920−30928.

(32) Fedde, K. N., Lane, C. C., and Whyte, M. P. (1988) Alkaline phosphatase is an ectoenzyme that acts on micromolar concentrations of natural substrates at physiologic pH in human osteosarcoma (SAOS-2) cells. *Arch. Biochem. Biophys. 264*, 400−409.

DOI: 10.1021/acs.biochem.7b00638
Biochemistry XXXX, XXX, XXX−XXX

(33) Hsu, H. H., Camacho, N. P., and Anderson, H. C. (1999) Further characterization of ATP-initiated calcification by matrix vesicles isolated from rachitic rat cartilage. Membrane perturbation by detergents and deposition of calcium pyrophosphate by rachitic matrix vesicles. *Biochim. Biophys. Acta, Biomembr. 1416*, 320−332.
(34) Fujiwara, S., Watanabe, T., Nagatsu, T., Gohda, J., Imoto, M., and Umezawa, K. (1997) Enhancement or induction of neurite formation by a protein tyrosine phosphatase inhibitor, 3,4-dephostatin, in growth factor-treated PC12h cells. *Biochem. Biophys. Res. Commun. 238*, 213−217.
(35) Umezawa, K. (1997) Induction of cellular differentiation and apoptosis by signal transduction inhibitors. *Adv. Enzyme Regul. 37*, 393−401.
(36) Umezawa, K., Kawakami, M., and Watanabe, T. (2003) Molecular design and biological activities of protein-tyrosine phosphatase inhibitors. *Pharmacol. Ther. 99*, 15−24.
(37) Barr, A. J. (2010) Protein tyrosine phosphatases as drug targets: strategies and challenges of inhibitor development. *Future Med. Chem. 2*, 1563−1576.
(38) Lipinski, C. A., Lombardo, F., Dominy, B. W., and Feeney, P. J. (2001) Experimental and computational approaches to estimate solubility and permeability in drug discovery and development settings. *Adv. Drug Delivery Rev. 46*, 3−26.
(39) Chen, V. B., Arendall, W. B., 3rd, Headd, J. J., Keedy, D. A., Immormino, R. M., Kapral, G. J., Murray, L. W., Richardson, J. S., and Richardson, D. C. (2010) MolProbity: all-atom structure validation for macromolecular crystallography. *Acta Crystallogr., Sect. D: Biol. Crystallogr. 66*, 12−21.

DOI: 10.1021/acs.biochem.7b00638
Biochemistry XXXX, XXX, XXX−XXX

APPENDIX 2

Published manuscript, Frank et al, 2018

AMERICAN SOCIETY FOR MICROBIOLOGY | mBio®

RESEARCH ARTICLE

Phagocytes from Mice Lacking the Sts Phosphatases Have an Enhanced Antifungal Response to *Candida albicans*

David Frank,[a,b] Shamoon Naseem,[b] Gian Luigi Russo,[b,c] Cindy Li,[b] Kaustubh Parashar,[b] James B. Konopka,[b] Nick Carpino[a,b]

[a]Program in Molecular and Cellular Pharmacology, Stony Brook University, Stony Brook, New York, USA

[b]Department of Molecular Genetics and Microbiology, Stony Brook University, Stony Brook, New York, USA

[c]Institute of Food Sciences, National Research Council, Avellino, Italy

ABSTRACT Mice lacking expression of the homologous phosphatases Sts-1 and Sts-2 ($Sts^{-/-}$ mice) are resistant to disseminated candidiasis caused by the fungal pathogen *Candida albicans*. To better understand the immunological mechanisms underlying the enhanced resistance of $Sts^{-/-}$ mice, we examined the kinetics of fungal clearance at early time points. In contrast to the rapid *C. albicans* growth seen in normal kidneys during the first 24 h postinfection, we observed a reduction in kidney fungal CFU within $Sts^{-/-}$ mice beginning at 12 to 18 h postinfection. This corresponds to the time period when large numbers of innate leukocytes enter the renal environment to counter the infection. Because phagocytes of the innate immune system are important for host protection against pathogenic fungi, we evaluated responses of bone marrow leukocytes. Relative to wild-type cells, $Sts^{-/-}$ marrow monocytes and bone marrow-derived dendritic cells (BMDCs) displayed a heightened ability to inhibit *C. albicans* growth *ex vivo*. This correlated with significantly enhanced production of reactive oxygen species (ROS) by $Sts^{-/-}$ BMDCs downstream of Dectin-1, a C-type lectin receptor that plays a critical role in stimulating host responses to fungi. We observed no visible differences in the responses of other antifungal effector pathways, including cytokine production and inflammasome activation, despite enhanced activation of the Syk tyrosine kinase downstream of Dectin-1 in $Sts^{-/-}$ cells. Our results highlight a novel mechanism regulating the immune response to fungal infections. Further understanding of this regulatory pathway could aid the development of therapeutic approaches to enhance protection against invasive candidiasis.

IMPORTANCE Systemic candidiasis caused by fungal *Candida* species is becoming an increasingly serious medical problem for which current treatment is inadequate. Recently, the Sts phosphatases were established as key regulators of the host antifungal immune response. In particular, genetic inactivation of Sts significantly enhanced survival of mice infected intravenously with *Candida albicans*. The $Sts^{-/-}$ *in vivo* resistance phenotype is associated with reduced fungal burden and an absence of inflammatory lesions. To understand the underlying mechanisms, we studied phagocyte responses. Here, we demonstrate that $Sts^{-/-}$ phagocytes have heightened responsiveness to *C. albicans* challenge relative to wild-type cells. Our data indicate the Sts proteins negatively regulate phagocyte activation via regulating selective elements of the Dectin-1–Syk tyrosine kinase signaling axis. These results suggest that phagocytes lacking Sts respond to fungal challenge more effectively and that this enhanced responsiveness partially underlies the profound resistance of $Sts^{-/-}$ mice to systemic fungal challenge.

KEYWORDS *Candida albicans*, cell signaling, effector functions, host-pathogen interactions, innate immunity

Received 10 April 2018 **Accepted** 20 June 2018 **Published** 17 July 2018

Citation Frank D, Naseem S, Russo GL, Li C, Parashar K, Konopka JB, Carpino N. 2018. Phagocytes from mice lacking the Sts phosphatases have an enhanced antifungal response to *Candida albicans*. mBio 9:e00782-18. https://doi.org/10.1128/mBio.00782-18.

Invited Editor Bruce Steven Klein, University of Wisconsin—Madison

Editor J. Andrew Alspaugh, Duke University Medical Center

Address correspondence to Nick Carpino, nicholas.carpino@stonybrook.edu.

In recent years, an increase in the numbers of invasive infections by fungal pathogens has raised concern (1). Of particular clinical concern are diverse *Candida* species, including *Candida albicans*. *C. albicans* is responsible for a number of infectious disorders, including oral candidiasis, chronic mucocutaneous candidiasis, and invasive candidiasis, a potentially lethal infection in which the fungus disseminates systemically and proliferates within internal tissues (2). *C. albicans* accounts for over 50,000 hospital-acquired systemic infections in the United States alone, with a 30% to 40% mortality rate associated with the invasive form of the disease (3, 4). Current antifungal medications used to treat systemic *C. albicans* infections have a number of drawbacks, including high cost, toxicity, and difficulties achieving appropriate bioavailability within infected tissues (1, 5). These limitations are compounded by difficulties in making a rapid and accurate disease diagnosis (6). In addition, the emergence of drug-resistant *Candida* strains is now considered a major threat by the CDC (7, 8).

Phagocytes of the innate immune system play a critical role in the immune response to *C. albicans* (9). Fungal cell wall constituents are recognized by cell-surface Toll-like receptors (TLRs) and C-type lectin receptors (CLRs), promoting the activation of cellular antimicrobial effector pathways (10). However, excessive inflammatory responses that occur in the context of fungal infections can also be counterproductive and lead to detrimental collateral tissue damage (11, 12). For example, in a mouse model of systemic candidiasis, progressive sepsis caused by a vigorous inflammatory response has been identified as the cause of death (13). In this context, it has been observed that reducing inflammation by reducing levels of proinflammatory factors can lead to improved host survival (14, 15). Optimizing clinical outcomes to *C. albicans* infection will require a more complete understanding of the biochemical mechanisms that underlie leukocyte antifungal inflammatory responses.

We recently reported that two homologous phosphatases, Sts-1 and Sts-2, play key roles in regulating the host response to systemic *C. albicans* infection (16). The Sts enzymes share overlapping and redundant functions as negative regulators of hematopoietic signaling pathways (17–19). They have a distinctive structure consisting of two protein interaction domains (UBA and SH3) and a C-terminal 2H-phosphatase domain that is structurally and enzymatically very distinct from those of other intracellular protein phosphatases known to regulate immune signaling pathways (20). Within hematopoietic cell populations, Sts-1 has been shown to negatively regulate signaling downstream of the TCR by targeting the Zap-70 kinase (17) and both GPVI-FcRγ signaling in platelets and FcεRI signaling in mast cells by targeting the Zap-70 homologue Syk (21, 22).

Sts$^{-/-}$ mice are profoundly resistant to disseminated candidiasis caused by supralethal inoculums, displaying significantly enhanced survival and an ability to clear the infection (16). To define the mechanisms underlying the enhanced resistance of Sts$^{-/-}$ mice, we investigated the role of Sts$^{-/-}$ leukocytes. Our results demonstrate that bone marrow-derived dendritic cells (BMDCs) lacking Sts expression have an enhanced ability to inhibit *C. albicans* growth and may contribute significantly to the resistance of Sts$^{-/-}$ mice. Further, we demonstrate that, within BMDCs, the Sts phosphatases negatively regulate the activation of select pathways downstream of the key fungal pathogen pattern recognition receptor Dectin-1. These observations define a novel role for Sts in regulating host antimicrobial effector responses and provide mechanistic insights into the ability of Sts$^{-/-}$ mice to resist lethal systemic *C. albicans* infection.

RESULTS

Inhibition of *C. albicans* growth within 24 h in Sts$^{-/-}$ mice. In the mouse model of invasive candidiasis, the kidneys are the predominant niche for *C. albicans* proliferation (23). Fungal germination is evident within 2 h postinfection, and kidney fungal CFU levels increase by 2 orders of magnitude over the course of 48 h (24, 25). Previous studies showed that Sts$^{-/-}$ mice exhibit a significantly lower kidney fungal burden that is especially evident by 48 h postinfection (16). To determine more precisely when levels of wild-type and Sts$^{-/-}$ kidney fungal CFU begin to diverge, we compared the

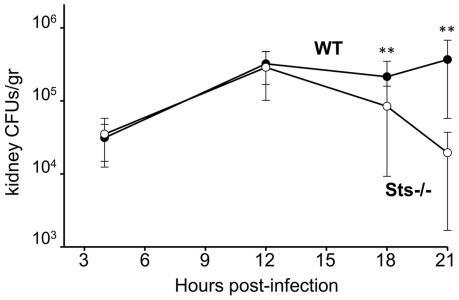

FIG 1 Reduced fungal CFU in Sts$^{-/-}$ kidneys at early time points postinfection. Kidneys from mice infected with 2.5×10^5 CFU were assessed for fungal burden prior to 24 h. Results represent averages of 2 to 3 independent experiments each carried out with 5 to 6 mice per group. **, $P < 0.001$ (by Mann-Whitney analysis) (error bars = standard deviations [SD] of means). WT, wild type.

fungal loads in wild-type and Sts$^{-/-}$ kidneys at early time points. Figure 1 illustrates that *C. albicans* within wild-type and Sts$^{-/-}$ kidneys proliferates at similar levels in the first 12 h following infection. However, while fungal CFU levels continue to increase after 12 h in wild-type kidneys, they begin to decrease in Sts$^{-/-}$ kidneys at between 12 and 18 h (Fig. 1). In this timeframe, similar numbers of leukocytes in wild-type and Sts$^{-/-}$ mice have entered the kidneys (16). These data indicate that within 12 to 18 h postinfection, mice lacking the Sts proteins are more effective than wild-type mice at inhibiting fungal growth and eliminating *C. albicans* cells from the kidney.

Hematopoietic stem cell (HSC)-derived cells contribute to the enhanced resistance of Sts$^{-/-}$ mice. Having established that enhanced kidney fungal restriction in Sts$^{-/-}$ animals becomes evident during the time period when bone marrow leukocyte populations begin to enter the renal compartment, we next determined if Sts$^{-/-}$ hematopoietic cells played a role. Transplantation of Sts$^{-/-}$ donor marrow into irradiated wild-type or Sts$^{-/-}$ recipients enhanced survival of *Candida* infection relative to the results seen with wild-type donor cells (Fig. 2A). Additionally, irradiated wild-type and Sts$^{-/-}$ mice reconstituted with Sts$^{-/-}$ bone marrow displayed a significant reduction in the 24-h fungal burden relative to mice receiving wild-type bone marrow (Fig. 2B). We also noted that Sts$^{-/-}$ recipients displayed improved survival relative to wild-type recipients given equivalent amounts of donor marrow (Fig. 2A), suggesting that a nonhematopoietic component also contributes to the increased survival of Sts$^{-/-}$ animals. To address whether phagocytic cells play a critical role in the Sts$^{-/-}$ resistance phenotype, we evaluated the 24-h fungal burden in mice that had been administered the phagocyte-depleting agent clodronate 24 h prior to infection (26). As expected, clodronate treatment led to higher fungal burdens. Noticeably, however, it also eliminated the 24-h fungal clearance advantage normally associated with Sts$^{-/-}$ animals (Fig. 2C). Together, these data suggest that the hematopoietic cell compartment makes an important contribution to the enhanced resistance of Sts$^{-/-}$ mice.

Enhanced candidacidal activity of Sts$^{-/-}$ leukocytes *ex vivo*. The regulatory role of the Sts proteins in innate leukocyte populations has not been explored. Both Sts-1 and Sts-2 are expressed by marrow cells at levels comparable to those within peripheral blood leukocytes and splenic cells (see Fig. S1A in the supplemental material). Therefore, we utilized an *in vitro* cell/fungal coculture assay to examine directly the interaction of bone marrow cells with fungal cells *ex vivo* (27). Marrow cells isolated from uninfected wild-type and Sts$^{-/-}$ mice were placed in culture and incubated with *C. albicans cph1*Δ *efg1*Δ cells. The *cph1*Δ *efg1*Δ mutant was used because it fails to undergo hyphal growth (28), thereby facilitating accurate quantification of fungal growth. After 24 h, we recovered equivalent CFU levels in cocultures containing untreated wild-type or Sts$^{-/-}$ marrow cells (Fig. 3A). In the presence of the immune cell activator phorbol myristate acetate (PMA), fewer fungal CFU were obtained (Fig. 3A). Significantly, PMA-treated Sts$^{-/-}$ marrow cells were more efficient at inhibiting fungal growth than treated wild-type marrow cells (Fig. 3A). This suggests that the antifungal

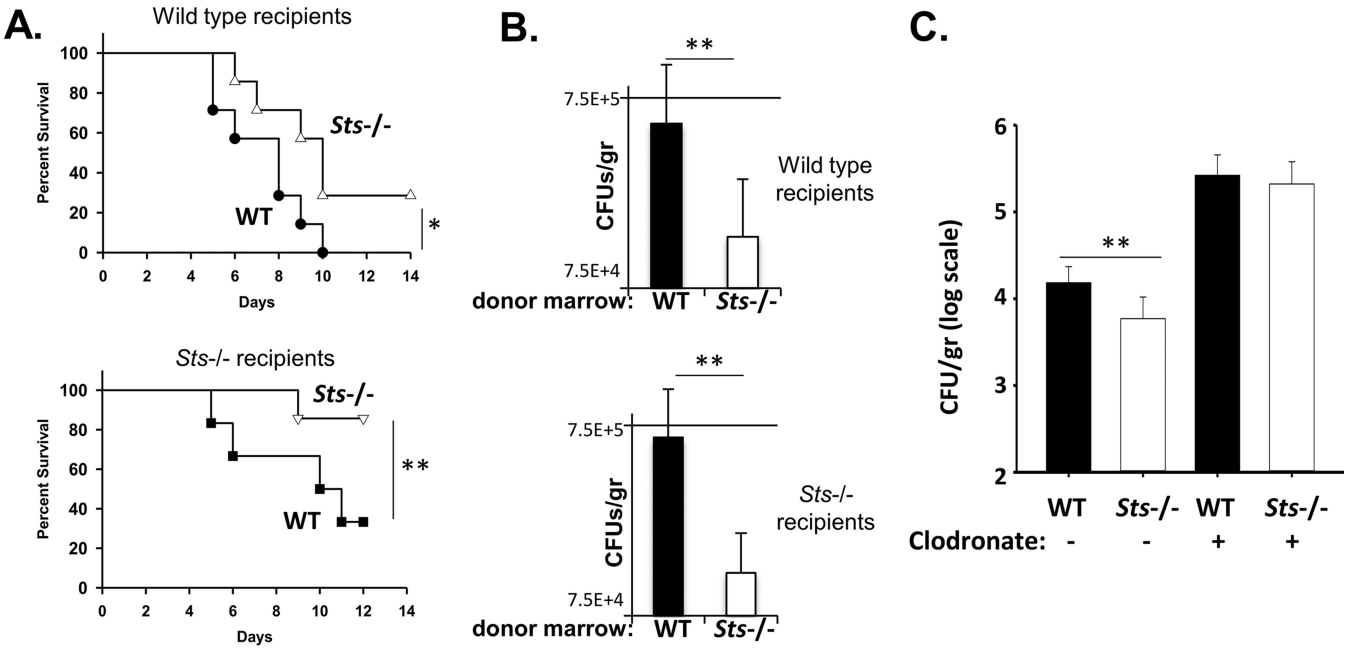

FIG 2 Contribution of Sts$^{-/-}$ hematopoietic stem cell (HSC)-derived cells to the heightened resistance of Sts$^{-/-}$ mice. (A) Radiation chimeras were infected with *C. albicans* (2.5×10^5 CFU) by bloodstream inoculation and monitored for 28 days. Wild-type (top) or Sts$^{-/-}$ (bottom) recipients receiving Sts$^{-/-}$ marrow demonstrated significantly enhanced survival, as indicated. *, $P < 0.05$ (by log rank analysis). (B) Radiation chimeras were infected with *C. albicans* (2.5×10^5 CFU) by bloodstream inoculation, and kidney CFU levels at 24 h postinfection were evaluated. Wild-type (top) or Sts$^{-/-}$ (bottom) recipients receiving Sts$^{-/-}$ marrow demonstrated significantly reduced 24-h kidney fungal CFU levels relative to mice receiving wild-type marrow. **, $P < 0.01$ (by Mann-Whitney analysis) (error bars = SD of means). (C) Mice treated with control liposomes (−) or a clodronate/liposome formulation (+) were infected 24 h later with 10^5 *C. albicans* cells. Sts$^{-/-}$ mice treated with clodronate failed to display enhanced fungal restriction in the kidney 24 h postinfection.

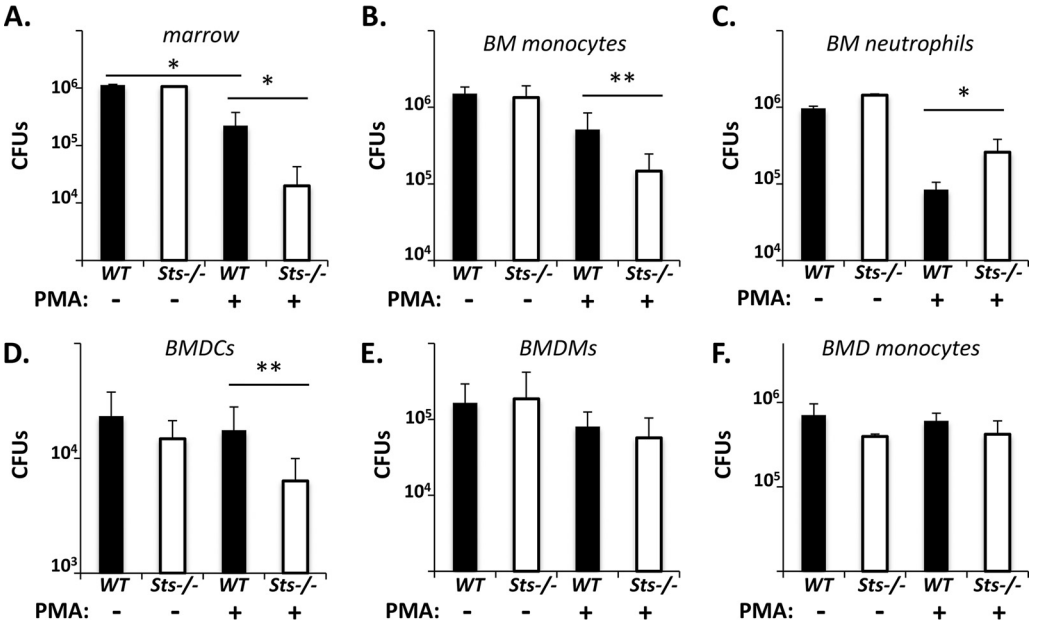

FIG 3 Increased antifungal activity of Sts$^{-/-}$ phagocytes *ex vivo*. (A) Nonfilamentous *C. albicans cph1*Δ *efg1*Δ cells were coincubated with untreated or PMA-treated bone marrow cells, and fungal CFU levels were determined after 24 h. Representative results of 3 experiments performed in triplicate are displayed. (B to F) Purified (B) bone marrow monocytes, (C) bone marrow neutrophils, (D) *ex vivo*-derived BMDCs, (E) BMDMs, or (F) BMD monocytes were cultured for 24 h with fungal cells, and CFU levels were enumerated as described for panel A. Results depict the average CFU of 3 experiments performed in triplicate. **, $P < 0.01$; *, $P < 0.05$ (by Mann-Whitney analysis) (error bars = SD of means).

properties of PMA-treated bone marrow cells are potentiated in the absence of Sts expression.

Marrow cell types associated with the initial innate immune response to systemic *C. albicans* infection include neutrophils and monocytes (29–31). Sts-1 and Sts-2 were found to be highly expressed in both cell populations (Fig. S1B and C [for cell purity data, see Fig. S2]). In order to examine the role of Sts in the antifungal responses of bone marrow monocytes and neutrophils, cells were purified from preparations of murine marrow. $Sts^{-/-}$ marrow monocytes exhibited 10-fold-greater inhibition of fungal growth than the corresponding wild-type cultures (Fig. 3B). As in the case of total bone marrow cell coculture, the increased fungal-growth-inhibitory properties displayed by $Sts^{-/-}$ monocytes was evident only when cells were pretreated with PMA. In contrast to marrow monocytes, PMA-treated neutrophils lacking Sts expression were less efficient at inhibiting fungal growth than wild-type neutrophils, although both were better at inhibiting fungal growth than untreated cells (Fig. 3C). We also examined the different phagocyte populations that can be obtained by culturing bone marrow *ex vivo* in the presence of different cytokines. These include bone marrow-derived dendritic cells (BMDCs) (32), bone marrow-derived macrophages (BMDMs) (33), and bone marrow-derived monocytes (BMD monocytes) (34) (see Fig. S1D to F). Similarly to bone marrow cells and marrow monocytes, $Sts^{-/-}$ BMDCs exhibited a significantly greater ability to restrict *C. albicans* growth *ex vivo* than wild-type BMDCs (Fig. 3D). In contrast, no differences were observed in the growth-inhibitory properties of wild-type and $Sts^{-/-}$ BMDMs and BMD monocytes (Fig. 3E and F). Cumulatively, our results suggest that the Sts proteins play a negative role in regulating antifungal properties of select phagocyte populations.

Increased *Candida*-induced ROS production in cells lacking Sts expression. Because $Sts^{-/-}$ BMDCs displayed enhanced fungal growth suppression *ex vivo* (Fig. 3D), we next investigated their antifungal effector functions. Members of the C-type lectin receptor (CLR) superfamily, including Dectin-1, are among the surface receptors engaged by fungal cells (35, 36). We stimulated cells with zymosan, a crude preparation of yeast cell wall extract that engages antifungal TLRs and CLRs, and observed a significantly greater zymosan-induced reactive oxygen species (ROS) response in $Sts^{-/-}$ BMDC cultures than in wild-type BMDCs. In particular, both the rate of ROS production and the peak ROS signal were significantly enhanced in cells lacking Sts (Fig. 4A, left). We then evaluated the ROS response of BMDCs treated with *C. albicans* cells. After addition of either live or heat-killed (HK) *C. albicans* to BMDC cultures, production of ROS became evident, although the onset of the ROS response was delayed relative to cells treated with zymosan (Fig. 4A, middle and right panels). Similarly to the response seen following zymosan treatment, ROS production by $Sts^{-/-}$ BMDCs following challenge with fungal cells was significantly augmented relative to the ROS response of wild-type BMDCs. In contrast to BMDCs, wild-type and $Sts^{-/-}$ neutrophils (Fig. 4B) and BMD monocytes (Fig. S3A) did not display any differences in fungus-induced ROS production, while BMDMs of both genotypes did not generate a fungus-induced ROS response (Fig. S3B). Stimulation of BMDCs with heat-killed *C. albicans cph1*Δ *efg1*Δ cells also produced a heightened ROS response in $Sts^{-/-}$ cells relative to wild-type cells (Fig. S4). Together, our data indicate that the Sts proteins negatively regulate the activation of fungus-induced ROS production in BMDCs.

In addition to ROS production, fungus-stimulated phagocytes produce diverse proinflammatory cytokines, including tumor necrosis factor alpha (TNF-α), interleukin-6 (IL-6), and IL-1β (37). In the case of the latter, activation of the NLRP3 inflammasome downstream of the fungal receptor Dectin-1 results in upregulation of IL-1β secretion (38). In contrast to the differential ROS responses observed between wild-type and $Sts^{-/-}$ BMDCs, we detected no differences in the production of TNF-α, IL-6, or IL-1β by cells lacking Sts expression relative to wild-type cells (Fig. 4C to E). Additionally, wild-type and $Sts^{-/-}$ cells upregulated Nos2 expression to similar extents following stimulation, resulting in identical levels of NO production (Fig. 4F and G). These results

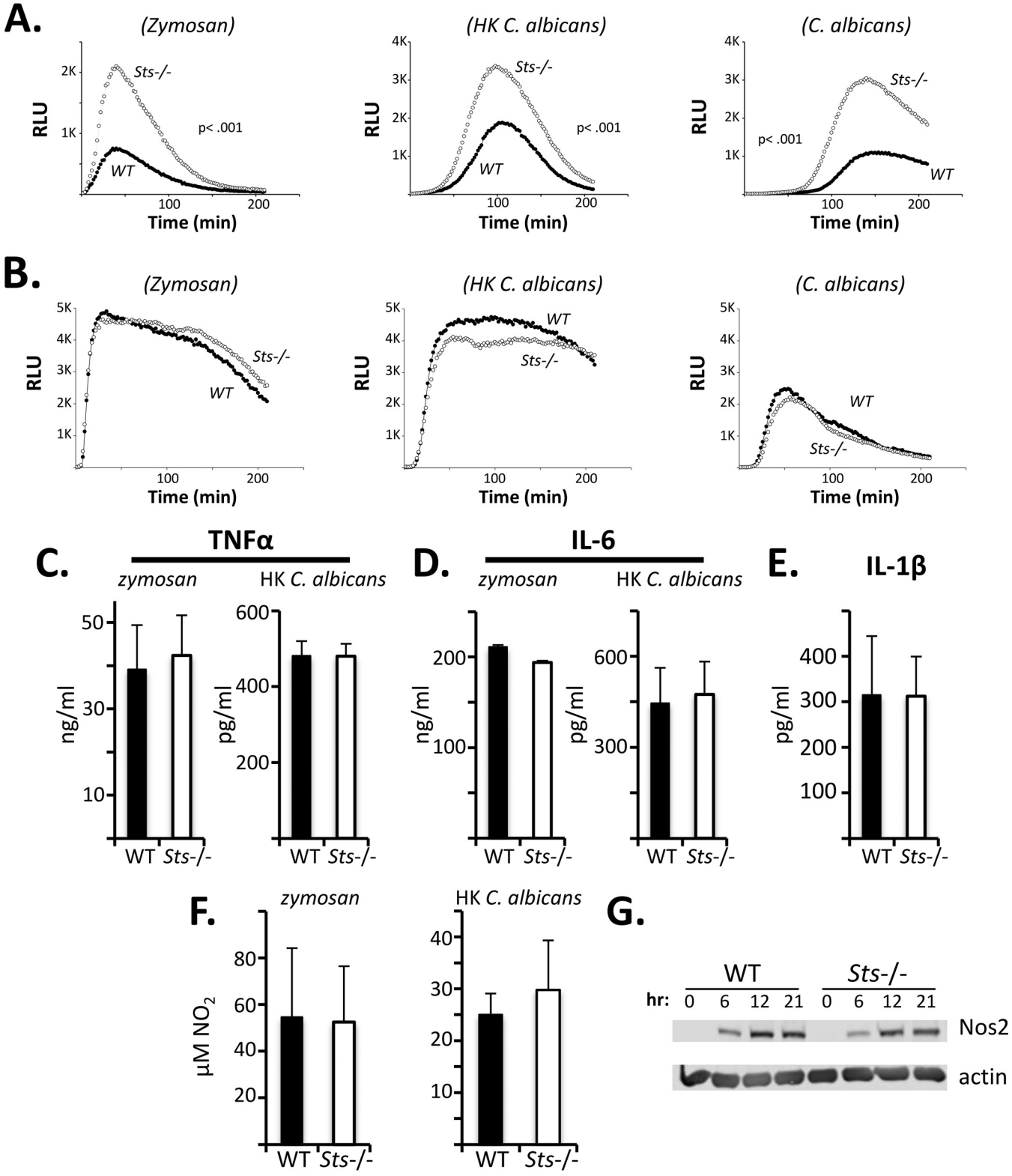

FIG 4 Increased *Candida*-induced ROS production in Sts$^{-/-}$ BMDCs. (A) Wild-type and Sts$^{-/-}$ BMDCs were stimulated with zymosan, heat-killed (HK) *C. albicans*, or live *C. albicans* as indicated, and levels of ROS production were assessed by luminol chemiluminescence. Average results of at least three separate experiments each conducted in triplicate are displayed. *P* values for the areas under each curve were calculated by Mann-Whitney analysis. RLU, relative light units. (B) Wild-type and Sts$^{-/-}$ neutrophils were stimulated as described for panel A and levels of ROS production assessed. (C) Equivalent levels of TNF-α in wild-type and Sts$^{-/-}$ BMDC culture supernatants stimulated with zymosan or HK *C. albicans* for 24 h, as indicated. Combined results of at least three separate experiments each conducted in duplicate are displayed. (D) Equivalent levels of IL-6 in wild-type and Sts$^{-/-}$ BMDC culture supernatants stimulated with zymosan or HK *C. albicans* for 24 h, as indicated. Representative (zymosan) or combined (HK *C. albicans*) results of at least three separate experiments each

(Continued on next page)

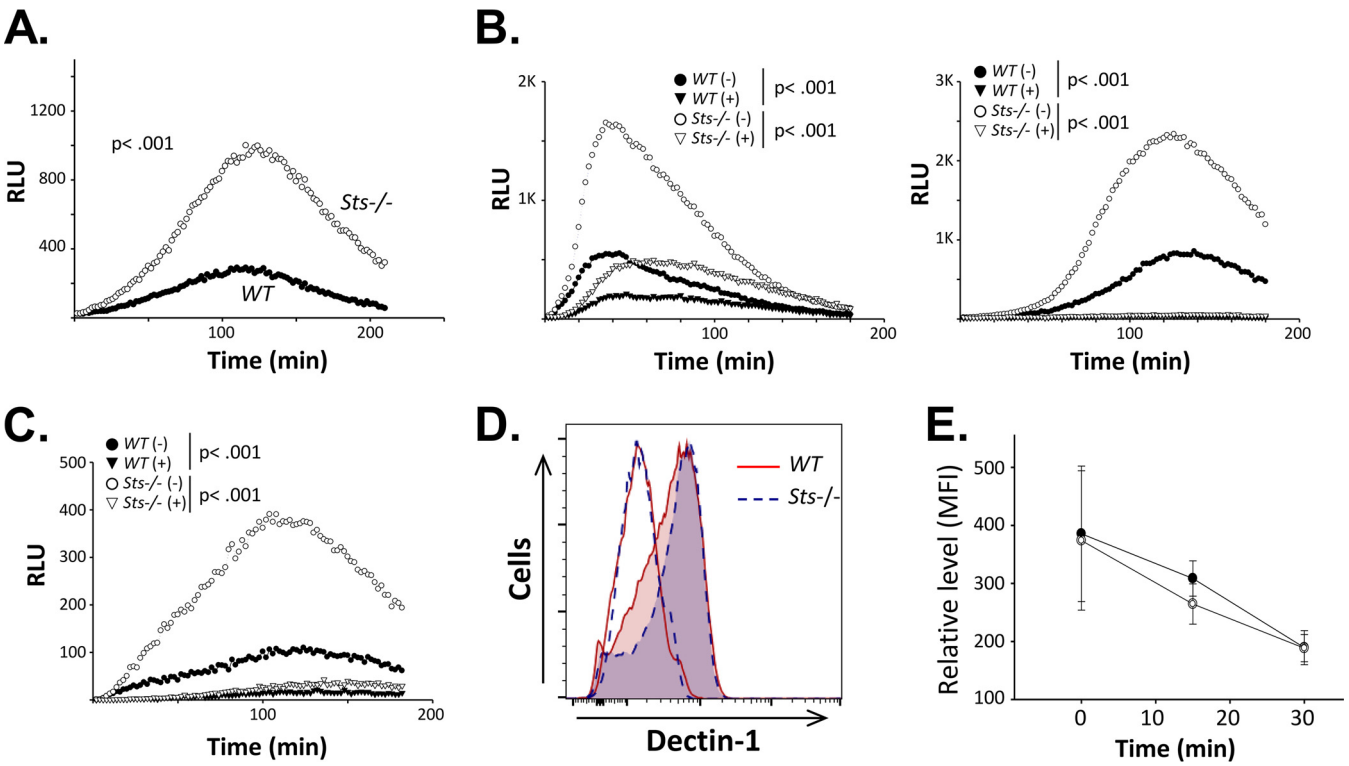

FIG 5 Sts regulates ROS production downstream of fungal CLR Dectin-1. (A) Wild-type and Sts$^{-/-}$ BMDCs were stimulated with particulate β-glucan, and then levels of ROS production were assessed by luminol chemiluminescence. (B) Zymosan-induced (left) or HK (heat-killed) wild-type *C. albicans*-induced (right) ROS production in wild-type and Sts$^{-/-}$ BMDCs was assessed in the absence (−) or presence (+) of soluble β-glucan, a specific inhibitor that blocks activation of Dectin-1 signaling pathways (46). (C) ROS production in wild-type and Sts$^{-/-}$ BMDCs was assessed in the absence (−) or presence (+) of a blocking anti-Dectin-1 antibody. (D) Equivalent levels of surface Dectin-1 receptor expressed on wild-type BMDCs (solid red line) and Sts$^{-/-}$ BMDCs (dotted dark blue line), evaluated by flow cytometry with a specific anti-Dectin-1 antibody. Nonshaded lines represent a nonspecific rat IgG control. (E) Equivalent levels of zymosan stimulation-dependent downregulation of surface Dectin-1 on wild-type (closed dot) and Sts$^{-/-}$ (open dot) BMDCs. MFI, mean fluorescence intensity. For panels A to C, average values from at least 3 independent experiments each performed in triplicate are presented. *P* values were calculated by Mann-Whitney analysis.

suggest that the Sts proteins regulate a subset of phagocyte antifungal effector functions that includes the production of reactive oxygen species.

Sts regulates ROS production downstream of fungal receptor Dectin-1. Dectin-1 is a CLR that is stimulated by *C. albicans* and mediates activation of numerous downstream pathways (39, 40). Among the ligands that stimulate Dectin-1 are polymeric forms of β-glucan that are components of fungal cell walls (10). To investigate the involvement of Dectin-1, we treated BMDCs with purified particulate β-1,3 glucan polymers and found that Sts$^{-/-}$ BMDCs demonstrated significantly increased ROS production relative to wild-type cells (Fig. 5A). Unlike polymeric β-glucan, soluble monomeric β-glucan acts in a competitive inhibitory fashion and blocks access to the Dectin-1 ligand-binding surface (41). After addition of soluble β-glucan to BMDC cocultures, the enhanced ROS response of Sts$^{-/-}$ cells following zymosan or HK *C. albicans* stimulation was inhibited (Fig. 5B). The elevated ROS response of Sts$^{-/-}$ BMDCs was also abrogated following addition of a blocking anti-Dectin-1 antibody to cocultures but not following addition of a control antibody (Fig. 5C). Importantly, we noted no difference in levels of surface expression of Dectin-1 on wild-type and Sts$^{-/-}$ BMDCs (Fig. 5D). Similarly, no differences in the stimulation-dependent downregulation of Dectin-1 from the cell surface were observed (Fig. 5E). These results suggest that the

FIG 4 Legend (Continued)
conducted in duplicate are displayed. (E) Equivalent levels of IL-1β in wild-type and Sts$^{-/-}$ BMDC culture supernatants stimulated for 24 h with 100 μg/ml zymosan. (F) Equivalent levels of nitrite, representative of NO production, in wild-type and Sts$^{-/-}$ BMDC culture supernatants stimulated with zymosan (left) or HK *C. albicans* (right) for 24 h. Combined results of at least three separate experiments each conducted in duplicate are displayed. (G) Induction of Nos2 in zymosan-stimulated BMDCs. Representative results of two separate experiments are displayed. (Error bars for panels C to F = SD of means).

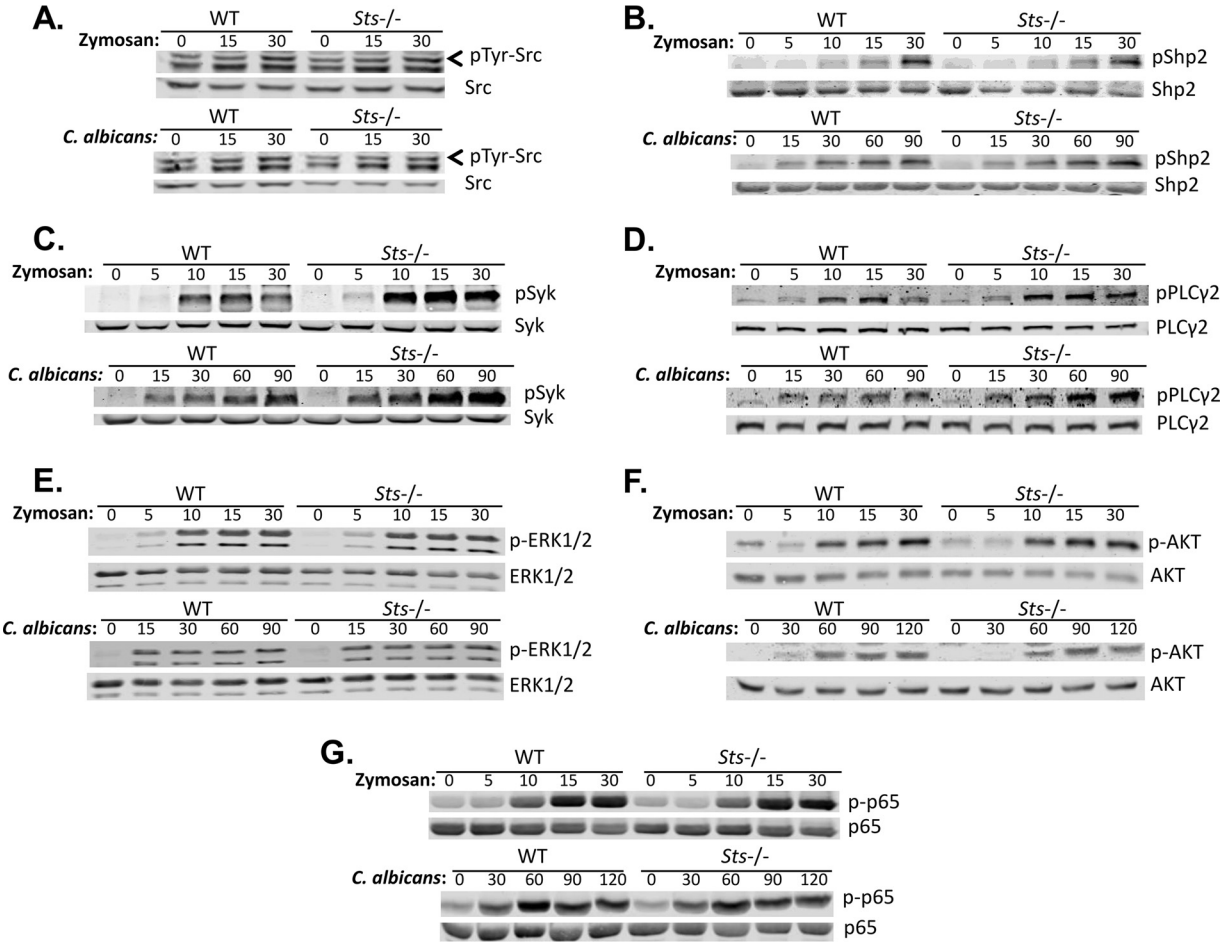

FIG 6 Increased activation of Syk and PLCγ2 downstream of Dectin-1. Wild-type or Sts$^{-/-}$ BMDCs were stimulated with either zymosan or live *C. albicans* (MOI of 0.5) for the indicated times, and levels of activation of (A) Src kinases; (B) Shp2 phosphatase; (C) Syk; (D) PLCγ2; (E) ERK1/2; (F) Akt; and (G) p65 NF-κB were determined with phosphospecific antibodies. Representative results from 3 independent experiments for each stimulation are displayed. Results for Syk and PLCγ2 were quantified and analyzed for statistical significance (see Fig. S5).

Sts proteins act downstream of Dectin-1 to negatively regulate activation of the fungus-induced ROS response.

Sts regulates levels of Syk activation induced by *C. albicans*. Among the first known biochemical events following Dectin-1 stimulation are upregulation of Src family member kinase activity and phosphorylation of Shp2 phosphatase (42, 43). Spleen tyrosine kinase (Syk), a nonreceptor protein kinase that is highly expressed in a variety of phagocytes, is then activated (44). We examined activation levels of Src family kinases in stimulated wild-type and Sts$^{-/-}$ cells using a phosphospecific antibody. No differences were observed in the levels of Src kinase activation following stimulation of BMDCs with zymosan or wild-type *C. albicans*. (Fig. 6A). Further, no differences between stimulated wild-type and Sts$^{-/-}$ cells in Shp2 phosphorylation levels were noted (Fig. 6B). In contrast, stimulation of wild-type and Sts$^{-/-}$ cells with either zymosan or *C. albicans* resulted in enhanced Syk tyrosine phosphorylation in Sts$^{-/-}$ cells (Fig. 6C; quantified in Fig. S5A). These observations suggest that the Sts phosphatases regulate Dectin-1 signaling at the level of Syk phosphorylation.

Engagement of Dectin-1 by fungus-associated ligands leads to activation of a number of intracellular signaling pathways. To investigate pathways downstream of Syk in Sts$^{-/-}$ phagocytes, we examined activation of PLCγ2, a downstream substrate of Syk (40). PLCγ2 was found to be hyperphosphorylated in stimulated Sts$^{-/-}$ BMDCs relative to wild-type cells (Fig. 6D; quantified in Fig. S5B). We also examined the activation of extracellular signal-regulated kinase-1/2 (ERK1/2) and phosphatidylinositol

3-kinase (PI3K), signaling molecules that play critical roles in transcriptional activation downstream of C-type lectin receptors. No differences were observed in the kinetics or extent of ERK1/2 activation (Fig. 6E), or in PI3K activation, as indicated by the kinetics and extent of Akt phosphorylation (Fig. 6F). Finally, levels of activation of p65 NF-κB in wild-type and Sts$^{-/-}$ cells following stimulation with either zymosan or *C. albicans* were identical (Fig. 6G). These results suggest that the Sts proteins could regulate a specific Syk-PLCγ2-ROS signaling axis downstream of Dectin-1 that is independent of the pathways regulating Dectin-1/Syk-induced cytokine gene expression.

DISCUSSION

Combination therapy that pairs the use of traditional antibiotics with agents to enhance beneficial host immune responses is considered an important therapeutic goal for the treatment of intractable infections and of those for which antibiotic resistance is a looming concern (11, 12). Interestingly, genetic inactivation of the Sts proteins dramatically improves host survival following lethal doses of intravenous *C. albicans*, suggesting that they are possible targets to enhance host antifungal immunity. Importantly, the resistance of Sts$^{-/-}$ mice is accompanied by rapid fungal clearance within the kidney, sharply decreased levels of inflammatory molecules, and an absence of inflammatory lesions. While our previous analysis revealed key differences in the immunological responses of wild-type versus Sts$^{-/-}$ mice (16), it did not provide mechanistic insights into how Sts inactivation alters immune responses and increases protection from systemic infection. In this study, therefore, we sought to identify underlying cellular and molecular components of the enhanced antifungal immune response displayed by Sts$^{-/-}$ mice.

Increased resistance to systemic *C. albicans* is mediated by Sts$^{-/-}$ leukocytes. Comparative analyses of fungal clearance within infected mice provided an important clue into underlying mechanisms. Critically, *C. albicans* grew similarly in wild-type and Sts$^{-/-}$ kidneys during the first 12 h postinfection. As kidney-resident phagocytes represent the primary innate immune cell population within uninfected kidneys (45), this observation suggests that the initial responses of resident phagocytes do not account for the differential abilities of wild-type and Sts$^{-/-}$ mice to control the infection. However, levels of fungal CFU within infected kidneys begin to differ between 12 and 18 h postinfection (Fig. 1), with Sts$^{-/-}$ CFU beginning to decline at a time when large numbers of leukocytes enter the renal compartment to counteract the infection (23, 31). This suggests that a key contribution is made by Sts$^{-/-}$ bone marrow-derived leukocytes, a hypothesis that is supported by our radiation chimera studies in which animals reconstituted with Sts$^{-/-}$ marrow had improved fungal clearance and enhanced survival relative to animals receiving wild-type marrow (Fig. 2). *Ex vivo* coculture analysis also demonstrated increased fungal growth suppression associated with Sts$^{-/-}$ phagocytes (Fig. 3). Together, these observations suggest that the Sts phosphatases negatively regulate intrinsic antifungal responses within key leukocyte populations.

Increased ROS production downstream of Dectin-1–Syk signaling in Sts$^{-/-}$ cells. After stimulating BMDCs with fungal ligands, we observed significantly heightened ROS production in Sts$^{-/-}$ cells but no differences in other antifungal responses such as cytokine production or generation of nitric oxide (Fig. 4). ROS production is known to be induced following engagement of the CLR Dectin-1 (46), and we confirmed the involvement of Dectin-1 using both a competitive inhibitor and blocking antibodies. While the signaling pathway from Dectin-1 to initiation of the ROS response has not been fully elucidated, one established component is the Syk kinase (38, 44, 47). Using a phosphospecific antibody that recognizes the tyrosine phosphorylated activation loop of Syk, we observed hyperphosphorylation of Syk in Sts$^{-/-}$ BMDCs following stimulation with zymosan or infection with *C. albicans* (Fig. 6). Under these conditions, there was no evidence of increased activation of upstream components such as Src kinases or Shp2. Therefore, our data suggest that Sts regulates signaling events downstream of Dectin-1 at the level of Syk phosphorylation and activation, perhaps by

direct dephosphorylation of Syk. The idea of a role for Sts in regulating Syk activity in BMDCs is supported by studies in other cell types that demonstrated that Syk is a Sts target (19, 21, 22).

Further evidence for heightened Syk kinase activity in Sts$^{-/-}$ BMDCs lies in the observation that PLCγ2, a putative Syk substrate, displays increased phosphorylation following stimulation of the Dectin-1 pathway. Interestingly, we did not observe any differences in the levels of activation of the mitogen-activated protein kinase (MAPK) and PI3K pathways, two signaling pathways also thought to be downstream of Syk (48). We also observed no differences between wild-type and Sts$^{-/-}$ cells in production of TNF-α, IL-6, and IL-1β, which are three cytokines that have been shown to lie downstream of the location of Syk activation (47). Together, these data highlight complexity in the regulation of Syk signaling that heretofore has not been described. In particular, the distinct effects on downstream effector pathways in Sts$^{-/-}$ cells suggest that Syk-mediated activation of downstream pathway components occurs in a differentially regulated manner. Whether this involves interaction of activated Syk with multiple distinct regulatory factors or differential subcellular localization of activated Syk is currently unclear. How Sts deficiency and increased Syk activation together lead selectively to increased ROS production is currently being investigated.

Cell-specific regulation of antifungal responses by Sts. Interestingly, our *ex vivo* analysis data suggest that Sts regulates leukocytes in a cell-specific manner. In particular, while Sts$^{-/-}$ BMDCs displayed increased candidacidal activity, BM-derived macrophages and BM-derived monocytes were unaffected by Sts inactivation. Furthermore, although bone marrow monocytes and neutrophils both expressed high levels of the Sts proteins, only Sts$^{-/-}$ monocytes displayed enhanced *C. albicans* growth-suppressive properties. The underlying basis for a cell-specific role for Sts in regulating antifungal responses is currently unclear, but it could indicate important differences in the manner in which different innate immune cells respond to fungal pathogens. These observations are consistent with a previous report from a study demonstrating that different bone marrow-derived cell lineages exhibit differential responses to fungal ligands (49). It will be interesting to determine how the cell specificity observed *ex vivo* influences the *in vivo* immune response to fungal infection.

Increasing resistance to *C. albicans* infection. Similarly to the Sts proteins, two other gene products (Jnk1 and Cbl-b) have recently been shown to negatively regulate phagocyte signaling pathways such that the corresponding gene deletions result in mice that have increased resistance to *C. albicans* bloodstream infection (12, 50–53). Jnk1, a member of the MAPK family of enzymes, negatively regulates activation of the transcription factor NFATc1. NFATc1 induces expression of the CLR CD23, and CD23 expression is upregulated in Jnk1$^{-/-}$ mice phagocytes, resulting in elevated levels of inducible nitric oxide synthase (iNOS) (Nos2) expression. Therefore, the protection of Jnk1$^{-/-}$ mice from systemic candidiasis appears to stem from increased fungus-induced NO production (50). The ubiquitin ligase Cbl-b mediates Dectin-1 internalization and degradation. In its absence, Dectin-1 surface expression is stabilized, resulting in Syk hyperactivation and enhanced phagocyte antifungal responses (51–53). Interestingly, while Cbl-b$^{-/-}$ BMDCs demonstrate increases in both ROS and cytokine production levels following infection with *C. albicans*, Sts$^{-/-}$ cells display an augmented ROS response without concomitant increases in cytokine production. Nonetheless, an intriguing property common to Jnk1$^{-/-}$, Cbl-b$^{-/-}$, and Sts$^{-/-}$ mutant mice is increased activation of phagocyte signaling pathways downstream of fungal CLRs, with consequent increases in antifungal effector activities. These observations offer insights into developing novel immune-enhancing therapeutics that could be paired with traditional antifungal antibiotics to ameliorate the destructive effects of systemic *C. albicans* infection.

MATERIALS AND METHODS

Mouse strains and cells. The generation of C57/B6 mice containing the Sts mutations has been previously described (17, 54, 55). Mice were housed in the Stony Brook University Animal Facility in

accordance with Division of Laboratory Animal Resources (DLAR) regulations. Animal protocols followed guidelines established within the "Guide for the Care and Use of Laboratory Animals" (8th ed.) published by the National Research Council of the National Academies. Protocols were approved by the Institutional Animal Care and Use Committee (IACUC) of Stony Brook University.

BMDCs were differentiated as previously described (32). Briefly, cells were cultured in RPMI medium containing 10% fetal bovine serum (FBS), 1 mM sodium pyruvate, 10 U/ml penicillin/streptomycin (Pen/Strep), 55 μM β-mercaptoethanol (BME), and 20 ng/ml granulocyte-macrophage colony-stimulating factor (GM-CSF). On days 3, 6, and 8, cells were provided fresh growth media. All BMDC experiments utilized nonadherent cells grown for 9 to 10 days in culture. BMDMs were cultured in DMEM containing 30% L929 cell supernatant (33), 20% FBS, and 1 mM sodium pyruvate for 4 days, after which cells were harvested, counted, and utilized as described. During the derivation of BMDMs, day 4 nonadherent cells were harvested as BM-derived monocytes (34).

For neutrophil purification, bone marrow cells were suspended in 4 ml of phosphate-buffered saline (PBS), placed on 3 ml Lymphoprep reagent (Axis-Shield, Oslo, Norway) (1.077 g/ml), and spun at 2,000 rpm. Alternatively, a murine neutrophil enrichment kit (Miltenyi) was utilized to obtain marrow neutrophils. Bone marrow monocytes were obtained with a murine monocyte isolation kit (Miltenyi) or an EasySep mouse monocyte kit (Stem Cell Technologies), according to the instructions of the manufacturers.

Reagents and antibodies. The following antibodies were purchased from Cell Signaling Technology, Inc.: pAKT S473 (9271), AKT (9272), p-ERK T202/Y204 (9106), ERK (9102), p-Syk Y525/526 (2710), p-PLCγ2 Y759 (3874), p-Src family Y416 (2101), Src (2110), p-Shp2 Y542 (3715), Shp2 (3397), p-P65 S536 (3033), and P65 (6956). Anti-Syk (Syk01) and anti-Nos2 (5C1B52) antibodies were from BioLegend. Antibodies to PLCγ2 (sc5283) were from Santa Cruz Biotechnology. Antibodies to Sts-1 and Sts-2 were previously described (17, 54). Dectin-1 antibody (2A11) was from Bio-Rad, and flow cytometry antibodies to CD45 (clone 30-F11), CD11b (clone M1/70), CD11C (clone N418), F4/80 (clone BM8), Ly6g (clone 1A8), Ly6c (clone AL-21), and I-A/I-E (clone M5/114.15.2) were from BioLegend. Luminol, PMA, horseradish peroxidase (HRP) type VI (P8375), and zymosan (Z4250) were from Sigma-Aldrich. Particulate β-glucan, soluble β-glucan, and depleted zymosan were obtained from InvivoGen.

Mouse infections. *Candida albicans* infections were carried out as previously described (16). Cells were harvested, washed twice in PBS, and counted, and cell counts were confirmed by plating dilutions onto yeast extract-peptone-dextrose (YPD) plates. Female mice were inoculated with 2.5×10^5 CFU via the lateral tail vein and monitored for 28 days. For clodronate depletion experiments, mice were administered by intravenous (i.v.) injection 1 mg clodronate/liposome formulation or control liposomes (Encapsula Nano Sciences, Brentwood, TN) 24 h prior to inoculation with *C. albicans* (1×10^5 CFU) (26). To obtain kidney CFU, kidneys were excised at the indicated times postinfection, placed in 5 ml PBS, and homogenized. The number of CFU per gram of tissue was determined by plating homogenate serial dilutions onto YPD medium plates and incubating at 30°C.

Derivation and use of radiation chimeras. Female mice (8 to 10 weeks of age) were dosed with 1,100 rads from a gamma cell irradiator (GammaCell 40; AEC Ltd.) and administered 8×10^6 bone marrow cells via tail vein injection within 1 h. Chimeric mice were housed for 12 weeks and then utilized for survival or organ CFU assays. Graphing and statistical analysis of survival after infection were carried out using a log rank test (Mantel-Haenszel test) with SigmaPlot software (SigmaPlot Systat Software, Inc., San Jose, CA).

***Ex vivo C. albicans* coculture assay.** Nonfilamentous *C. albicans* mutant *cph1*Δ *efg1*Δ cells (28) were grown overnight, reinoculated into fresh medium, and grown to an optical density at 600 nm (OD_{660}) of 0.7 to 0.9. Cells were washed twice in PBS and coincubated with cells obtained from male or female mice in RPMI media at a multiplicity of infection (MOI) of 0.0375 to 0.125, with or without 10 ng/ml PMA, for 24 h in a 96-well plate. Wells were washed once with water and collected in 1 ml of deionized water to lyse nonfungal cells. Fungal CFU were obtained by plating serial dilutions onto YPD plates.

Pathway analysis. Cells obtained from male or female mice were stimulated, washed, and lysed in buffer containing 0.05 M Tris, 0.15 M sodium chloride, 5 μM EDTA, 0.2 mM pervanadate, 0.5 mg/ml phenylmethylsulfonyl fluoride (PMSF), and 1× Roche protease inhibitors. Lysates were clarified by centrifugation, subjected to SDS-PAGE, and transferred to nitrocellulose (Whatman). Membranes were probed with specific antibody and the appropriate secondary antibody and were developed with an Odyssey CLx imaging system (Li-COR). Immunoprecipitations were conducted by rotating lysates with specific antibody for 2 h at 4°C, followed by 1 h at 4°C with protein A Sepharose beads (Sigma). Beads were washed three times in lysis buffer, and proteins were eluted with 2× Laemmli sample buffer and separated by SDS-PAGE. Dectin-1 downregulation was evaluated using a FACScan cytometer (Cytek Biosciences).

Measurement of ROS and NO production. Levels of reactive oxygen species were measured as previously described (56). Briefly, BMDCs (1×10^5 cells/well) or neutrophils (4×10^5 cells/well) were plated in triplicate wells of a 96-well plate. Stimuli were prepared in RPMI media containing 600 μM luminol and 16 units of HRP/ml. Reagent medium (100 μl) was added to 100 μl of preplated cells, and luminescence was measured at regular intervals on a Filtermax F5 96-well plate reader using Softmax Pro software (Molecular Devices, Sunnyvale, CA). Griess reagent was used to evaluate levels of NO_2 production in cell culture supernatants per the instructions of the manufacturer (Promega).

Cytokine measurements. Cells were placed in a 6-well tissue culture plate and stimulated with zymosan (100 μg/ml) or heat-killed SC5314 (MOI of 2). The supernatant was collected and frozen at −80°C until measured. IL-6, TNF-α (BioLegend), and IL-1β (Thermo Fisher Invitrogen) levels were measured by enzyme-linked immunosorbent assay (ELISA) according to provided instructions.

SUPPLEMENTAL MATERIAL

Supplemental material for this article may be found at https://doi.org/10.1128/mBio.00782-18.

FIG S1, TIF file, 1.9 MB.
FIG S2, TIF file, 0.8 MB.
FIG S3, TIF file, 1.5 MB.
FIG S4, TIF file, 0.4 MB.
FIG S5, TIF file, 0.9 MB.

ACKNOWLEDGMENTS

We thank Laurie Levine, Jean Rooney, and other staff members of the Stony Brook DLAR for help with animal studies. We also acknowledge the technical support provided by Todd Rueb and Rebecca Connor of the Stony Brook University Flow Cytometry Core for help with fluorescence-activated cell sorting. We thank Michael Hayman and members of the laboratories of N.C. and J.B.K. for discussions.

This work was supported by grants to N.C. from Stony Brook University; the Stony Brook Medical Center Dean's Office; the National Heart, Lung, and Blood Institute (NIH) under award UO1HL127522 (Clinton Rubin, principal investigator [PI]); and the Office of the Assistant Secretary of Defense for Health Affairs through Peer-Reviewed Medical Research Program W81XWH-16-PRMRP-DA (PR161377) and by funds from the National Institutes of Health awarded to N.C. (R21 AI130859) and J.K. (R01 AI047837). G.L.R. thanks the Fullbright Research Scholar Program (United States-Italy) and the Short Term Mobility Program of the National Research Council (Italy) for support. The funders had no role in the study design, data collection and interpretation, or the decision to submit work for publication.

We declare that we have no financial conflict of interest.

REFERENCES

1. Brown GD, Denning DW, Levitz SM. 2012. Tackling human fungal infections. Science 336:647. https://doi.org/10.1126/science.1222236.
2. Lionakis MS, Iliev ID, Hohl TM. 2017. Immunity against fungi. JCI Insight 2:e93156. https://doi.org/10.1172/jci.insight.93156.
3. Lionakis MS. 2014. New insights into innate immune control of systemic candidiasis. Med Mycol 52:555–564. https://doi.org/10.1093/mmy/myu029.
4. Pfaller MA, Diekema DJ. 2010. Epidemiology of invasive mycoses in North America. Crit Rev Microbiol 36:1–53. https://doi.org/10.3109/10408410903241444.
5. Perlin DS. 2009. Antifungal drug resistance: do molecular methods provide a way forward? Curr Opin Infect Dis 22:568–573. https://doi.org/10.1097/QCO.0b013e3283321ce5.
6. Kullberg BJ, Arendrup MC. 2015. Invasive candidiasis. N Engl J Med 373:1445–1456. https://doi.org/10.1056/NEJMra1315399.
7. Spampinato C, Leonardi D. 2013. *Candida* infections, causes, targets, and resistance mechanisms: traditional and alternative antifungal agents. BioMed Res Int 2013:204237 https://doi.org/10.1155/2013/204237.
8. CDC. 2013. Antibiotic resistance threats in the United States, 2013. http://www.cdc.gov/drugresistance/threat-report-2013/pdf/ar-threats-2013-508.pdf.
9. Romani L. 2011. Immunity to fungal infections. Nat Rev Immunol 11:275–288. https://doi.org/10.1038/nri2939.
10. Erwig LP, Gow NA. 2016. Interactions of fungal pathogens with phagocytes. Nat Rev Microbiol 14:163–176. https://doi.org/10.1038/nrmicro.2015.21.
11. Duggan S, Leonhardt I, Hünniger K, Kurzai O. 2015. Host response to *Candida albicans* bloodstream infection and sepsis. Virulence 6:316–326. https://doi.org/10.4161/21505594.2014.988096.
12. Carpino N, Naseem S, Frank DM, Konopka JB. 2017. Modulating host signaling pathways to promote resistance to infection by Candida albicans. Front Cell Infect Microbiol 7:481. https://doi.org/10.3389/fcimb.2017.00481.
13. Spellberg B, Ibrahim AS, Edwards JE, Jr, Filler SG. 2005. Mice with disseminated candidiasis die of progressive sepsis. J Infect Dis 192:336–343. https://doi.org/10.1086/430952.
14. Zwolanek F, Riedelberger M, Stolz V, Jenull S, Istel F, Köprülü AD, Ellmeier W, Kuchler K. 2014. The non-receptor tyrosine kinase Tec controls assembly and activity of the noncanonical caspase-8 inflammasome. PLoS Pathog 10:e1004525. https://doi.org/10.1371/journal.ppat.1004525.
15. Lionakis MS, Fischer BG, Lim JK, Swamydas M, Wan W, Richard Lee CCR, Cohen JI, Scheinberg P, Gao JL, Murphy PM. 2012. Chemokine receptor Ccr1 drives neutrophil-mediated kidney immunopathology and mortality in invasive candidiasis. PLoS Pathog 8:e1002865. https://doi.org/10.1371/journal.ppat.1002865.
16. Naseem S, Frank D, Konopka JB, Carpino N. 2015. Protection from systemic *Candida albicans* infection by inactivation of the Sts phosphatases. Infect Immun 83:637–645. https://doi.org/10.1128/IAI.02789-14.
17. Carpino N, Turner S, Mekala D, Takahashi Y, Zang H, Geiger TL, Doherty P, Ihle JN. 2004. Regulation of ZAP-70 activation and TCR signaling by two related proteins, Sts-1 and Sts-2. Immunity 20:37–46. https://doi.org/10.1016/S1074-7613(03)00351-0.
18. Newman TN, Liverani E, Ivanova E, Russo GL, Carpino N, Ganea D, Safadi F, Kunapuli SP, Tsygankov AY. 2014. Members of the novel UBASH3/STS/TULA family of cellular regulators suppress T-cell-driven inflammatory responses in vivo. Immunol Cell Biol 92:837–850. https://doi.org/10.1038/icb.2014.60.
19. Tsygankov AY. 2013. Tula-family proteins: a new class of cellular regulators. J Cell Physiol 228:43–49. https://doi.org/10.1002/jcp.24128.
20. Mikhailik A, Ford B, Keller J, Chen Y, Nassar N, Carpino N. 2007. A phosphatase activity of Sts-1 contributes to the suppression of TCR signaling. Mol Cell 27:486–497. https://doi.org/10.1016/j.molcel.2007.06.015.
21. Reppschläger K, Gosselin J, Dangelmaier CA, Thomas DH, Carpino N, McKenzie SE, Kunapuli SP, Tsygankov AY. 2016. TULA-2 protein phosphatase suppresses activation of Syk through the GPVI platelet receptor for collagen by dephosphorylating Tyr(P)-346, a regulatory site of Syk. J Biol Chem 291:22427–22441. https://doi.org/10.1074/jbc.M116.743732.
22. de Castro RO, Zhang J, Groves JR, Barbu EA, Siraganian RP. 2012. Once phosphorylated, tyrosines in the carboxyl terminus of protein-tyrosine kinase Syk interact with signaling proteins, including TULA-2, a negative regulator of mast cell degranulation. J Biol Chem 287:8194–8204. https://doi.org/10.1074/jbc.M111.326850.

23. Lionakis MS, Lim JK, Lee CC, Murphy PM. 2011. Organ-specific innate immune responses in a mouse model of invasive candidiasis. J Innate Immun 3:180–199. https://doi.org/10.1159/000321157.
24. Lionakis MS, Swamydas M, Fischer BG, Plantinga TS, Johnson MD, Jaeger M, Green NM, Masedunskas A, Weigert R, Mikelis C, Wan W, Lee CCR, Lim JK, Rivollier A, Yang JC, Laird GM, Wheeler RT, Alexander BD, Perfect JR, Gao JL, Kullberg BJ, Netea MG, Murphy PM. 2013. CX3CR1-dependent renal macrophage survival promotes Candida control and host survival. J Clin Invest 123:5035–5051. https://doi.org/10.1172/JCI71307.
25. Xu W, Solis NV, Ehrlich RL, Woolford CA, Filler SG, Mitchell AP. 2015. Activation and alliance of regulatory pathways in *C. albicans* during mammalian infection. PLoS Biol 13:e1002076. https://doi.org/10.1371/journal.pbio.1002076.
26. Qian Q, Jutila MA, Van Rooijen N, Cutler JE. 1994. Elimination of mouse splenic macrophages correlates with increased susceptibility to experimental disseminated candidiasis. J Immunol 152:5000–5008.
27. Marcil A, Harcus D, Thomas DY, Whiteway M. 2002. *Candida albicans* killing by RAW 264.7 mouse macrophage cells: effects of *Candida* genotype, infection ratios, and gamma interferon treatment. Infect Immun 70:6319–6329. https://doi.org/10.1128/IAI.70.11.6319-6329.2002.
28. Lo HJ, Köhler JR, DiDomenico B, Loebenberg D, Cacciapuoti A, Fink GR. 1997. Nonfilamentous *C. albicans* mutants are avirulent. Cell 90:939–949. https://doi.org/10.1016/S0092-8674(00)80358-X.
29. Domínguez-Andrés J, Feo-Lucas L, Minguito de la Escalera M, González L, López-Bravo M, Ardavín C. 2017. Inflammatory Ly6C^{high} monocytes protect against candidiasis through IL-15-driven NK cell/neutrophil activation. Immunity 46:1059–1072.e4. https://doi.org/10.1016/j.immuni.2017.05.009.
30. Swamydas M, Gao JL, Break TJ, Johnson MD, Jaeger M, Rodriguez CA, Lim JK, Green NM, Collar AL, Fischer BG, Lee CCR, Perfect JR, Alexander BD, Kullberg BJ, Netea MG, Murphy PM, Lionakis MS. 2016. CXCR1-mediated neutrophil degranulation and fungal killing promote *Candida* clearance and host survival. Sci Transl Med 8:322ra10. https://doi.org/10.1126/scitranslmed.aac7718.
31. Ngo LY, Kasahara S, Kumasaka DK, Knoblaugh SE, Jhingran A, Hohl TM. 2014. Inflammatory monocytes mediate early and organ-specific innate defense during systemic candidiasis. J Infect Dis 209:109–119. https://doi.org/10.1093/infdis/jit413.
32. Lutz MB, Kukutsch N, Ogilvie AL, Rössner S, Koch F, Romani N, Schuler G. 1999. An advanced culture method for generating large quantities of highly pure dendritic cells from mouse bone marrow. J Immunol Methods 223:77–92. https://doi.org/10.1016/S0022-1759(98)00204-X.
33. Doyle CR, Pan JA, Mena P, Zong WX, Thanassi DG. 2014. TolC-dependent modulation of host cell death by the Francisella tularensis live vaccine strain. Infect Immun 82:2068–2078. https://doi.org/10.1128/IAI.00044-14.
34. Francke A, Herold J, Weinert S, Strasser RH, Braun-Dullaeus RC. 2011. Generation of mature murine monocytes from heterogeneous bone marrow and description of their properties. J Histochem Cytochem 59:813–825. https://doi.org/10.1369/0022155411416007.
35. Sancho D, Reis e Sousa C. 2012. Signaling by myeloid C-type lectin receptors in immunity and homeostasis. Annu Rev Immunol 30:491–529. https://doi.org/10.1146/annurev-immunol-031210-101352.
36. Drummond RA, Brown GD. 2013. Signalling C-type lectins in antimicrobial immunity. PLoS Pathog 9:e1003417. https://doi.org/10.1371/journal.ppat.1003417.
37. Brown GD. 2011. Innate antifungal immunity: the key role of phagocytes. Annu Rev Immunol 29:1–21. https://doi.org/10.1146/annurev-immunol-030409-101229.
38. Gross O, Poeck H, Bscheider M, Dostert C, Hannesschläger N, Endres S, Hartmann G, Tardivel A, Schweighoffer E, Tybulewicz V, Mocsai A, Tschopp J, Ruland J. 2009. Syk kinase signalling couples to the Nlrp3 inflammasome for anti-fungal host defence. Nature 459:433–436. https://doi.org/10.1038/nature07965.
39. Reid DM, Gow NA, Brown GD. 2009. Pattern recognition: recent insights from Dectin-1. Curr Opin Immunol 21:30–37. https://doi.org/10.1016/j.coi.2009.01.003.
40. Plato A, Willment JA, Brown GD. 2013. C-type lectin-like receptors of the dectin-1 cluster: ligands and signaling pathways. Int Rev Immunol 32:134–156. https://doi.org/10.3109/08830185.2013.777065.
41. Goodridge HS, Reyes CN, Becker CA, Katsumoto TR, Ma J, Wolf AJ, Bose N, Chan ASH, Magee AS, Danielson ME, Weiss A, Vasilakos JP, Underhill DM. 2011. Activation of the innate immune receptor Dectin-1 upon formation of a 'phagocytic synapse'. Nature 472:471–475. https://doi.org/10.1038/nature10071.
42. Page TH, Smolinska M, Gillespie J, Urbaniak AM, Foxwell BM. 2009. Tyrosine kinases and inflammatory signalling. Curr Mol Med 9:69–85. https://doi.org/10.2174/156652409787314507.
43. Deng Z, Ma S, Zhou H, Zang A, Fang Y, Li T, Shi H, Liu M, Du M, Taylor PR, Zhu HH, Chen J, Meng G, Li F, Chen C, Zhang Y, Jia XM, Lin X, Zhang X, Pearlman E, Li X, Feng GS, Xiao H. 2015. Tyrosine phosphatase SHP-2 mediates C-type lectin receptor-induced activation of the kinase Syk and anti-fungal TH17 responses. Nat Immunol 16:642–652. https://doi.org/10.1038/ni.3155.
44. Kerrigan AM, Brown GD. 2011. Syk-coupled C-type lectins in immunity. Trends Immunol 32:151–156. https://doi.org/10.1016/j.it.2011.01.002.
45. Nelson PJ, Rees AJ, Griffin MD, Hughes J, Kurts C, Duffield J. 2012. The renal mononuclear phagocytic system. J Am Soc Nephrol 23:194–203. https://doi.org/10.1681/ASN.2011070680.
46. Underhill DM, Rossnagle E, Lowell CA, Simmons RM. 2005. Dectin-1 activates Syk tyrosine kinase in a dynamic subset of macrophages for reactive oxygen production. Blood 106:2543–2550. https://doi.org/10.1182/blood-2005-03-1239.
47. Poeck H, Ruland J. 2010. SYK kinase signaling and the NLRP3 inflammasome in antifungal immunity. J Mol Med 88:745–752. https://doi.org/10.1007/s00109-010-0631-4.
48. Blanco-Menéndez N, Del Fresno C, Fernandes S, Calvo E, Conde-Garrosa R, Kerr WG, Sancho D. 2015. SHIP-1 couples to the Dectin-1 hemITAM and selectively modulates reactive oxygen species production in dendritic cells in response to *Candida albicans*. J Immunol 195:4466–4478. https://doi.org/10.4049/jimmunol.1402874.
49. Goodridge HS, Shimada T, Wolf AJ, Hsu YM, Becker CA, Lin X, Underhill DM. 2009. Differential use of CARD9 by dectin-1 in macrophages and dendritic cells. J Immunol 182:1146–1154. https://doi.org/10.4049/jimmunol.182.2.1146.
50. Zhao X, Guo Y, Jiang C, Chang Q, Zhang S, Luo T, Zhang B, Jia X, Hung MC, Dong C, Lin X. 2017. JNK1 negatively controls antifungal innate immunity by suppressing CD23 expression. Nat Med 23:337–346. https://doi.org/10.1038/nm.4260.
51. Wirnsberger G, Zwolanek F, Asaoka T, Kozieradzki I, Tortola L, Wimmer RA, Kavirayani A, Fresser F, Baier G, Langdon WY, Ikeda F, Kuchler K, Penninger JM. 2016. Inhibition of CBLB protects from lethal Candida albicans sepsis. Nat Med 22:915–923. https://doi.org/10.1038/nm.4134.
52. Xiao Y, Tang J, Guo H, Zhao Y, Tang R, Ouyang S, Zeng Q, Rappleye CA, Rajaram MVS, Schlesinger LS, Tao L, Brown GD, Langdon WY, Li BT, Zhang J. 2016. Targeting CBLB as a potential therapeutic approach for disseminated candidiasis. Nat Med 22:906–914. https://doi.org/10.1038/nm.4141.
53. Zhu LL, Luo TM, Xu X, Guo YH, Zhao XQ, Wang TT, Tang B, Jiang YY, Xu JF, Lin X, Jia XM. 2016. E3 ubiquitin ligase Cbl-b negatively regulates C-type lectin receptor-mediated antifungal innate immunity. J Exp Med 213:1555–1570. https://doi.org/10.1084/jem.20151932.
54. Carpino N, Kobayashi R, Zang H, Takahashi Y, Jou ST, Feng J, Nakajima H, Ihle JN. 2002. Identification, cDNA cloning, and targeted deletion of p70, a novel, ubiquitously expressed SH3 domain-containing protein. Mol Cell Biol 22:7491–7500. https://doi.org/10.1128/MCB.22.21.7491-7500.2002.
55. San Luis B, Sondgeroth B, Nassar N, Carpino N. 2011. Sts-2 is a phosphatase that negatively regulates zeta-associated protein (ZAP)-70 and T cell receptor signaling pathways. J Biol Chem 286:15943–15954. https://doi.org/10.1074/jbc.M110.177634.
56. Frohner IE, Bourgeois C, Yatsyk K, Majer O, Kuchler K. 2009. *Candida albicans* cell surface superoxide dismutases degrade host-derived reactive oxygen species to escape innate immune surveillance. Mol Microbiol 71:240–252. https://doi.org/10.1111/j.1365-2958.2008.06528.x.

Supplemental Information Legends

Figure S1. Expression of Sts-1 and Sts-2 in murine hematopoietic cells. Representative western blots illustrate levels of Sts-1 & -2 in (**A**) bone marrow (BM), blood and spleen; (**B**) purified monocytes (Mo) isolated from preparations of marrow cells; (**C**) purified neutrophils (Neu) isolated from heterogeneous marrow populations; (**D**) BMDMs derived by culturing marrow cells in CSF-1 over a 5-day period and removing non-adherent cells; (**E**) BMD-monocytes derived by culturing marrow cells in CSF-1 over a 4-day period and harvesting non-adherent cells; and (**F**) BM-derived dendritic cells (BMDCs) derived by culturing cells in GM-CSF for 10 days, harvesting non-adherent cells, and purifying them by flow cytometry ($CD45^+CD11b^+MHCII^+CD11c^+$).

Figure S2. Isolation of hematopoietic bone marrow cells. Representative FACS plot of (**A**) purified $Ly6C^{hi}$ bone marrow monocytes; or (**B**) $Ly6G^+$ bone marrow neutrophils used for *ex vivo* co-culture assays (Figure 2).

Figure S3. Sts does not regulate ROS production in BMD-monocytes or BMDMs. Wild type and *Sts*-/- (**A**) marrow-derived monocytes, and (**B**) BMDMs were stimulated with zymosan, HK *C. albicans*, or live *C. albicans* as indicated, and levels of ROS production were assessed by luminol chemiluminescence. Average results of at least two separate experiments each conducted in triplicate are displayed.

Figure S4. Increased ROS production from heat killed non-filamentous *C. albicans*. *Left*, Wild type and *Sts*-/- BMDCs were stimulated with HK *C. albicans cph1*Δ/*efg1*Δ (MOI 50) and levels of ROS production were assessed by luminol chemiluminescence. *Right*,

Average results (areas under the curve, AUC) of two separate experiments each conducted in triplicate are displayed. **, $p < 0.01$ by Mann-Whitney analysis (error bars = SD of mean).

Figure S5. Increased phosphorylation of signaling molecules downstream of Dectin-1. Levels of site-specific phosphorylation at (**A**) Syk Tyr-525/526 and (**B**) PLCγ2 Tyr-759 in zymosan-stimulated (top) or wild type *C. albicans*-stimulated (bottom) BMDCs were determined by quantifying the fluorescent intensities of protein bands using a LI-COR Odyssey Imaging System and normalizing to the level of total Syk protein. Each measurement was expressed as a value relative to the normalized level of site-specific phosphorylation observed in wild-type cells. The illustrated data represent the average of three to four separate experiments. **= ($p<0.01$), *=($p < 0.05$), by Student's t-test.

Figure S1

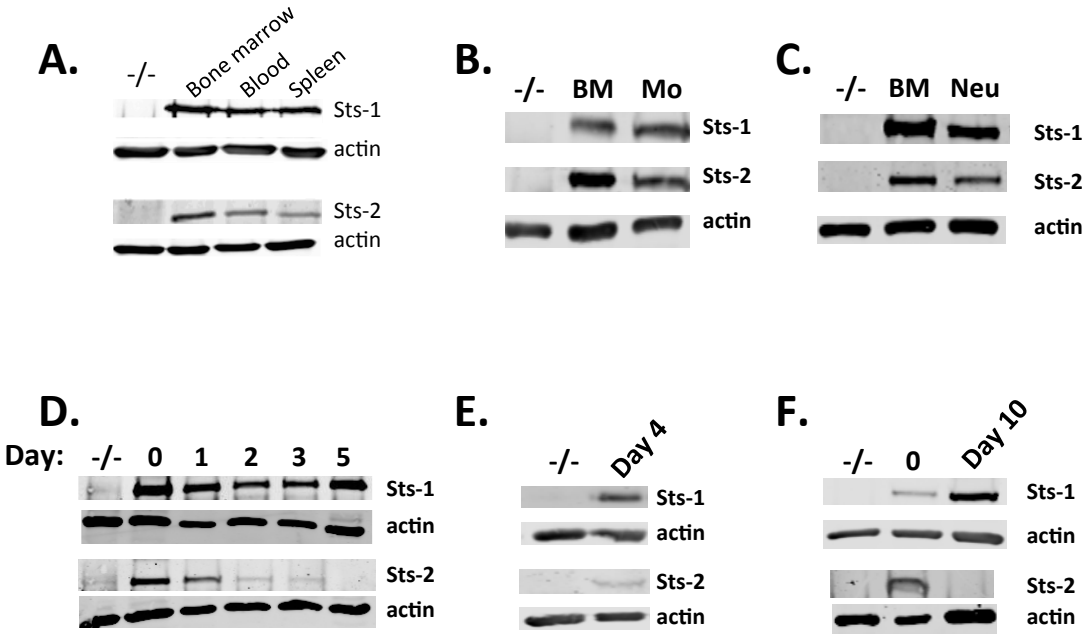
A.
-/-
Bone marrow
Blood
Spleen
Sts-1
actin
Sts-2
actin
B.
-/-
BM
Mo
Sts-1
Sts-2
actin
C.
-/-
BM
Neu
Sts-1
Sts-2
actin
D.
Day:
-/-
0
1
2
3
5
Sts-1
actin
Sts-2
actin
E.
-/-
Day 4
Sts-1
actin
Sts-2
actin
F.
-/-
0
Day 10
Sts-1
actin
Sts-2
actin

Figure S2

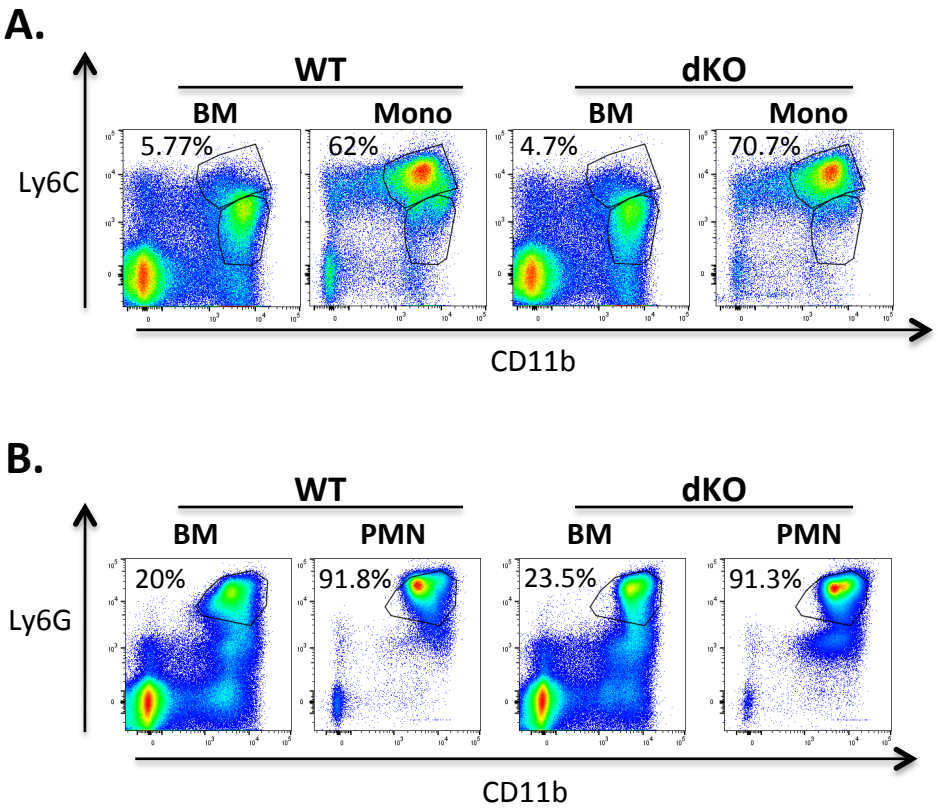
A.
WT
dKO
BM
Mono
BM
Mono
5.77%
62%
4.7%
70.7%
Ly6C
CD11b
B.
WT
dKO
BM
PMN
BM
PMN
20%
91.8%
23.5%
91.3%
Ly6G
CD11b

Figure S3

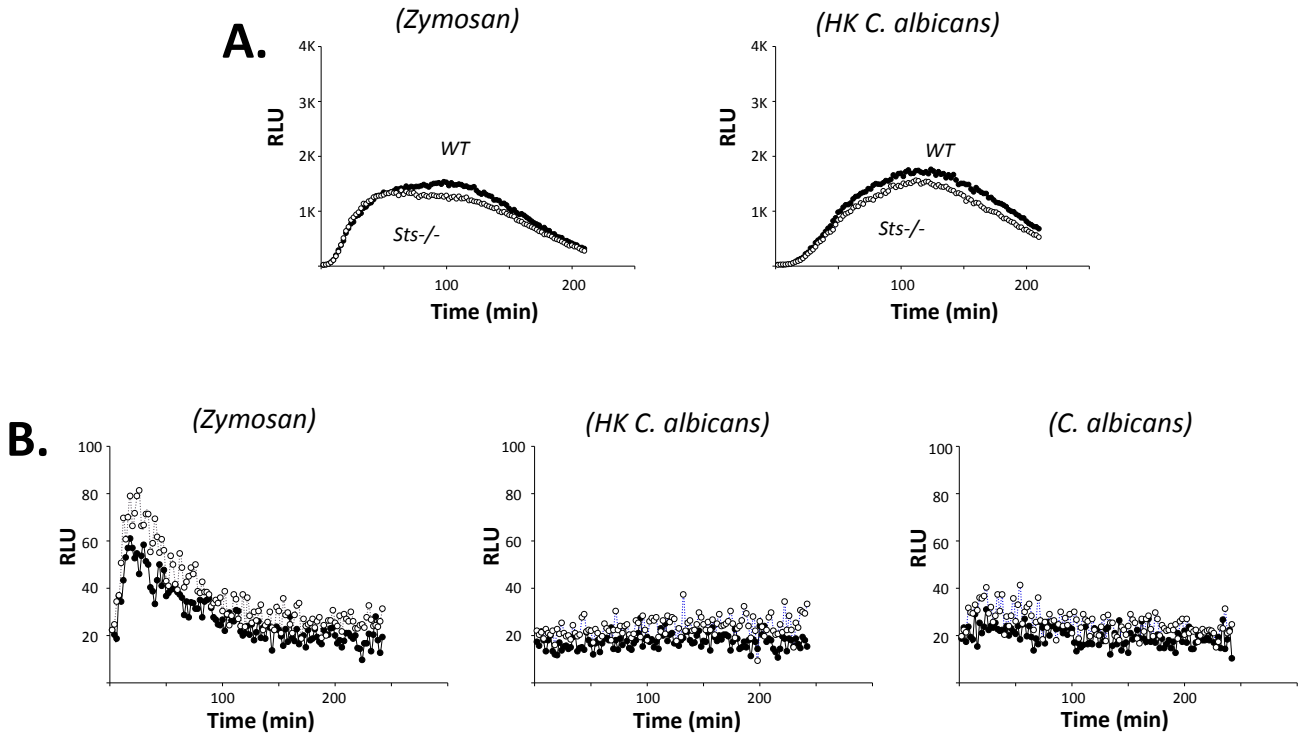
A.
(Zymosan)
(HK C. albicans)
RLU
4K
3K
2K
1K
WT
Sts-/-
100
200
Time (min)
B.
(Zymosan)
(HK C. albicans)
(C. albicans)
RLU
100
80
60
40
20
100
200
Time (min)

Figure S4

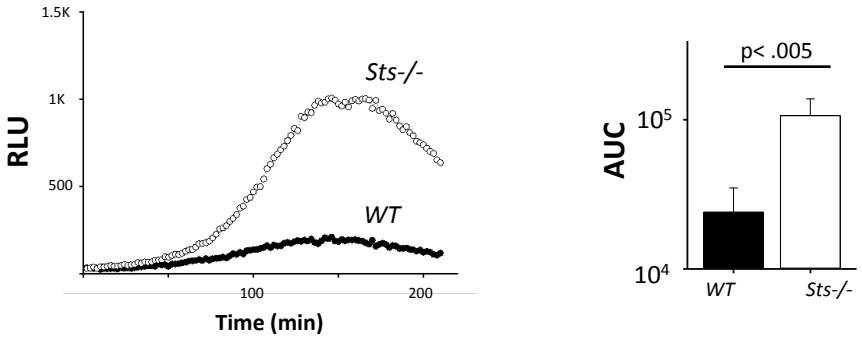

Figure S5

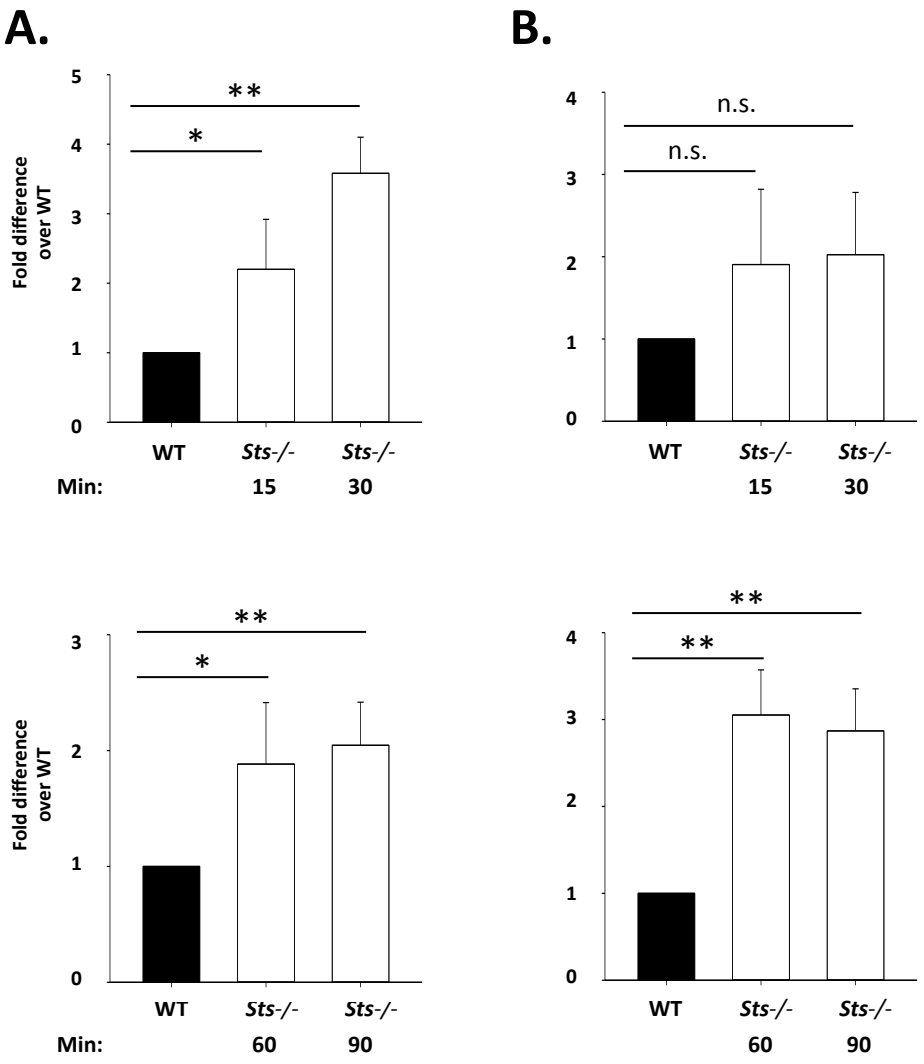

APPENDIX 3

From Parashar et al, Manuscript in Preparation, 2018.

FIGURE LEGENDS

Figure 1. Bone marrow monocytes lacking Sts expression display heightened IFNγ secretion following infection with *F. tularensis LVS*, MOI 5 (Left). IFNγ production is suppressed at MOI 20. Production of TNFα and IL-6 in infected monocytes is unaffected by the absence of Sts (middle and right).

Figure 2. Wild type and Sts-/- bone marrow monocytes lacking Sts expression were infected with F. tularensis LVS (MOI 5) and treated with identical Units of IFNγ. *Sts*-/- monocytes display heightened restriction of intracellular bacteria.

Figure 1

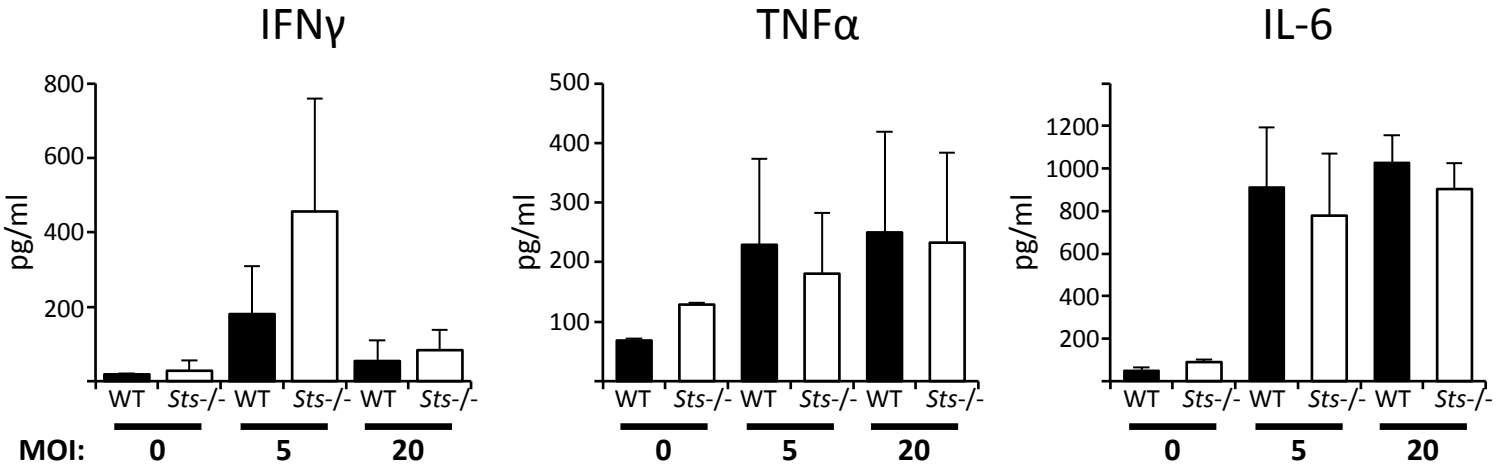
IFNγ
TNFα
IL-6
pg/ml
800
600
400
200
500
300
100
1200
1000
WT
Sts-/-
MOI:
0
5
20

Figure 2

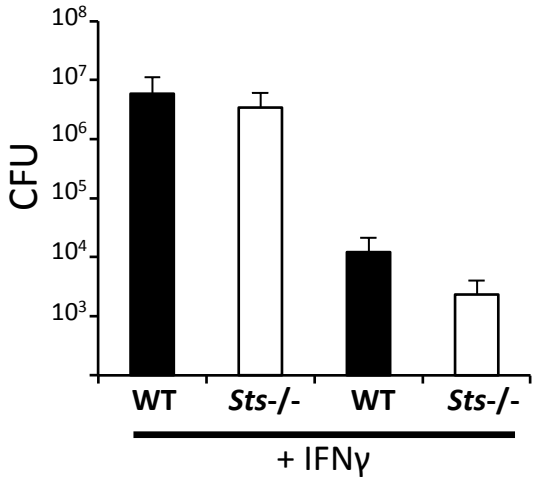

APPENDIX 4

Zhou et al, Manuscript in Preparation, 2018.

Discovery and Characterization of Two Classes of Selective Inhibitors of the Suppressor of TCR Signaling Family of Proteins

Weijie Zhou[1], Yue Yin[1], Emery Smith[2], Jacqueline Chou[1], Justin Shumate[2], Louis Scampavia[2], Timothy P. Spicer[2], Nicholas Carpino[3], and Jarrod B. French[1,4,*]

1. Department of Chemistry, Stony Brook University, Stony Brook, NY 11794

2. Department of Molecular Medicine, The Scripps Research Institute Molecular Screening Center, Jupiter FL 33458

3. Department of Molecular Genetics and Microbiology, Stony Brook University, Stony Brook, NY 11794

4. Department of Biochemistry and Cell Biology, Stony Brook University, Stony Brook, NY 11794

* Corresponding author

JBF: jarrod.french@stonybrook.edu

ABSTRACT

The Suppressor of T cell receptor Signaling (Sts) proteins, particularly Sts-1, have recently emerged as potential immunostimulatory targets for drug development. Genetic inactivation of the Sts proteins dramatically increases host survival of systemic infection and leads to improved pathogen clearance. The protein tyrosine phosphatase (PTP) activity of these proteins arises from a C-terminal 2-histidine phosphatase (HP) domain. To identify new inhibitors of the HP activity of Sts-1 we miniaturized a phosphatase assay to 1,536-well format and conducted a 20,580 compound screen. Among the hits (IC_{50} < 10 μM) were two classes of structurally related compounds, tetracycline variants and sulfonated azo dyes. These hits had low micromolar to nanomolar IC_{50} values. Orthogonal screening confirmed the validity of these inhibitors and demonstrated that both act competitively on Sts-1 phosphatase activity. When tested on other PTPs, PTP1B and SHP1, the tetracycline variant, doxycycline, and the sulfonated azo dye, Congo red, are selective inhibitors of Sts-1_{HP} with selectivity indices ranging from 19 to as high as 200. The planar polyaromatic moieties present in both classes of compounds suggested a common binding mode. Mutation of either tryptophan 494 or tyrosine 596, located near the active site of the protein, reduced the K_i of the inhibitors from 3- to 18-fold, indicating that these residues may help promote binding of substrates with aromatic groups. This work provides new insights into substrate selectivity mechanisms and describes two classes of compounds that can serve as probes of function or as a basis for future drug discovery.

INTRODUCTION

The T cell Receptor (TCR) complex recognizes antigens and is responsible for activating T cells. The TCR signaling pathway is highly regulated, both positively and negatively, by tyrosine kinases and protein tyrosine phosphatases (PTPs) (1-3). Two members of the Suppressor of TCR Signaling (Sts) family of proteins, Sts-1 and Sts-2, act as negative regulators of signaling pathways downstream of the TCR (4, 5). Functional inactivation of the Sts proteins (*Sts*$^{-/-}$) in mice leads to profound resistance to systemic infection by the fungal pathogen *Candida albicans*, and the bacterial pathogen *Francisella tularensis* (6-9). This resistance phenotype is characterized by enhanced survival, rapid clearance of the pathogen and altered inflammatory response. Systemic *C. albicans* infections, with close to 50,000 cases per year in the United States alone, have high mortality rates that have not decreased in the last 20 years (10-12). *F. tularensis*, which is the causative agent of tularemia (rabbit fever), is one of the most infectious pathogens known and is classified as a category A bioterrorism agent (13, 14). Untreated, patients with tularemia have a fatality rate of 50 to 60% (15). The striking resistance phenotype and enhanced survival rates of *Sts*$^{-/-}$ mice suggest that therapeutic inactivation of Sts function generates a unique immune response that helps to reduce pathogen burden and prevent the accompanying destructive inflammation. As such, the pharmacological inhibition of Sts activity presents a potential opportunity to generate immuno-stimulatory therapies, to be used in combination with existing standard-of-care antibiotics or antifungals, as a means to treat deadly pathogen infections.

Sts-1 and Sts-2, which share 40% sequence identify, are multi-domain proteins composed of an N-terminal ubiquitin association (UBA) domain, a Src-homology 3 (SH3) domain, and a C-terminal histidine phosphatase (HP) domain. The UBA and SH3 domains are believed to mediate protein-protein interactions and may be involved in spatiotemporal regulation of the Sts catalytic function (16-18). The HP domain of these proteins are homologous to the phosphoglycerate mutase (PGM) family, a subgroup of the histidine phosphatase superfamily (5, 19, 20). The HP domain of the Sts proteins, like other members of the PGM family, employs a 2-step catalytic mechanism that involves nucleophilic

attack by one of the two conserved histidine residues and formation of a phosphor-histidine intermediate (19, 21-24). While the Sts proteins are known to catalyze the dephosphorylation of phosphotyrosines on protein substrates, they are structurally, functionally and mechanistically distinct from canonical protein tyrosine phosphatases (PTPs) such as PTP1B and SHP1.(5, 20) An established substrate of both Sts-1 and Sts-2, *in vivo*, is the kinase Zap-70 (4, 5, 25). For this substrate, and all others measured, Sts-1 has substantially greater catalytic activity than Sts-2. Similarly, Sts-1 appears to play the predominant role in the observed resistance phenotype (8).

The striking resistance to pathogen infection observed in Sts-deficient mice presents an obvious opportunity for pharmacological interventions. Despite the potential as an immunostimulatory target, little has been reported regarding drug discovery or development. X-ray crystal structures, and complementary biochemical data, suggest that Sts-1 has a well-defined and seemingly druggable active site that is structurally unlike other PTPs or PGMs (19, 20). To date, however, no specific inhibitors of either Sts-1 or Sts-2 have been reported. These proteins can be inhibited with the general competitive inhibitor, orthovanadate, and the SHP-2 inhibitor PHPS1 (4-[2-[1,5-dihydro-3-(4-nitrophenyl)-5-oxo-1-phenyl-4H-pyrazol-4-ylidene]hydrazinyl]-benzenesulfonic acid) inhibits Sts-1 with a K_i of 1 μM (20, 26, 27).

To identify small molecule inhibitors of Sts-1 for use as functional probes or as a basis for further drug development we miniaturized an established phosphatase assay and conducted a 20,000 compound high throughput screen of the Sts-1 phosphatase domain Sts-1_{HP}. The screen yielded 51 active compounds (IC_{50} < 10 μM) that were inactive in an enzyme-minus counter-screen. Within these hits were several groups of compounds with similar structural scaffolds. Among these, tetracycline analogs and sulfonate-containing azo dyes, were the largest two groups, with more than 10 and 5 variants present in the screening results, respectively. Both compound classes were determined to be competitive inhibitors of Sts-1_{HP} that selectively inhibit this phosphatase, when compared to the PTPs

SHP1 and PTP1B. Based on the conserved planar, aromatic structures of these inhibitors we speculated that aromatic residues on the protein were likely involved in critical protein-inhibitor interactions. Consistent with this hypothesis, mutation of either a tyrosine or tryptophan residue near the active site of Sts-1 reduces the effectiveness of these inhibitors without altering the kinetic parameters of the enzyme. Taken together, these data confirm the druggability of the Sts-1 phosphatase active site and provide the first examples of selective Sts-1 inhibitors. The results from the screen, as well as the initial structure-activity and mechanism of action data, provide a foundation for future drug development efforts.

RESULTS

Assay design, miniaturization and testing

The goal of the high-throughput screening (HTS) was to identify potential inhibitors of the histidine phosphatase activity of Sts-1. As previously reported, the isolated HP domain of Sts-1 displays similar kinetics as the intact protein (20). For ease of protein expression and purification, we conducted the screen with Sts-1_{HP}. To assay the phosphatase activity of Sts-1_{HP} we chose to use the 3-O-methylfluorescein phosphate (OMFP) as a substrate. Sts-1_{HP} generates the fluorescent product, 3-O-methylfluorescien, with reasonable kinetics (K_m of 190 μM, k_{cat} of 786 s^{-1}) (20). The assay was optimized and miniaturized to a 1,536-well format. To test the assay performance in this format, we first conducted a 1,280 compound pilot screen, in triplicate, using the bioactive small molecules in the Library of Pharmacologically Active Compounds (LOPAC – Sigma Aldrich) (Fig. 1A). The Sts-1 inhibitor, PHPS1, was used as a positive control (Fig. 1B). The assay performed well with an average Z' value of 0.69 ± 0.02 and signal-to-background ratio (S:B) of 2.03 ± 0.10 (n=3 plates). A standard cutoff of three times the standard deviation of the average percent activity of the compounds tested was used, and yielded 10 hits for a hit rate of 0.86% (Fig. 1C). Table 1 lists the hits from this pilot screen and the average percent response for each.

20,580 compound screen

The general workflow from assay optimization through to completion of our screen is shown in Fig. 2A. After validating the miniaturized assay and conducting the pilot screen, Sts-1_{HP} was screened against a subset of the Scripps Drug Discovery Library (SDDL) consisting of 20,580 compounds (Fig 2B). All the compounds were tested in singlicate using the same protocol as the LOPAC pilot. The performance of the assay was excellent, with an average Z' of 0.83 ± 0.03 and an average S:B of 3.76 ± 0.26 (n=17 plates) (Fig. 2C). The assay yielded 115 active compounds (0.56% hit rate), 105 of which were distinct compounds, using a standard cut-off (3xSD of average response; 23.12%) (Fig 2B). A titration assay was then conducted for all actives (98 were available to test) using the same reagents, protocols and detection system as the primary assay. Each compound was tested using a 10-point dose-response titration in triplicate. The titration assay performed well with an average Z' of 0.77 ± 0.04 and an average S:B of 3.82 ± 0.06. This was followed by a counterscreen, where the compounds were added after the reaction was quenched, to identify compounds that non-specifically affect the fluorescence of the assay. The counterscreen had an average Z' of 0.84 ± 0.03 and an average S:B of 5.44 ± 0.08. All compounds selected for titration were also subjected to LC-MS analysis to confirm mass and sample purity. At the completion of the screen, 51 compounds were identified that were considered active (IC_{50} < 10 μM) in the primary OMFP assay, and inactive (IC_{50}>10 μM) in the counterscreen.

Major inhibitor classes identified in screen

While the 51 active compounds that emerged from the screen displayed a relatively broad chemical diversity, several structural scaffolds appeared with a high degree of frequency. One large class of hits, which contained 12 variants in the primary screen, was the tetracycline derivatives. The structures of the six best tetracycline compounds from the HTS are shown in Figure 3. These compounds displayed IC_{50} values that ranged from low micromolar to high nanomolar (Table 2). Another large, structurally similar, class of compounds that was identified was the sulfonated azo dyes (Fig. 4). These azo dyes also showed low to sub-micromolar IC_{50} values in the primary screen. Additional compound classes

included a small set of 3,4-dihydroxyphenylalanine (L-dopa) variants, and a number of 6-hydroxyuracil (barbituric acid) derivatives.

Secondary screening and mechanism of action

To confirm if these classes of compounds were genuine hits and not false positives (nonspecifically binding), we conducted a secondary screen using an orthogonal assay (based on the hydrolysis of *p*-nitrophenylphosphate) and determined the mechanism of action (MOA). We selected three tetracycline derivatives (methacycline, tetracycline and doxycycline) and two azo dyes (Congo red and Evans blue) for these analyses. The experimentally determined K_i values for the tetracyclines ranged from 99 to 326 μM (Table 2), while the azo dyes had sub-micromolar inhibition constants (Table 3). To determine MOA, double reciprocal plots were constructed using several inhibitor concentrations for doxycycline (Fig. 5A) and for Congo red (Fig. 5B). In both cases, the results are consistent with competitive inhibition. The initial rates of progress curves were linear, suggesting rapid equilibrium inhibition, and confirmatory dilution experiments did not suggest any time dependence of the inhibition (28, 29).

Specificity of inhibitors

Sts-1 is a protein tyrosine phosphatase but is structurally distinct from canonical PTPs (20). To determine the selectivity of the inhibitors for Sts-1_{HP}, we quantified the effect of a tetracycline derivative and an azo dye on the activity of the non-receptor type PTPs PTP1B and SHP1. Doxycycline did not inhibit PTP1B or SHP1 at any concentration tested (up to 2 mM), while Congo red inhibited these PTPs at low μM concentrations (Table 4). This suggests that both the tetracyclines and the sulfonated azo dyes are likely to be selective inhibitors, with doxycycline having a selectivity index (SI) of greater than 200 while Congo red exhibited an SI of nearly 20.

Key structural features of Sts-1 that contribute to inhibitor binding

Structural comparison of the hits from the screen, and the two classes highlighted above in particular, yielded several initial structure-activity relationship observations. Both the tetracycline derivatives and sulfonated azo dyes all possess a high number of hydrogen bond donors and acceptors. The azo dyes, specifically, also have multiple sulfonates, which can potentially act as phosphate surrogates in the Sts active site. The stereochemistry of the compounds also played a key role, something that is most evident in the comparison of the tetracycline analogs (Fig. 3 and Table 2). Subtle stereochemical changes yield several-fold differences in potency. Perhaps the most striking similarity amongst the inhibitor classes discovered in the screen was the almost universal presence of relatively planar, polyaromatic groups. This observation led us to speculate that planar aromatic amino acid sidechains would be important for the Sts-inhibitor interactions. Examination of the structure of Sts-1_{HP} reveals the presence of a tryptophan residue (W494) and a tyrosine residue (Y596) at the periphery of the active site (Fig. 6). To test whether these residues play a significant role in inhibitor binding, we generated several mutants and compared the inhibition constants of the mutants to the native enzyme (Table 5). Mutation of W494 to either phenylalanine, histidine or leucine reduces the potency (measured by the ratio of K_i of mutant to K_i of native Sts-1_{HP}) of doxycycline by 7 – 15 fold and of Congo red by 13 – 18 fold. The contribution of Y596 to inhibitor binding was apparently much smaller. Mutation of Y596 to phenylalanine or leucine led to only small decreases (< 5) in inhibitor potency. The single exception was the Y596L mutant, which was inhibited by Congo red with a 12-fold lower potency.

DISCUSSION

The Sts proteins, particularly Sts-1, have recently emerged as potential targets for the treatment of deadly pathogen infections (refs). An altered immune response and increased fungal or bacterial clearance in Sts knockout mice generates a profound resistance phenotype (refs). Small molecules that can potently and selectively inhibit Sts-1 phosphatase activity would be extremely valuable, both as probes of function and as a foundation for drug development. We set out to conduct a high-throughput screen with the goal of identifying one or more class of compounds that inhibit Sts-1 phosphatase

activity, and do so selectively when compared to canonical PTPs. After testing several established phosphatase assays, we settled on the OMFP-based fluorescence assay to screen for inhibitors of Sts-1_{HP}.(ref) We were able to successfully miniaturize this assay to 1,536-well plate format and confirmed that it behaved well, yielding satisfactory statistics (Z´ = 0.69 ± 0.02, S:B of 2.03 ± 0.10; n=3 plates). We next tested our methods using the LOPAC collection of 1,280 pharmacologically active compounds. As expected, the assay ran well and we initially identified 10 active compounds for a 0.86% hit rate (Fig. 1). Among these hits, listed in Table 1, were several known PTP inhibitors including aurintricarboxylic acid, morin, dephostatin and 3,4-methyldephostatin (30-34). These results confirmed that our assay could be used in high-throughput to effectively screen for inhibitors of the Sts-1 phosphatase activity.

Having established the efficacy of our approach, we conducted a screen of 20,580 compounds. These compounds were a subset of the Scripps Drug Discovery Library (SDDL) selected to maximize structural diversity in the screen. The assay, conducted in 1,536-well format in singlicate, performed well (Figs. 2B and C) and initially yielded 115 hits (0.56% hit rate). After performing a counterscreen to eliminate false positives, 98 commercially available compounds were advanced. A 10-point dose response titration, using a 3-fold dilution series, was used to establish IC_{50} values for these compounds. After completing the titrations and additional counterscreen, 51 active compounds, defined as having an IC_{50} < 10 μM, were identified. A flowchart showing the progress through testing and screening is shown in Figure 2A.

To investigate initial SAR in the data, we mined the screening results for obvious structural classes of compounds. While several classes of compounds were identified, two groups in particular represented nearly 30% of the total number of actives. The first, and most numerous, were the tetracycline derivatives (Fig. 3), with 12 total variants observed amongst the 51 compounds with IC_{50} < 10 μM in our screen. The structures and IC_{50} values from the initial titrations of the top 6 derivatives are given in Table 2. Based on the dose response curves, these compounds have IC_{50} values in the low to sub-

218 micromolar range. They also exhibited relatively low promiscuity indices (from 1 to 6), a measure of
219 how often a compound shows up in screens. To confirm that these inhibitors are specifically inhibiting
220 the Sts phosphatase activity and not interfering with the assay, we determined the inhibition constants
221 of a subset of these compounds with an orthogonal approach. Using an absorbance-based assay,
222 which relies on detection of *p*-nitrophenol, we calculated the K_i values for the inhibition of Sts-1_{HP} by
223 methacycline, tetracycline and doxycycline (Table 2). While the results show the same trend as the
224 primary screen IC_{50} data, the values reflect a significantly lower level of inhibition. Further analysis of
225 the protein-inhibitor interactions (see below) suggests that these tetracycline derivatives may be binding
226 peripherally at the active site. This may allow partial access of the smaller *p*-nitrophenyl phosphate
227 (PNPP) substrate while more effectively blocking access of the larger OMFP substrate. This would
228 explain why the titration data, which employed the OMFP substrate, shows a much higher level of
229 inhibition. As Sts-1 is a protein tyrosine phosphatase and the native substrate is, as such, a protein
230 molecule, the IC_{50} values determined using the OMFP assay are likely more indicative of the
231 physiologically relevant response to these inhibitors.
232
233 Another class of structurally similar compounds, the sulfonated azo dyes (Fig. 4), also appeared with
234 high frequency in our screening results (6 of the 51 active compounds). These compounds had IC_{50}
235 values from the low micromolar to sub-micromolar (Table 3). Likely owing to their inherent fluorescence,
236 some of these compounds also show up in a large number of other screens. Two of the compounds,
237 NF-279 and PPNDS, had a reasonably low promiscuity index ($\leq$ 5). These two compounds are both
238 potent and selective inhibitors of P2X receptors (35, 36). To rule out that these compounds were non-
239 specifically interfering with the assay, we determined the inhibition constants for two representative
240 sulfonated azo dyes using the PNPP assay. Both Congo red and Evans blue were potent inhibitors with
241 nanomolar K_i values (Table 3). As observed in the primary screen, Congo red was several-fold more
242 potent than Evans blue. Unlike the tetracyclines, the sulfonated azo dyes show high levels of inhibition
243 regardless of the substrate used in these assays. This indicates that these compounds more fully

occupy the active site, precluding even the smaller PNPP substrate. Analysis of the conserved structural features of these azo dyes suggests that the naphthalenesulfonate group may act as a phosphotyrosine surrogate. The catalytic histidine residues are likely to bind the sulfonate group, as observed in the sulfate-bound crystal structure of Sts-1_{HP} (Fig. 6A) (20). The conserved arginine residues would then be oriented to make cation-π interactions with the naphthyl group. Additional protein-inhibitor interactions would likely occur between the peripheral aromatic residues in the active site and the phenyl, benzyl, pyridoxal or methoxybenzyl group (see further discussion below).

To examine MOA we determined the kinetics of the Sts-1_{HP} phosphatase reaction at several inhibitor concentrations for doxycycline and Congo Red. Analysis of the double reciprocal plots of the data show a reduction in K_m and no effect on the maximal rate, indicating competitive inhibition (Fig. 5). We then examined the effect of these inhibitors on PTP1B and SHP1 to determine if they selectively inhibit Sts-1 over these other PTPs. The data, in Table 4, shows that Congo red is approximately 20- and 50-fold more active against Sts-1 than either PTP1B or SHP1, respectively. Similarly, doxycycline is more than 200-fold more potent against Sts-1 than the other PTPs. These data demonstrates that these compounds are relatively potent and selective competitive inhibitors of Sts phosphatase activity. In addition, this illustrates the effectiveness of the screening approach as a means of lead generation for drug development.

In looking for common structural motifs present in the active compounds and, specifically, the two major classes of inhibitors described, we observed a large number of the hits had relatively planar, polycyclic aromatic substituents. This propensity for Sts-1 to bind flat, polyaromatic compounds is also seen in the substrate specificity. The larger coumarin derivative DiFMUP and fluorescein derivative OMFP are significantly better substrates (k_{cat}/K_m = 5 × 10^7 and 4 × 10^6, respectively) than the phosphotyrosine mimic *p*-nitrophenyl phosphate (k_{cat}/K_m = 5 × 10^3) (20). This trend likely is indicative of structural

features of the protein that confer selectivity for the native substrate(s). To determine if specific residues at or near the active site make significant contributions to the binding of polycyclic aromatic inhibitors, we reexamined the inhibition kinetics using several Sts-1 mutants. The residues that we deemed most likely to participate in recruiting these types of inhibitors were a tyrosine residue (Y596) and a tryptophan residue (W494) that are found near the Sts active site (Figs. 6A and B). While mutations of W494 or Y596 had little effect on the K_m, mutation of the tryptophan reduced the potency of doxycycline or Congo red by a factor of approximately 15- to 20-fold (Table 5). Mutation of the tyrosine also had an effect, albeit more subtle, showing levels of inhibition that were only 3- to 12-fold lower than the native enzyme. These results indicate that both of these residues contribute to ligand binding, and that W494 plays a more significant role in this regard. Comparison of the sulfate-bound to the unliganded Sts-1_{HP} structures show that, while the conserved histidine and arginine sidechains remain fixed, both W494 and Y596 move upon substrate binding (20). W494, in particular, undergoes a slight (~10°) rotation leaving the nitrogen atom more than 2Å from its position in the unliganded structure. In addition, in the X-ray crystal structure, W494 had one of the highest B-factor values (which measure the extent to which the electron density is spread out in the model). This indicates that this tryptophan residue has a high degree of local mobility. This flexibility may contribute to how the protein recognizes and binds to substrates. Taken together, this data suggests that these aromatic residues at the active site, particularly W494, may serve as a selectivity filter for native substrates. While the protein-protein interacting domains of Sts-1, SH3 and UBA, may help to recruit specific protein targets for dephosphorylation, a selectivity mechanism would almost certainly be required to distinguish between the many phosphotryrosine residues on the target protein. Zap-70, a known substrate of Sts-1, has over 25 tyrosine residues, many of which are clustered together. Both Sts-1 and Sts-2 show varying levels of phosphatase activity for different tyrosine residues on Zap-70, suggesting that a mechanism for selectivity is in place (37, 38). Further analysis of protein-ligand interactions and the structural features that determine these interactions is needed in order to fully define this selectivity mechanism.

Immunotherapies have become of increasing interest of late, particularly in their promise to treat infection and different types of cancers (39-43). For the treatment of infectious disease, there are definite advantages in the use of immunomodulatory agents, either alone or in combination with standard of care antibiotics. Central among these is the decreased potential to generate antibiotic resistance (40). While there are a number of immunostimulatory therapies currently in use, they are primarily in the form of peptides and other biomolecules, and new targets are actively being sought. The Sts proteins are a highly promising new target for the development of immunomodulatory therapies. Genetic inactivation of these proteins leads to a profound resistance phenotype and accelerated clearance of several types of dangerous human pathogens (8, 9). As a first step towards developing Sts-targeted drugs, we have identified two new classes of selective inhibitors of Sts-1 phosphatase activity using a high-throughput screening approach. These compounds, a series of tetracycline derivatives and several sulfonated azo dyes, are the first reported inhibitors that are both potent and selective for Sts-1. The results of the screen and accompanying characterization of the hits provides important insights into substrate binding and is strong evidence supporting the druggability of this class of protein.

MATERIALS AND METHODS

Cloning, expression and purification of Sts-1_{HP} and mutants

Sts-1_{HP} (residues 373-636) was cloned with a 6xhis tag in the pTHT vector (a modified form of pET-28 with a Tobacco Etch Virus protease site in place of the thrombin site). To generate mutants, wild-type Sts-1_{HP} construct was used as DNA templates for PCR-based site-directed mutagenesis. All constructs were sequence-verified to ensure accuracy. Wild-type Sts-1_{HP} and mutants were expressed using BL21(DE3) cells and purified as previously described (20).

Fluorescence assay protocol in 1,536-well plate format

The optimized conditions for the HTS assay in 1,536-well plate format are summarized in Table 6. Assay buffer was prepared fresh daily and contained 30 mM Tris HCl, 75 mM NaCl, 1 mM EDTA and 1m M DTT (all reagents from Sigma Aldrich). STS-1_{HP} was prepared in assay buffer to a final concentration of 750 ng/ml. 4 µL of STS-1_{HP}, or buffer only, were dispensed to the appropriate wells of a 1,536-well black solid bottom microtiter plates (Greiner BioOne) using an FRD (Aurora Biosciences). Test compounds in DMSO or DMSO alone were added to the appropriate wells using the automated GNF/Kalypsis robotic platform. A 10 mM stock of OMFP, freshly prepared in neat DMSO, was diluted in water and the assay was started by dispensing 2 µL of OMFP fluorescent substrate to all wells to yield a 50 µM final concentration. Plates were centrifuged and incubated for 20 minutes at room temperature. To stop the reaction, a 0.7 N NaOH solution was added at 1 µL to a final concentration of 100 mM. After centrifugation, the plates were read at 485 nm excitation and 525 nm emission using a Viewlux plate reader (PerkinElmer Life Sciences).

Compound library

For the pilot screen, a 1,280 compound library known as the Library of Pharmacologically Active Compounds (LOPAC, Sigma Aldrich) was used. The compounds were tested in triplicate at a single nominal concentration of 5.8uM. In the 20,580-compound screen, a subset of the Scripps Drug Discovery Library (SDDL) was profiled in the HTS campaign. The SDDL currently consists of >650K unique compounds, representing a diversity of drug-like scaffolds targeted to traditional and non-traditional drug-discovery biology. The SDDL has been curated from over 20 commercial and academic sources and contains more than 20,000 compounds unique to Scripps. The SDDL compounds have been selected based on scaffold novelty, physical properties and spatial connectivity (44-49). We selected compounds for the 20K pilot effort that included a heavy concentration of approved drugs (~3,200), or drug like molecules such as the Cayman bioactive lipids (>1,000), TOCRIS, Prestwick, and for diversity, portions of the Chembridge, Enamine, Life Chemicals and Microscources collections.

Data Analysis

In both the LOPAC pilot screen and the HTS, compounds were tested at a single concentration at a final nominal concentration of 5.8 μM using the protocol summarized in Table 6. The activity of each well was normalized on a per-plate basis using the following equation:

$$\%\ Inhibition = \ 100 \times \frac{Test\ well - Median\ Low\ Control}{Median\ High\ Control - Median\ Low\ Control}$$

Where *Test well* is defined as wells containing enzyme/substrate in the presence of test compound, *Low Control* is defined as the median of the wells containing test compounds and *High Control* is defined as the wells containing DMSO and OMFP in the absence of the Sts-1_{HP} enzyme. The reference compound, PHPS1, was used to monitor the stability of the assay, but was not used in the calculation of the controls or the normalization. Data was normalized on a per plate basis, and each assay plate underwent a quality control check. A value greater than 0.5 for Z´ was required before further analysis (50). Similar to other HTS campaigns, nominally inhibiting compounds (hit cutoff) were selected as those that had response values above three times the standard deviation of the average percent response from all compounds tested (51). Data was visualized with a randomized scatterplot of all compound activity (Figs. 1A and 2B), generated using Spotfire Pro (TIBCO Software Inc.).

Counterscreen and concentration response assays

The concentration response curves (CRCs) were generated using assays that employed the same reagents, protocols, and detection systems as the primary assay, but also utilized a counterscreen assay where the compounds were added after the NaOH step to help identify fluorescent quenchers and other non-specific inhibitors. The assays tested compounds as 10-point dose-response titration (3-fold dilutions) in triplicate. For each test compound, percent activity was plotted against compound concentration. A four parameter equation describing a sigmoidal dose-response curve was then fitted

with adjustable baseline using Assay Explorer software (Symyx Technologies Inc.). The reported IC_{50} values were generated from fitted curves by solving for the X-intercept value at the 50% activity level of the Y-intercept value. Compounds with an IC_{50} greater than 10 μM were considered inactive while compounds with an IC_{50} equal to or less than 10 μM were considered active. Only those compounds that were active in the primary screen and inactive in the counterscreen advanced for further analysis.

QA/QC

All samples in the SDDL have been tested for purity and structural confirmation *via* LC-MS and/or NMR to provide adequate QA/QC. In addition, after completion of the 20K screen, all compounds that proceeded through the titration phase were subjected to LC-MS analysis using samples obtained directly from the same source plates used in the assay. This allowed for reconfirmation of hit sample purity (single peak) and mass (correct molecular weight). Only those samples that passed LC-MS analysis for both purity and mass were advanced for further analysis.

Steady-State Kinetics

The steady-state kinetics were conducted using a spectrophotometric phosphatase assay making use of p-nitrophenyl phosphate (pNPP). The assay was run as described previously (20). Briefly, $Sts\text{-}1_{HP}$ was assayed in a buffer containing a final concentration of 20 mM Tris (pH 7.5), 150 mM sodium chloride, 5 mM magnesium chloride and 1 mM βME and varying concentrations of pNPP as a substrate. Activity was measured by following the increase in absorbance at 405 nm due to the production of pNP. The initial reaction rate (<10 % reaction completion) was plotted against pNPP concentration. The data were fit with a rectangular hyperbola using the Michaelis-Menten equation and values for K_m and k_{cat} were determined from the graph (Kaleidagraph, Synergy Software).

Inhibition Analysis

The pNPP assay was used for the follow-up inhibition analysis after completion of the 20K pilot screen and for MOA studies. The initial velocity, as a function of substrate concentration, was measured at several fixed concentrations of the inhibitor of interest (20). Lineweaver-Burk (double reciprocal) plots were constructed in each case and a linear fit was used. All the kinetic experiments were conducted in triplicate, and the error bars shown are the standard error from triplicate measurements. Error values given in tables report the error in the fit to the equation. For the double reciprocal plots, the data was fit using the following equation for competitive inhibition:

$$v = \frac{v_{max}[subs\qquad\qquad]}{K_m\left(1 + \frac{[Inhibitor]}{K_i}\right) + [substrate]}$$

K_i was calculated from the K_m value determined in the presence of inhibitor using the following equation:

$$k_m^{app} = k_m\left(1 + \frac{[Inhibitor]}{K_i}\right)$$

The error values provided in all tables are standard errors from triplicate measurements.

ACKNOWLEDGEMENTS

This work was supported by the National Heart, Lung, and Blood Institute of the National Institutes of Health (NIH) through Award Number U01HL127522 (JBF, NC), the National Institute of Allergy and Infectious Disease of the NIH through Award Number R21AI130859 (JBF, NC), and the Office of the Assistant Secretary of Defense for Health Affairs through the Peer Reviewed Medical Research Program under Award No. W81XWH17-1-0147 (JBF, NC). In addition, parts of this work were supported by the National Institutes of General Medical Sciences of the NIH under grant R35GM124898 (JBF). **Add any Scripps support.** The content is solely the responsibility of the authors and does not necessarily represent the official views of the National Institutes of Health or the Department of Defense. Additional support was provided by the Center for Biotechnology, a New York

State Center for Advanced Technology, Stony Brook University, Cold Spring Harbor Laboratory, Brookhaven National Laboratory and Feinstein Institute for Medical Research.

REFERENCES

1. Mustelin T, Tasken K. 2003. Positive and negative regulation of T-cell activation through kinases and phosphatases. Biochem J 371:15-27.
2. Smith-Garvin JE, Koretzky GA, Jordan MS. 2009. T cell activation. Annu Rev Immunol 27:591-619.
3. Singer AL, Koretzky GA. 2002. Control of T cell function by positive and negative regulators. Science 296:1639-40.
4. Carpino N, Turner S, Mekala D, Takahashi Y, Zang H, Geiger TL, Doherty P, Ihle JN. 2004. Regulation of ZAP-70 Activation and TCR Signaling by Two Related Proteins, Sts-1 and Sts-2. Immunity 20:37-46.
5. Mikhailik A, Ford B, Keller J, Chen Y, Nassar N, Carpino N. 2007. A phosphatase activity of Sts-1 contributes to the suppression of TCR signaling. Mol Cell 27:486-97.
6. Carpino N, Naseem S, Frank DM, Konopka JB. 2017. Modulating Host Signaling Pathways to Promote Resistance to Infection by Candida albicans. Front Cell Infect Microbiol 7:481.
7. Frank D, Naseem S, Russo GL, Li C, Parashar K, Konopka JB, Carpino N. 2018. Phagocytes from Mice Lacking the Sts Phosphatases Have an Enhanced Antifungal Response to Candida albicans. MBio 9.
8. Naseem S, Frank D, Konopka JB, Carpino N. 2015. Protection from systemic Candida albicans infection by inactivation of the Sts phosphatases. Infect Immun 83:637-45.
9. Parashar K, Kopping E, Frank D, Sampath V, Thanassi DG, Carpino N. 2017. Increased Resistance to Intradermal Francisella tularensis LVS Infection by Inactivation of the Sts Phosphatases. Infect Immun 85.
10. Brown GD, Denning DW, Gow NA, Levitz SM, Netea MG, White TC. 2012. Hidden killers: human fungal infections. Sci Transl Med 4:165rv13.
11. Brown GD, Denning DW, Levitz SM. 2012. Tackling human fungal infections. Science 336:647.

12. Mayer FL, Wilson D, Hube B. 2013. Candida albicans pathogenicity mechanisms. Virulence 4:119-28.
13. Asare R, Kwaik YA. 2010. Exploitation of host cell biology and evasion of immunity by francisella tularensis. Front Microbiol 1:145.
14. McLendon MK, Apicella MA, Allen LA. 2006. Francisella tularensis: taxonomy, genetics, and Immunopathogenesis of a potential agent of biowarfare. Annu Rev Microbiol 60:167-85.
15. Oyston PC. 2008. Francisella tularensis: unravelling the secrets of an intracellular pathogen. J Med Microbiol 57:921-30.
16. Hicke L, Schubert HL, Hill CP. 2005. Ubiquitin-binding domains. Nat Rev Mol Cell Biol 6:610-21.
17. Musacchio A. 2002. How SH3 domains recognize proline. Adv Protein Chem 61:211-68.
18. Tsygankov AY. 2013. TULA-family proteins: a new class of cellular regulators. J Cell Physiol 228:43-9.
19. Rigden DJ. 2008. The histidine phosphatase superfamily: structure and function. Biochem J 409:333-48.
20. Zhou W, Yin Y, Weinheimer AS, Kaur N, Carpino N, French JB. 2017. Structural and Functional Characterization of the Histidine Phosphatase Domains of Human Sts-1 and Sts-2. Biochemistry 56:4637-4645.
21. Bond CS, White MF, Hunter WN. 2001. High resolution structure of the phosphohistidine-activated form of Escherichia coli cofactor-dependent phosphoglycerate mutase. J Biol Chem 276:3247-53.
22. Bond CS, White MF, Hunter WN. 2002. Mechanistic implications for Escherichia coli cofactor-dependent phosphoglycerate mutase based on the high-resolution crystal structure of a vanadate complex. J Mol Biol 316:1071-81.
23. San Luis B, Nassar N, Carpino N. 2013. New insights into the catalytic mechanism of histidine phosphatases revealed by a functionally essential arginine residue within the active site of the Sts phosphatases. Biochem J 453:27-35.

24. Zheng Q, Jiang D, Zhang W, Zhang Q, Zhao Q, Jin J, Li X, Yang H, Bartlam M, Shaw N, Zhou W, Rao Z. 2014. Mechanism of dephosphorylation of glucosyl-3-phosphoglycerate by a histidine phosphatase. J Biol Chem 289:21242-51.

25. Luis BS, Carpino N. 2014. Insights into the suppressor of T-cell receptor (TCR) signaling-1 (Sts-1)-mediated regulation of TCR signaling through the use of novel substrate-trapping Sts-1 phosphatase variants. FEBS J 281:696-707.

26. Chen Y, Jakoncic J, Carpino N, Nassar N. 2009. Structural and functional characterization of the 2H-phosphatase domain of Sts-2 reveals an acid-dependent phosphatase activity. Biochemistry 48:1681-90.

27. Chen Y, Jakoncic J, Parker KA, Carpino N, Nassar N. 2009. Structures of the phosphorylated and VO(3)-bound 2H-phosphatase domain of Sts-2. Biochemistry 48:8129-35.

28. Copeland RA. 2003. Mechanistic considerations in high-throughput screening. Anal Biochem 320:1-12.

29. Copeland RA. 2005. Evaluation of enzyme inhibitors in drug discovery. A guide for medicinal chemists and pharmacologists. Methods Biochem Anal 46:1-265.

30. Imoto M, Kakeya H, Sawa T, Hayashi C, Hamada M, Takeuchi T, Umezawa K. 1993. Dephostatin, a novel protein tyrosine phosphatase inhibitor produced by Streptomyces. I. Taxonomy, isolation, and characterization. J Antibiot (Tokyo) 46:1342-6.

31. Umezawa K, Kawakami M, Watanabe T. 2003. Molecular design and biological activities of protein-tyrosine phosphatase inhibitors. Pharmacol Ther 99:15-24.

32. Watanabe T, Takeuchi T, Otsuka M, Tanaka S, Umezawa K. 1995. Synthesis and protein tyrosine phosphatase inhibitory activity of dephostatin analogs. J Antibiot (Tokyo) 48:1460-6.

33. Gupta SC, Phromnoi K, Aggarwal BB. 2013. Morin inhibits STAT3 tyrosine 705 phosphorylation in tumor cells through activation of protein tyrosine phosphatase SHP1. Biochem Pharmacol 85:898-912.

34. Liang F, Huang Z, Lee SY, Liang J, Ivanov MI, Alonso A, Bliska JB, Lawrence DS, Mustelin T, Zhang ZY. 2003. Aurintricarboxylic acid blocks in vitro and in vivo activity of YopH, an essential virulent factor of Yersinia pestis, the agent of plague. J Biol Chem 278:41734-41.
35. Damer S, Niebel B, Czeche S, Nickel P, Ardanuy U, Schmalzing G, Rettinger J, Mutschler E, Lambrecht G. 1998. NF279: a novel potent and selective antagonist of P2X receptor-mediated responses. Eur J Pharmacol 350:R5-6.
36. Lambrecht G, Rettinger J, Baumert HG, Czeche S, Damer S, Ganso M, Hildebrandt C, Niebel B, Spatz-Kumbel G, Schmalzing G, Mutschler E. 2000. The novel pyridoxal-5'-phosphate derivative PPNDS potently antagonizes activation of P2X(1) receptors. Eur J Pharmacol 387:R19-21.
37. Chen X, Ren L, Kim S, Carpino N, Daniel JL, Kunapuli SP, Tsygankov AY, Pei D. 2010. Determination of the substrate specificity of protein-tyrosine phosphatase TULA-2 and identification of Syk as a TULA-2 substrate. J Biol Chem 285:31268-76.
38. San Luis B, Sondgeroth B, Nassar N, Carpino N. 2011. Sts-2 is a phosphatase that negatively regulates zeta-associated protein (ZAP)-70 and T cell receptor signaling pathways. J Biol Chem 286:15943-54.
39. Fuge O, Vasdev N, Allchorne P, Green JS. 2015. Immunotherapy for bladder cancer. Res Rep Urol 7:65-79.
40. Masihi KN. 2001. Fighting infection using immunomodulatory agents. Expert Opin Biol Ther 1:641-53.
41. Sagiv-Barfi I, Czerwinski DK, Levy S, Alam IS, Mayer AT, Gambhir SS, Levy R. 2018. Eradication of spontaneous malignancy by local immunotherapy. Sci Transl Med 10.
42. Syn NL, Teng MWL, Mok TSK, Soo RA. 2017. De-novo and acquired resistance to immune checkpoint targeting. Lancet Oncol 18:e731-e741.
43. Yang Y. 2015. Cancer immunotherapy: harnessing the immune system to battle cancer. J Clin Invest 125:3335-7.

44. Lovering F, Bikker J, Humblet C. 2009. Escape from flatland: increasing saturation as an approach to improving clinical success. J Med Chem 52:6752-6.
45. Lipinski CA, Lombardo F, Dominy BW, Feeney PJ. 2001. Experimental and computational approaches to estimate solubility and permeability in drug discovery and development settings. Adv Drug Deliv Rev 46:3-26.
46. Kolb HC, Sharpless KB. 2003. The growing impact of click chemistry on drug discovery. Drug Discov Today 8:1128-37.
47. Ding S, Gray NS, Wu X, Ding Q, Schultz PG. 2002. A combinatorial scaffold approach toward kinase-directed heterocycle libraries. J Am Chem Soc 124:1594-6.
48. Congreve M, Carr R, Murray C, Jhoti H. 2003. A 'rule of three' for fragment-based lead discovery? Drug Discov Today 8:876-7.
49. Baell JB, Holloway GA. 2010. New substructure filters for removal of pan assay interference compounds (PAINS) from screening libraries and for their exclusion in bioassays. J Med Chem 53:2719-40.
50. Zhang JH, Chung TD, Oldenburg KR. 1999. A Simple Statistical Parameter for Use in Evaluation and Validation of High Throughput Screening Assays. J Biomol Screen 4:67-73.
51. Madoux F, Tanner A, Vessels M, Willetts L, Hou S, Scampavia L, Spicer TP. 2017. A 1536-Well 3D Viability Assay to Assess the Cytotoxic Effect of Drugs on Spheroids. SLAS Discov 22:516-524.

Figure Legends

Figure 1. Pilot screen. The % response (A) for the 1,280 LOPAC library compounds, conducted in triplicate, is shown. The high control is plotted in red, the low control is plotted in green, the PHPS1 standard is plotted in magenta, and the samples are plotted in black. Compounds that had a response greater than three times the standard deviation (31.8% response in this case) were selected as active. The potent Sts-1 inhibitor, PHPS1, which has an IC_{50} of 17.6 μM (B), was used as a positive control. A correlation plot (C) of the compounds screened in duplicate plates is shown. The hit cutoffs are designated by red lines ($R^2 = 0.933$).

Figure 2. 20,580 compound high-throughput screen. The 20K screen, summarized in (A), yielded 101 initial hits using a standard cutoff (23.12% response, in this case) (B). After retesting and counterscreens, 51 active compounds (with $IC_{50} < 10$ μM) were identified and advanced for further testing. All of the assays performed well, yielding reasonable Z´ and signal-to-background values (C).

Figure 3. Tetracycline derivatives identified in the screen. Shown are the structures and names of the top tetracycline active compounds ($IC_{50} < 10$ μM) selected in the screening campaign.

Figure 4. Sulfonated azo dyes. Shown are the structures and names of the top sulfonated azo dye variants that were identified as active compounds ($IC_{50} < 10$ μM) in the screening campaign.

Figure 5. Mechanism of action. Double reciprocal plots for inhibition of $Sts\text{-}1_{HP}$ by the tetracycline derivative doxycycline (A) and the azo dye Congo red (B). For each, three concentrations of the inhibitor were used (shown as inset on each graph) and a linear fit was used. The lines fit to the data intersect the X-axis at a value close to zero, in both cases, indicating a competitive mode of inhibition.

Figure 6. Active site of the histidine phosphatase domain of Sts-1. In addition to the catalytic histidine residues (H379 and H565; shown in ball-and-stick representation with green carbon atoms and blue nitrogen atoms) and conserved asparagine residues (R379, R383 and R462; shown in ball-and-stick representation with green carbon atoms and blue nitrogen atoms), two aromatic residues (W494 and Y596; shown in ball-and-stick representation with black carbon atoms, blue nitrogen atoms and red oxygen atoms) occupy the phosphatase active site of Sts-1 (A). A sulfate molecule (shown in ball-and-stick representation with the sulfate atom shown in orange and oxygen atoms shown in red) in the structure acts as a phosphate surrogate and marks the site where catalysis occurs. An overall view of the Sts-1_{HP} dimer (B; the left protomer shows a surface representation where the conserved His and Arg residues are colored blue, while W494 and Y596 are colored black) illustrates how Trp494 and Tyr596 are at the periphery of the active site and could serve a role in positioning planar aromatic inhibitors to block access to the active site.

584 **Table 1.** Active compounds from LOPAC screen

Name	Molecular Weight (g/moL)	Average Response (%)
Aurintricarboxylic Acid	422.34	89.95
6-Hydroxy-DL-DOPA	213.19	64.86
Reactive Blue 2	774.16	58.99
L-α-methyl DOPA	211.21	57.45
Methyl-3,4-Dephostatin	168.15	46.07
Doxycycline	444.43	45.03
Morin	302.24	44.94
Hispidin	246.22	44.44
Dephostatin	168.15	43.47
Minocycline	456.49	32.59

585

586

Table 2. Active Tetracycline derivatives identified in 20K compound screen

Name	Mol. Weight (g/mol)	Primary IC_{50} (μM)	Counterscreen IC_{50} (μM)	Promiscuity Index[a]	K_i (μM)	logP
Methacycline	478.9	0.67	>14.5	6 of 73	326 ± 35	-3.5
Meclocycline	476.9	1.8	>14.5	3 of 67	ND[b]	-2.9
Tetracycline	444.4	1.9	>14.5	3 of 73	199 ± 20	-3.5
Oxytetracyline	460.4	3.6	>14.5	4 of 67	ND	-4.5
Doxycycline	444.4	4.1	>14.5	5 of 73	99 ± 19	-3.3
Demeclocycline	464.9	4.7	>14.5	1 of 67	ND	-3.2

[a] The promiscuity index is the number of times this compound appeared as a hit in a screen compared to the number of total screens conducted that contained this compound – a lower number is desirable.

[b] ND: Not determined

Table 3. Active sulfonated azo dyes identified in 20K compound screen

Name	Mol. Weight (g/mol)	Primary IC_{50} (μM)	Counterscreen IC_{50} (μM)	Promiscuity Index[a]	K_i (μM)	logP
Congo Red	696.7	0.92	>14.5	11 of 73	0.079 ± 0.02	3.57
Chicago Sky Blue	992.8	1.0	>14.5	8 of 67	ND[b]	-4.1
NF-279	1401.1	2.4	>29	5 of 75	ND	4.55
Evans Blue	960.8	3.1	23.6	19 of 82	0.39 ± 0.11	-2.7
PPNDS	694.4	6.9	>29	3 of 75	ND	-2.1

[a] The promiscuity index is the number of times this compound appeared as a hit in a screen compared to the number of total screens conducted that contained this compound – a lower number is desirable.

[b] ND: Not determined

602 **Table 4**. Selectivity of inhibitors for Sts-1_{HP} over other PTPs

Protein	K_m (mM)	K_i Doxycycline (mM)	K_i Congo red (μM)
Sts-1_{HP}	2.64 ± 0.48	0.099 ± 0.019	0.079 ± 0.02
PTP-1B	5.39 ± 1.07	No Inhibition	1.47 ± 0.34
SHP1	3.28 ± 0.26	No Inhibition	3.88 ± 0.59

603

604

605

606

607 **Table 5.** Inhibition of Sts-1_{HP} mutants

Construct	K_m (mM)	K_i Doxycycline (mM)	Doxycycline K_i Ratio[a]	K_i Congo Red (μM)	Congo Red K_i Ratio[a]
Sts-1_{HP}	2.64 ± 0.48	0.099 ± 0.019	1	0.079 ± 0.02	1
W494F	5.70 ± 1.05	1.42 ± 0.11	14.3	1.42 ± 0.32	18.0
W494L	6.90 ± 0.95	0.73 ± 0.04	7.4	1.46 ± 0.13	18.5
W494H	6.32 ± 0.83	1.48 ± 0.09	14.9	1.07 ± 0.03	13.5
Y596F	3.65 ± 0.49	0.39 ± 0.04	3.9	0.23 ± 0.02	2.9
Y596L	3.88 ± 0.74	0.49 ± 0.05	4.9	0.94 ± 0.05	11.9

608

609 [a] Defined as the ratio of the K_i of the mutant Sts-1_{HP} to that of the K_i of the wild-type Sts-1_{HP} enzyme

610

611

612

613

Table 6. Summary of Sts-1 HTS assay protocol for 1,536-well plate format

Step	Description	Quantity/ Condition	Comments
1	$Sts\text{-}1_{HP}$ addition in buffer	4 µL/well	750 ng/mL STS-1 in Assay buffer (30 mM Tris HCl, 75 mM NaCl, 1 mM EDTA, 1 mM DTT)
2	Pin compound or DMSO	30 nL/well	5.8 nM compound in 0.4% DMSO final
3	OMFP addition in water	2 µL/well	50uM final
4	Incubation	20 minutes	Room temperature in the dark
5	NaOH addition	1 µL/well	100 mM final, stops reaction
6	Read fluorescence	Viewlux	Ex: 480 nm; Em: 520 nm

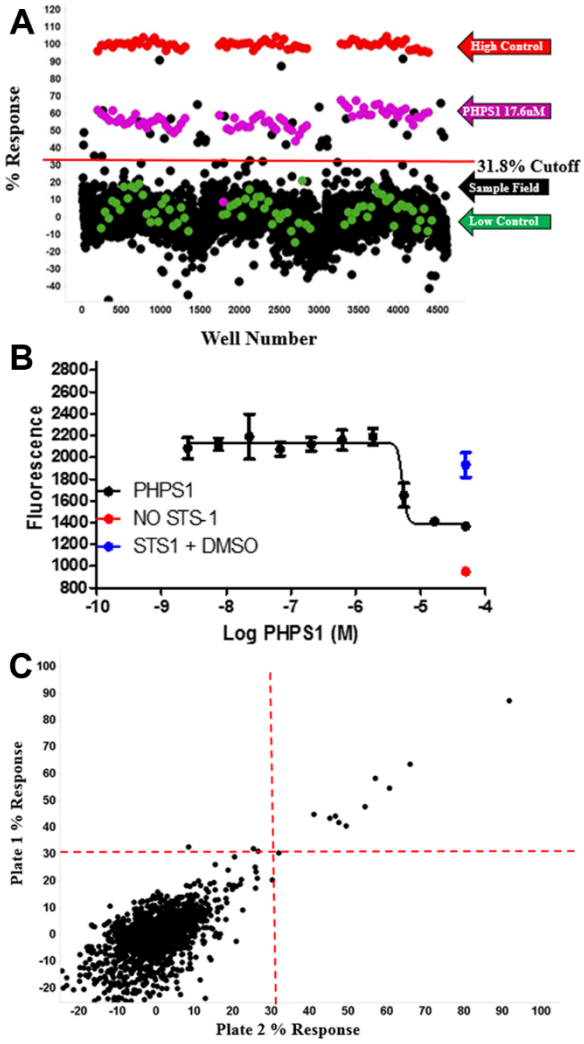
A
% Response
High Control
PHPS1 17.6uM
31.8% Cutoff
Sample Field
Low Control
Well Number
B
Fluorescence
PHPS1
NO STS-1
STS1 + DMSO
Log PHPS1 (M)
C
Plate 1 % Response
Plate 2 % Response

Figure 1.

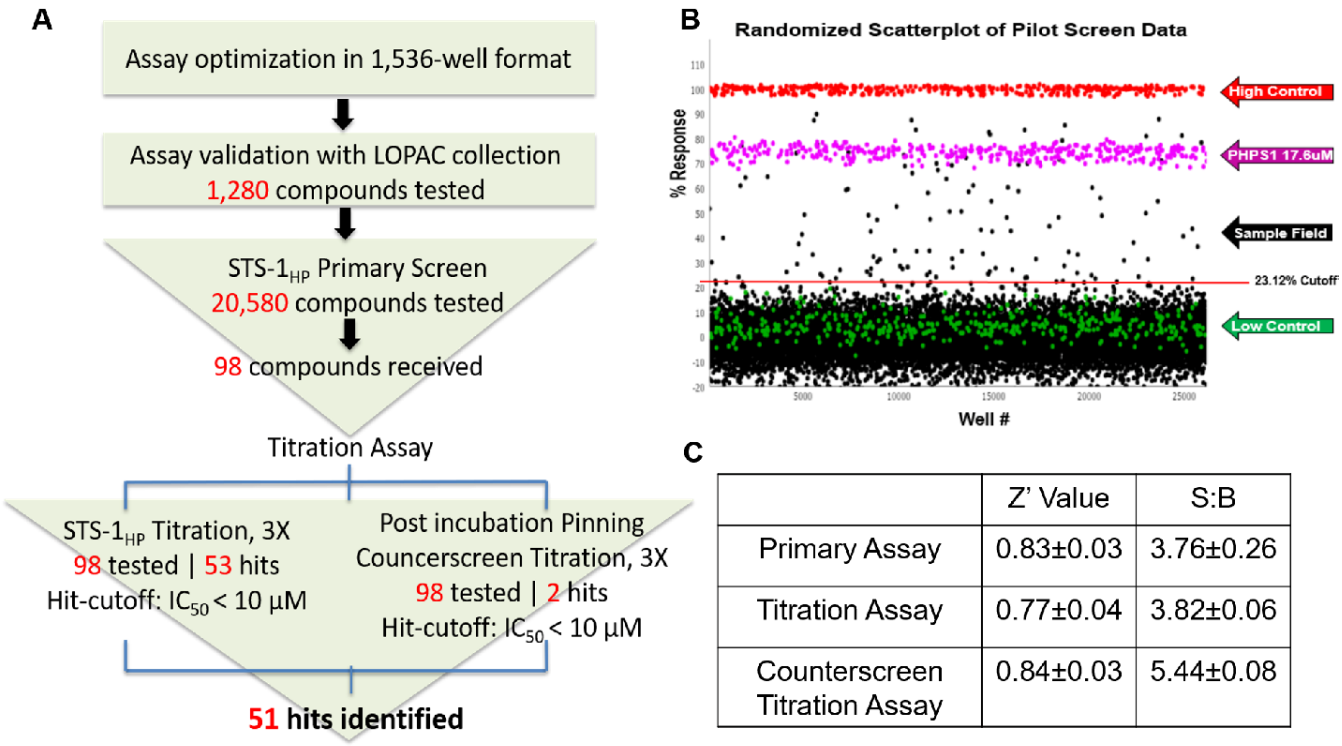

	Z' Value	S:B
Primary Assay	0.83±0.03	3.76±0.26
Titration Assay	0.77±0.04	3.82±0.06
Counterscreen Titration Assay	0.84±0.03	5.44±0.08

Figure 2.

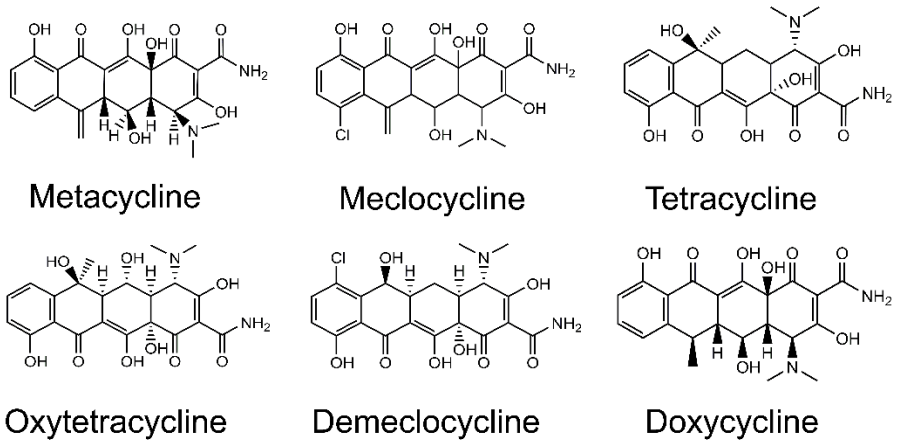

630

631

632 **Figure 3.**

633

634

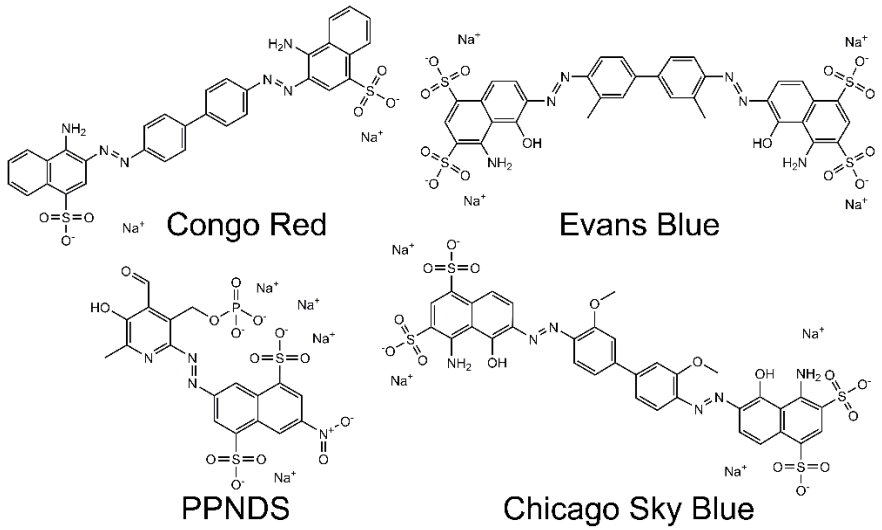

635

636

637 **Figure 4.**

638

639

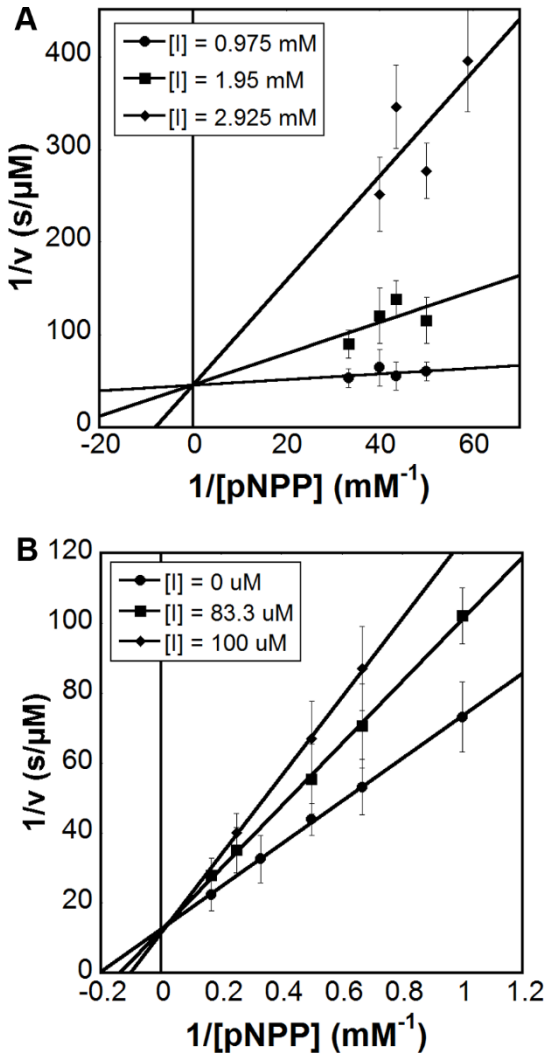

640

641

642 **Figure 5.**

643

644

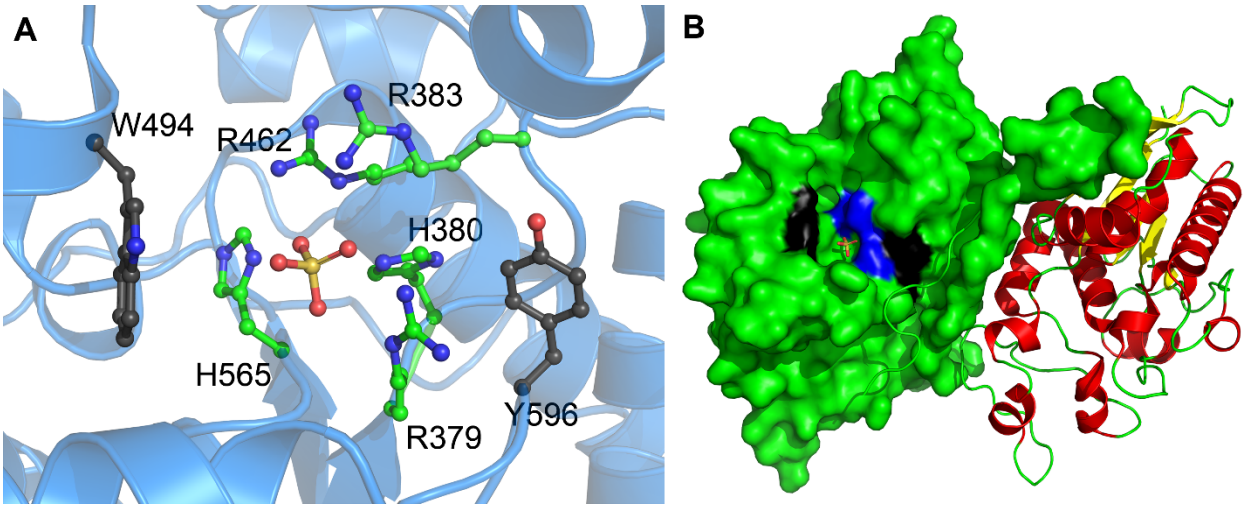

Figure 6.

APPENDIX 5

Supplementary Figure 5.1

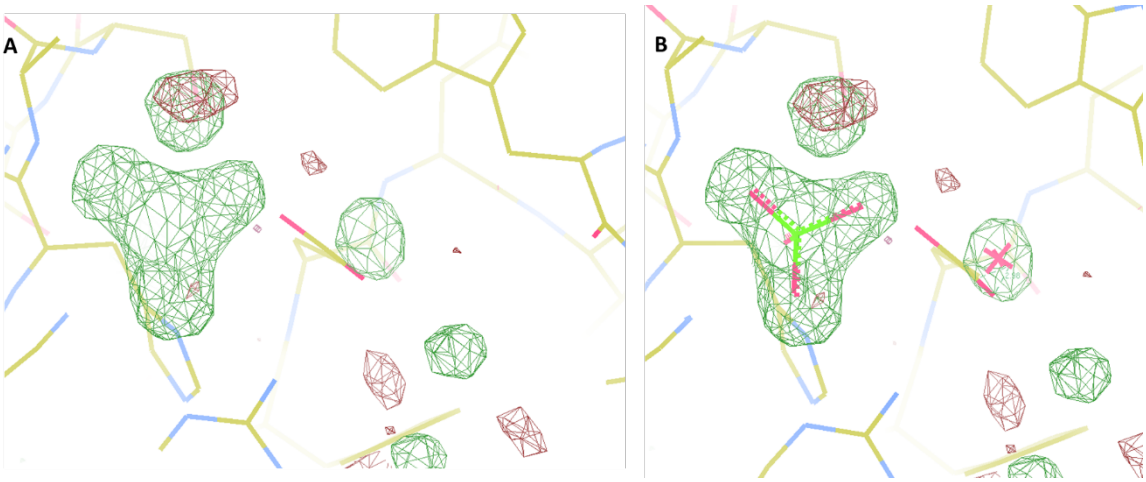

Typical electron density (A) observed at the active site of the Sts-1_{HP} domain (similar to what is reported in Zhou *et al.* – Appendix 1). This electron density clearly fits a sulfate molecule as seen modeled in B.

Supplementary Figure 5.2

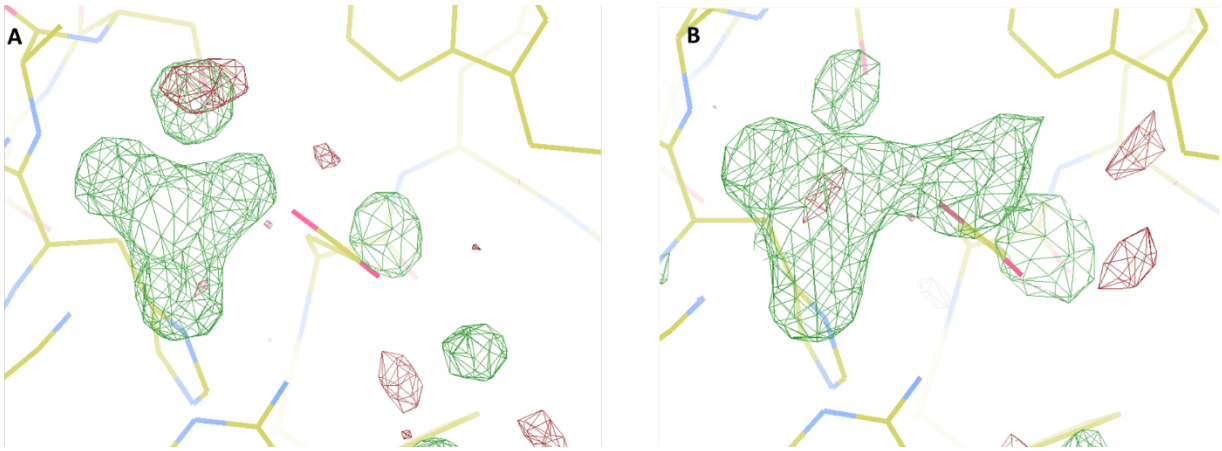

The same electron density (A) from Figure 5.1 (A) is shown alongside the density observed in the active site (B) when the substrate 3-amino-pyridine is soaked into the crystals just prior to data collection. Note that there is additional, continuous, electron density that cannot be accurately modeled with a sulfate ion and that the position of the water molecule (see below) has shifted in the data shown in B.

Supplementary Figure 5.3

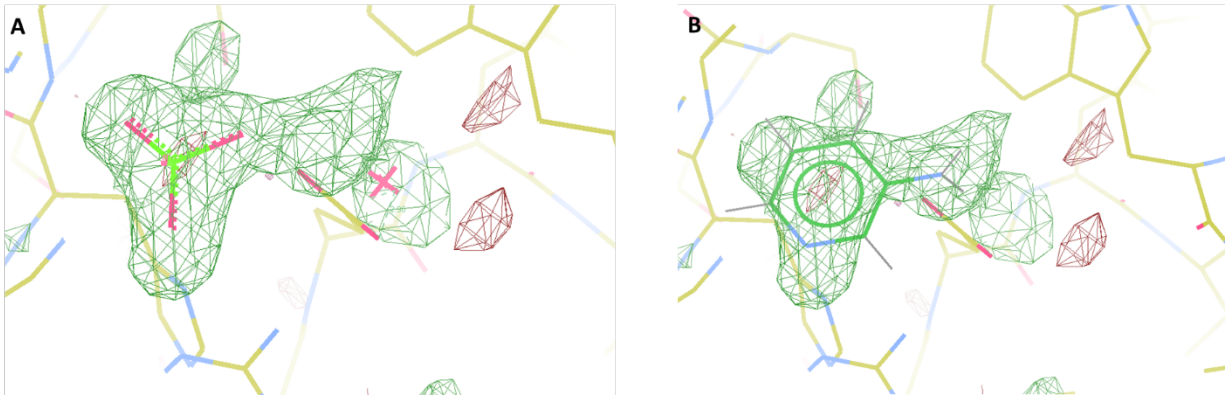

The electron density observed after soaking the crystals in a solution containing 3-aminopyridine (as described in 5.2B above) does not clearly fit either a sulfate ion (A) or the ligand that was added (B). Also note that the electron density for the water molecule (the water is modeled as a red X in A) no longer fits the position of the water molecule and appears shifted away from the arginine residue.

Supplementary Figure 5.4

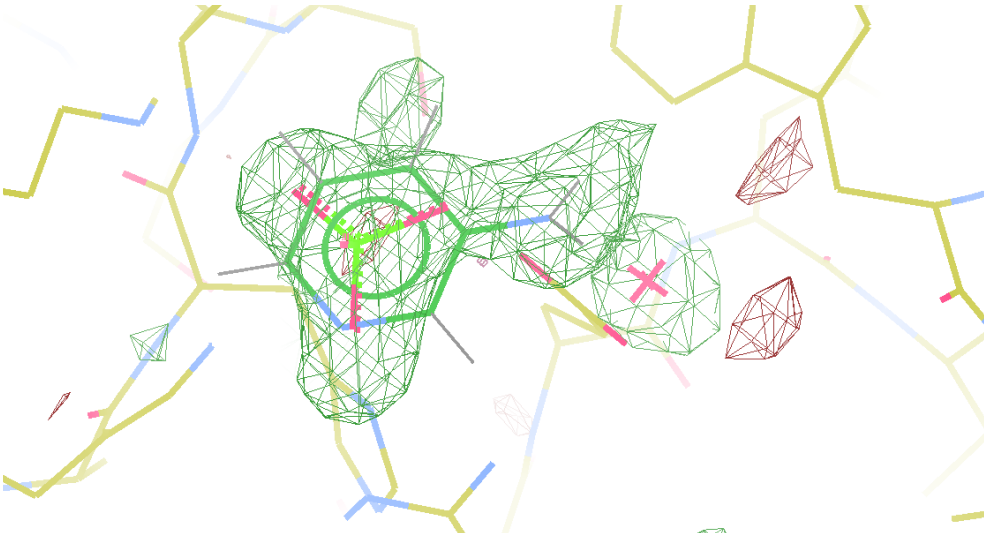

The most likely explanation for the observed density is that of partial occupancy of both the sulfate ion and the 3-aminopyridine ligand. This would lead to ‘averaged’ electron density in the maps and could explain the hybrid density observed. We are currently working to optimize the conditions to obtain crystals fully occupied with 3-aminopyridine in order to obtain